A Reduced Switch-Count Power Cell Configuration for Medium Voltage Cascaded Cell Motor Drives

A REDUCED SWITCH-COUNT POWER CELL CONFIGURATION FOR MEDIUM VOLTAGE CASCADED CELL MOTOR DRIVES

BY

DOHO KANG, B.Eng.

A THESIS

SUBMITTED TO THE DEPARTMENT OF ELECTRICAL & COMPUTER ENGINEERING

AND THE SCHOOL OF GRADUATE STUDIES

OF MCMASTER UNIVERSITY

IN PARTIAL FULFILMENT OF THE REQUIREMENTS

FOR THE DEGREE OF

MASTER OF APPLIED SCIENCE

Master of Applied Science (2022) McMaster University

(Electrical & Computer Engineering) Hamilton, Ontario, Canada

TITLE: A Reduced Switch-Count Power Cell Configuration for Medium Voltage Cascaded Cell Motor Drives

AUTHOR: Doho Kang

B. Eng.

McMaster University, Hamilton, ON, Canada

SUPERVISOR: Dr. Mehdi Narimani

NUMBER OF PAGES: viii, 154

To my parents, Jung A & Sung Wook.

Abstract

Multilevel inverters (MLI) are the foundation of motor drives in medium and high-voltage applications, allowing low voltage devices in high power applications. The Cascaded H-Bridge (CHB) is a multilevel inverter with significant popularity and unique advantages due to its modular structure. The modularity of the CHB allows a scalable design that accommodates various power ratings with minimal changes. In a typical CHB, a six-pulse diode rectifier and an H-Bridge inverter provide power from the grid to the load. As a diode rectifier only allow unidirectional power flow, the typical CHB is confined to only receiving power from the grid. The unidirectional nature of the typical CHB can propose energy loss if used in regenerative applications. A regenerative CHB with two-level voltage source inverters rather than diode rectifiers has been introduced to address the unidirectional power flow. However, this solution proposes a significant increase in the system's complexity, cost, and size. As the demand for efficient energy increases, the

research on more suitable-sized and economical regenerative CHBs has gained substantial attention.

In this thesis work, two new reduced switch-count regenerative CHB power cells are proposed. Both proposed power cells reduce the number of switches per cell by four. The challenges that arise are addressed by introducing new control and carrier phase-shifting techniques. The switch-count reduction aims to reduce the complexity, cost, and size of the conventional regenerative CHB.

The theoretical analysis and simulation studies demonstrate the potential of the new reduced switch-count regenerative power cells and its capability to replace the conventional regenerative CHB power cell.

Experimental validation of one of the proposed power cells is conducted with a single-cell configuration. The experimental result for conventional regenerative, three-phase reduced switch-count and the new proposed power cells are presented to compare their operation. The future work of this thesis includes experimental validation of the new proposed power cell in a 7-level regenerative CHB drive and operation of the system with a regenerative motor load.

Acknowledgements

First and foremost, I would like to express sincere gratitude to my supervisor, Dr. Mehdi Narimani, for the support, guidance, and advice throughout my graduate studies. He has helped me immensely personally, academically, and professionally, and I am genuinely grateful for the knowledge and opportunities.

I want to thank my colleagues in HiPEL for their help in my research. Sarah Badawi has never hesitated to share and discuss key concepts and ideas throughout my graduate studies, providing helpful feedback on my research. Zhituo Ni has helped by sharing his knowledge and experience to aid my research. I am thankful for the assistance I have received in building up the experimental prototype and the knowledge provided.

I would also like to thank Dr. Navid Zargari and Dr. George Cheng from the R&D team in Rockwell Automation Canada. Their guidance, insight, and support as our industrial research partner are invaluable and helped my research work.

Finally, I would like to thank my parents and my brother. I cannot thank them enough for the endless support, love, and encouragement they provide me with everything that I do.

Contents

List of Figures

List of Tables

Chapter 1

Introduction

1.1 Background

The motor drives' development started in the 1980s with the development of the three-level neutral-point-clamped (NPC) inverter [1]. The development of motor drives allowed the conversion of fixed input frequency and voltage to variable output frequency and voltage, ultimately providing control of the motor's speed and torque. The three-level NPC inverter utilized Bipolar Junction Transistors (BJT) as switching devices with an induction motor load rated at 200V and 2.2kW [1]. As the technologies advanced in power semiconductor devices in the mid-1980s, especially with Insulated Gate Bipolar Transistor (IGBT), motor drives have progressed in output power capabilities from several hundred watts to hundreds of megawatts [2].

For high power applications, medium voltage (MV) motor drives cover power ratings from 0.4 to 40MW with a voltage rating of 2.3-13.8kV. The high power MV motor drives have many applications in the industry. Some of the applications include pipeline pumps in the petrochemical industry, fans in the cement industry, pumps in water pumping stations, traction applications in the transportation industry, and steel rolling mills in the metals industry [3].

According to a market study [4,5], the global MV drive market is expected to grow continuously. One of the significant markets for MV motor drives is a retrofit application. Many MV motors in the field operate at a fixed speed without using an MV motor drive. With the fixed speed motor application, flow control for devices such as fans, pumps, or compressors is regulated by mechanical methods such as throttle control, inlet damping, and flow control valve. The installation of an MV motor drive to replace mechanical forms of flow regulation allow approximately 25% in savings in electricity cost. The reduction in operating costs allows MV motor drive to have a typical payback time of 1-2 years [4].

Many MV drive products are available in the market today. The MV drives in the market use various power converter topologies and control schemes to offer unique features and some limitations [3]. Some of the MV drive products marketed by major drive manufacturers can be seen in Table 1.1.

TABLE 1.1. EXAMPLES OF MV DRIVE PRODUCTS.

Manufacturer and Product	Power Converter Topology	Power Range (MVA)
Alstom VDM5000 [6]	Two-Level Voltage Source Inverter (2L-VSI)	1.4 – 7.2
ABB ACS 1000 [7]	Neutral Point Clamped (NPC)	0.3 – 5
GE Power Conversion MV7000 [8]		3 – 21
Siemens SIMOVERT-MV [9]		0.6 – 7.2
Siemens GH180 [10]	Cascaded H-Bridge (CHB)	0.3 – 60
Hitachi HIVECOL-HVI [11]		0.31 – 16.7
Rockwell Automation PowerFlex 6000 [12]		0.32 – 5.6
Alstom VDM6000 [6]	Flying Capacitor (FC)	0.5 – 9

Although many different MV drive topologies exist in the market, the basic structure of MV drives can be simplified, as illustrated in Fig. 1.1.

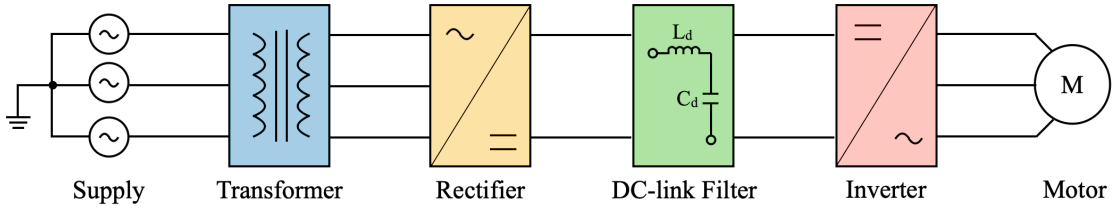

Fig. 1.1. Basic Structure of a MV Drive [3]

Based on the topology and the system requirements of the motor drive, filters may be added on the supply or motor side. The basic components of the MV drive are given as follows:

- **Transformer:** Often used for reduction in line current distortion.
- **Rectifier:** convert the supply voltage to a DC voltage.
- **DC-link Filter:** Used to provide a stable DC voltage.
- **Inverter:** Used to convert the DC voltage to controlled AC voltage.

From the design perspective, there are four main technical requirement and challenges that directly corresponds to the topologies and components employed in the general structure of the MV Drive. These technical requirements and challenges can be listed [3]:

1) Line-side Requirements

- Compliance with grid connection standards.
- High input power factor.
- Suppression of LC resonance if filters are used.

2) Motor-side Challenges

- Minimization of dv/dt and common mode voltage stress.
- Low harmonic distortion.
- Suppression of LC resonance if filters are used.

3) Switching Device Constraints

- Adequate switching frequency to balance between minimizing switching power loss and waveform distortion.
- Voltage equalization when using series-connected devices.

4) Drive System Requirements

- High efficiency, reliability, and fault-tolerance.
- Low cost, size, and complexity.

The line-side requirement for an MV motor is commonly met with multi-pulse rectifiers. A single diode rectifier can convert the three-phase AC supply voltage to a DC voltage. However, a diode rectifier will introduce line current distortion that affects the ability to fulfill the line-side requirement. A phase-shifting transformer with multiple

secondary windings coupled with a set of diode rectifiers can be utilized to provide a single DC source or multiple isolated DC sources and ensure that the line-side requirements are met [3]. Fig. 1.2 illustrates the different configurations of multi-pulse rectifiers.

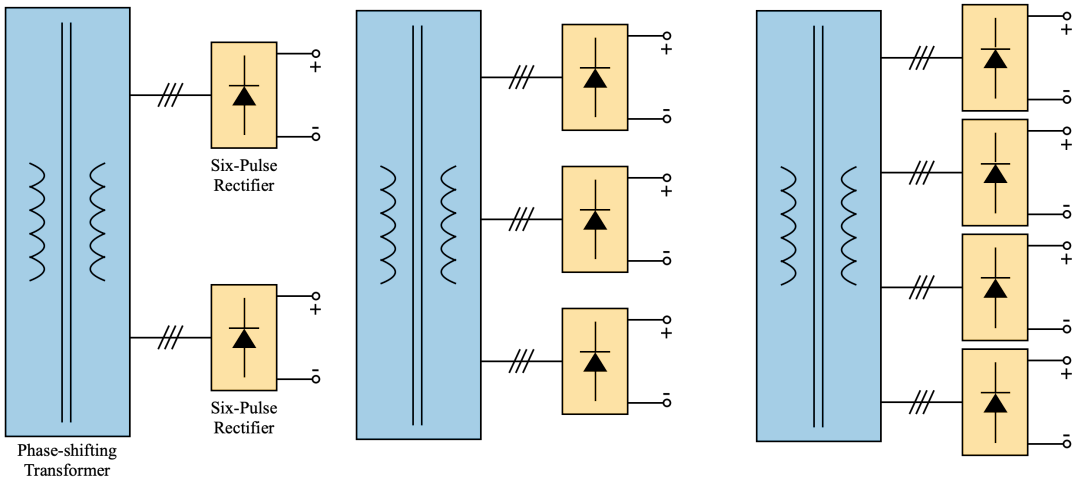

(a) 12-pulse Rectifier (b) 18-pulse Rectifier (c) 24-pulse Rectifier

Fig. 1.2. Multi-pulse Diode Rectifiers [3]

The other technical requirements and challenges rely on the inverter used in an MV drive. Different inverter topologies provide different benefits and drawbacks that need to be considered. Fig. 1.3 shows four topologies seen in Table 1.1.

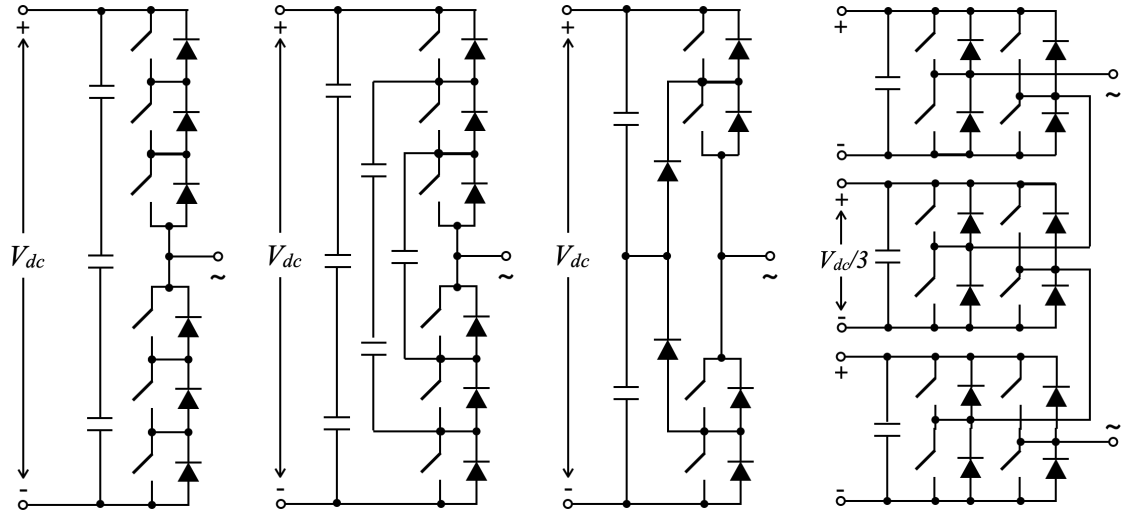

(a) 2L-VSI (b) NPC Inverter (c) FC Inverter (d) CHB Inverter

Fig. 1.3. MV Inverter Topologies [3]

Based on the four topologies shown in Fig. 1.3, the inverter topologies are categorized by their output voltage levels. The 2L-VSI, in Fig 1.3(a), is only able to output two voltage levels, while the NPC, FC, and CHB inverters, in Fig 1.3(b)-(d), can output multiple voltage levels. The inverters that output multiple voltage levels are referred to as Multi-Level Inverters (MLIs), and Fig. 1.4 shows the output line voltage of the inverters.

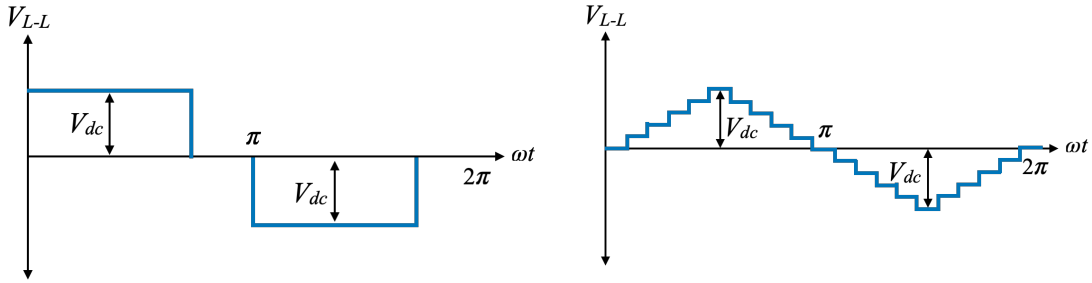

(a) Output Line Voltage of 2L-VSI (b) Output Line Voltage of MLIs

Fig. 1.4. Output Line Voltage of MV inverters

The output voltage of the 2L-VSI is synthesized by switching between two voltage levels. The significant voltage difference between output voltage levels results in high dv/dt and common mode voltage. In addition, as the switching devices need to withstand the entire DC-link voltage, switching devices need to be connected in series in medium voltage applications. The output voltage of the MLIs consists of multiple small voltage levels which synthesize the desired output voltage. The MLI topologies are designed such that the DC-link voltage is split into multiple small voltage levels that are added to the output voltage. Multiple output voltage levels allow the MLIs to have significantly lower dv/dt and common mode voltage, no devices connected in series, and much lower switching frequency due to its improvement in harmonic distortion [3]. Based on an MV drive's technical requirements and challenges, MLIs are much more suitable for medium voltage and high voltage applications.

1.2 Motivation

The Cascaded H-Bridge inverter is a popular MLI as the CHB has a modular structure. As seen in Fig. 1.3(d), three separate modules called power cells are connected in series to provide a controlled AC voltage. Each power cell contributes to the total number of voltage levels that the CHB inverter can provide. An additional power cell can be added to provide more voltage levels or a higher output voltage. The unique design of the CHB offers a few advantages compared to the other MLI:

- Scalable system that accommodates multiple power ratings by changing the number of power cells [3], [13]
- Easy maintenance due to its modular power cell structure [13]
- No capacitor voltage is balancing required [13]
- Fault-tolerant due to its high redundancy states and modularity [13]

With a conventional MV CHB drive, each power cells utilize a diode rectifier to provide the necessary DC voltage. However, as a diode rectifier only allows unidirectional power flow, the conventional MV CHB drive can incur excess energy loss in certain applications. In applications such as downhill conveyors, cranes, and hoists, the load can overhaul the motor causing the motor to regenerate energy back to the CHB MV drive [5]. The regenerated energy from the motor must be dissipated safely as the DC-bus capacitors are energy storage devices and will cause the DC voltage of the power cell to increase [14]. A braking chopper circuit can be used to dissipate the regenerated energy [14]. However, a braking chopper circuit dissipates the energy with a resistor as heat, making the conventional MV CHB drive inefficient in this mode of operation.

A regenerative power cell has been introduced to allow bidirectional power flow from the grid and the motor. Instead of utilizing diode rectifiers to convert the three-phase input voltage to the required DC voltage, a 2L-VSI is used [15]-[17]. The non-regenerative and regenerative CHB power cell is shown in Fig. 1.5.

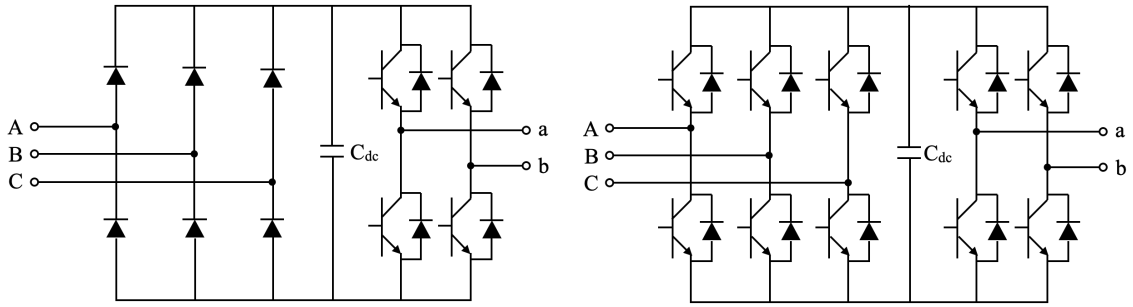

(a) Non-Regenerative CHB Power Cell (b) Regenerative CHB Power Cell

Fig. 1.5. Conventional Non-Regenerative and Regenerative CHB Power Cells [15]-[17]

The regenerative power cell allows the energy to return to the grid rather than dissipate the energy with a resistor. The regenerative power cell addresses the inefficiencies apparent in the conventional non-regenerative CHB drive. However, the regenerative power cell requires a significant increase in switching devices, leading to a more complex system, higher cost, and higher failure probability.

The motivation of this thesis work is to provide an economical version of a regenerative CHB drive that can address the significant increase in switching devices seen in the traditional regenerative power cell. This work introduces two new reduced switch-count regenerative power cells for a CHB drive. The switch count reduction in both power cell topologies proposes challenges that will be analyzed and addressed in the thesis. The proposed analysis and solutions will be verified through simulation using MATLAB/Simulink and experimentally through a scaled-down single power cell setup.

1.3 Contributions

The contributions of the presented work can be outlined as follows:

- A comprehensive review of the existing reduced switch-count regenerative power cells for a CHB drive. Each topology's structure, performance, and control system are investigated. A comparison of the existing reduced switch-count regenerative power cells is provided to identify the benefit and drawbacks of each topology.
- Proposal of a new reduced switch-count regenerative CHB power cell (Topology I) based on a Four Switch Three Phase Inverter and an H-Bridge with a shared inverter leg. The proposed power cell reduces the number of switching devices per power cell by four. A thorough analysis of the new configurations and challenges is provided.
- Proposal of a new reduced switch-count regenerative CHB power cell (Topology II) based on a Four Switch Three Phase Inverter and a half-bridge inverter. The proposed power cell reduces the number of switching devices per power cell by four. The analysis of control, performance, and challenges are provided.
- Proposal of a control scheme to address the current unbalance for the proposed reduced switch-count regenerative power cell (Topology II).
- Proposal of a triplen harmonic elimination method for the reduced switch-count regenerative power cell (Topology II).
- Proposal of two carrier shifting techniques to eliminate the carrier and sideband harmonics (Topology II).
- Simulation studies of the two new reduced switch-count regenerative power cells in a regenerative CHB motor drive under motoring and regenerative mode of operation.

- Experimental implementation and validation of the conventional regenerative CHB power cell, three-phase Reduced Switch-Count Cell, and the new proposed reduced switch-count regenerative power cell (Topology II) using a scaled-down single-cell setup.

1.4 Thesis Structure

The thesis is structured as follows:

Chapter 2 reviews the traditional non-regenerative and regenerative CHB motor drives. This chapter aims to review and provide the knowledge to understand the work.

Chapter 3 provides a comprehensive review of the existing reduced switch-count regenerative power cell configurations for a CHB motor drive. The structure, control, operation, and challenges are reviewed in detail. This chapter aims to provide the current state of existing reduced switch-count regenerative power cell designs, the knowledge of how the reduction is achieved, and the challenges that arise.

Chapter 4 analyzes the first proposed reduced switch-count regenerative power cell based on a Four-Switch Three Phase Inverter (FSTPI) Active Front End (AFE) and an H-Bridge inverter. The structure, operation, modulation techniques, and challenges are presented. Simulation studies to verify the analysis will be included in this chapter.

Chapter 5 analyzes the second proposed reduced switch-count regenerative power cell based on an FSTPI AFE and a half-bridge inverter. The structure, operation, modulation techniques, and challenges are presented. Methods to address the challenges identified and the simulation studies of a CHB using the proposed power cell are included in this chapter.

Chapter 6 provides the experimental result of the conventional, three-phase reduced switch-count and the second proposed reduced switch-count regenerative power cell. The operational differences and validation of the simulation studies will be provided in this chapter.

The last chapter, chapter 7, concludes the thesis. This chapter will summarize the work, conclusions, and future work.

Chapter 2

Cascaded H-Bridge (CHB) Medium-Voltage (MV) Drives

2.1 Conventional Non-Regenerative CHB MV Drive

2.1.1 Structure

The basic structure of a conventional non-regenerative CHB MV drive and its power cell is shown in Fig. 2.1. In a CHB MLI, a modular component called power cells are connected in series. The power cells in a CHB drive operate at a significantly lower than the rated voltage of the CHB drive, and the total output voltage of the CHB corresponds to the sum of the power cell output voltages connected in series [3].

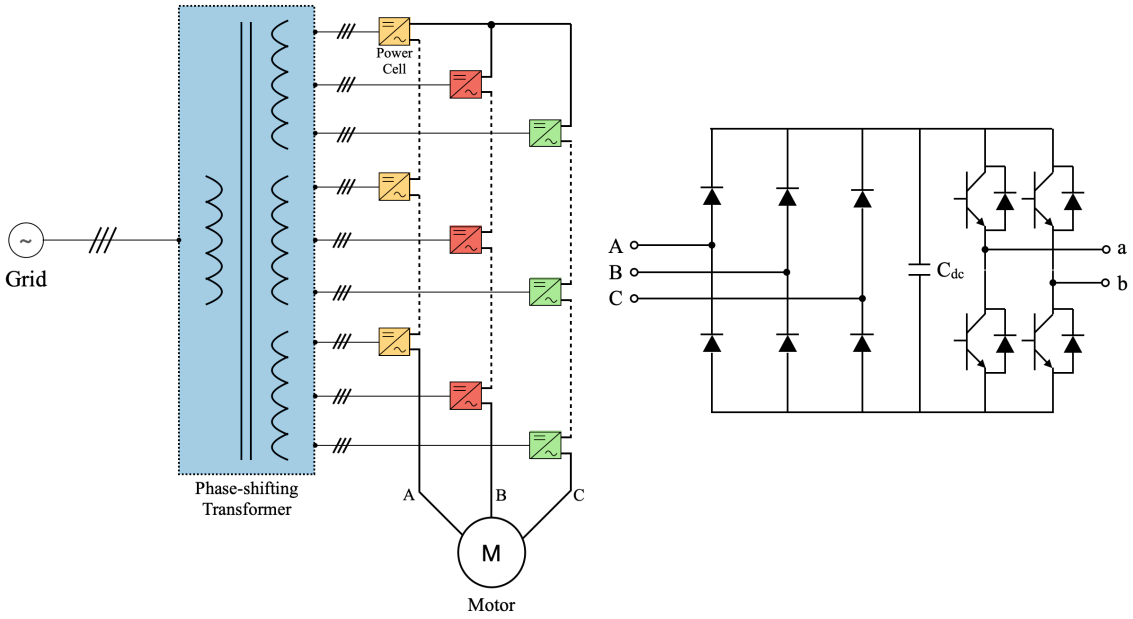

(a) Block Diagram of a CHB MV Drive. (b) Typical Non-Regenerative Power Cell.

Fig. 2.1. CHB MV Drive.

Each power cell consists of a diode rectifier, DC-bus capacitors, and an H-Bridge inverter. The function of each component in a power cell is as follows:

- **Diode Rectifier:** Converts the three-phase input voltage to DC voltage
- **DC-bus Capacitor:** Reduce the voltage ripples caused by the rectifier and inverter
- **H-Bridge inverter:** Provide controlled AC voltage to the output

The series connection of the power cells in a CHB topology provides two features: multilevel and high output voltage using low voltage switching devices.

2.1.2 Grid Connection

The structure of the CHB motor drive requires each power cell to have an isolated DC voltage source. The six-pulse diode rectifier in each power cell converts the three-phase voltages to rectified DC voltage. The rectified DC voltage from the diode rectifier contains oscillations, and as a result, a DC-link capacitor is present in each power cell to provide a smooth DC voltage. The average power cell DC-link voltage is expressed by (2.1) [3].

$$V_{dc} = \frac{3\sqrt{2}}{\pi} V_{LL} \tag{2.1}$$

Where V_{LL} represents the input line-to-line voltage from the secondary side of the transformer.

The uncontrolled nature of the diode rectifier confines the average DC-link voltage to the input line-to-line voltage. In the conventional CHB, the secondary voltage of the phase-shifting transformer can be used to adjust the DC-link voltage. Additionally, the phase-shifting transformer provides the following purposes [18]:

- Isolated input voltages for each power cell
- Reduction of grid voltages to an appropriate cell input voltage
- Mitigation of the common mode voltage stress
- Cancellation of low order harmonics produced by the diode rectifier

2.1.3 Motor Side Modulation

The conventional non-regenerative power cell is constructed with a single-phase H-Bridge inverter shown in Fig 2.2.

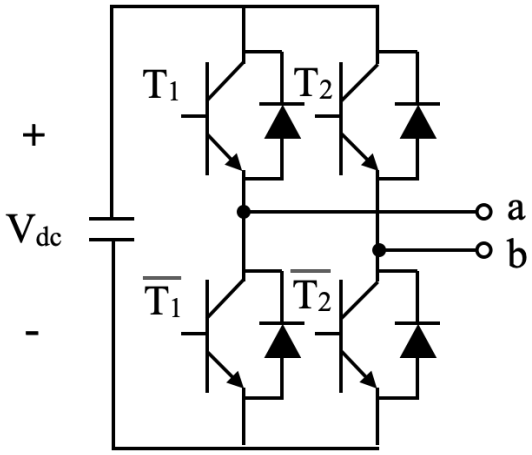

Fig. 2.2. Single-phase H-Bridge Inverter.

Space Vector Modulation (SVM) [19] or Sinusoidal Pulse-Width Modulation (SPWM) [3] can be used to control the single-phase H-Bridge Inverter in a CHB. However, SPWM is the most common modulation technique. Two variants of SPWM, bipolar and unipolar, exist. In both types of SPWM, the bottom switches, $\overline{T_1}$ and $\overline{T_2}$, are complementary to the upper switches, T_1 and T_2. Therefore, only two independent gate signals must be generated [3].

Bipolar modulation utilizes a single sinusoidal modulating wave, v_m, with a triangular carrier, v_{cr}, to generate the gating signals for the two upper switches. In bipolar modulation, the upper switch T_2 is complimentary to T_1, and the bottom switches complement the upper switches. Fig 2.3 illustrates the implementation of the bipolar SPWM method and its resulting output voltage.

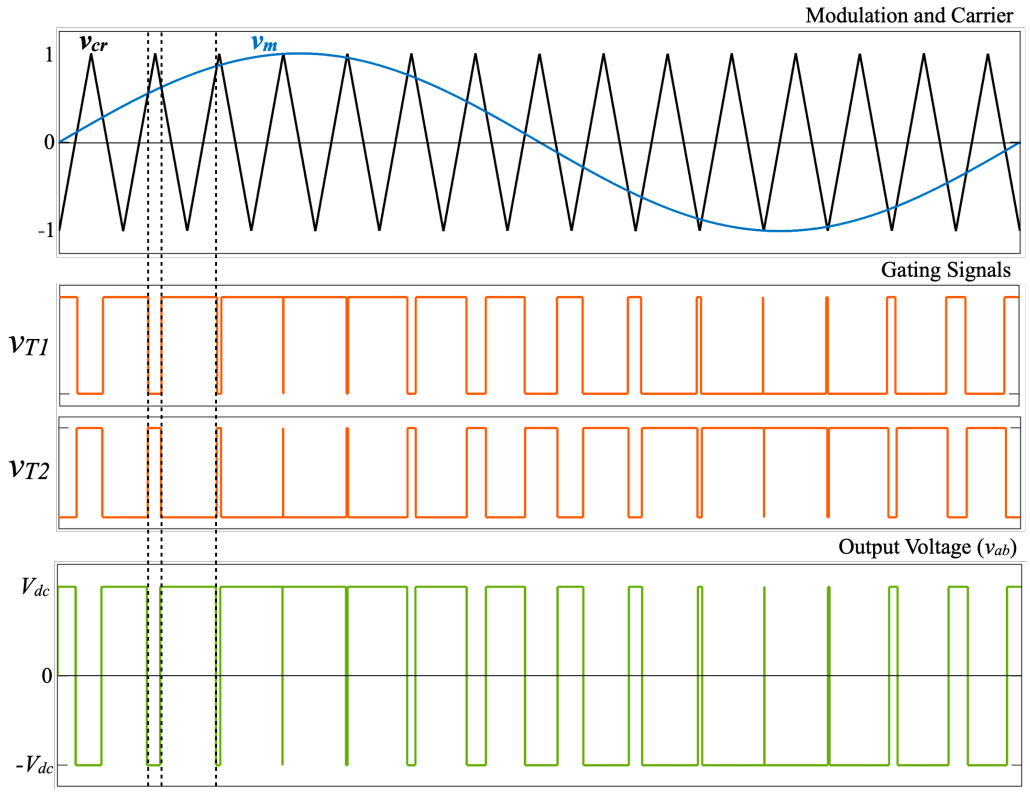

Fig. 2.3. Bipolar Modulation Technique

Unipolar modulation compares a sinusoidal modulating wave, v_m, with two triangular carriers, v_{cr+} and v_{cr-}, to generate the necessary gating signals for the two upper switches. The gating signal for switch T_1 is determined by the modulating wave, v_m, and triangular carrier, v_{cr+}. In contrast, the gating signal for switch T_2 is determined by the modulating wave, v_m, and triangular carrier, v_{cr-} [3]. Fig. 2.4 illustrates the implementation of the unipolar SPWM method and its resulting output voltage.

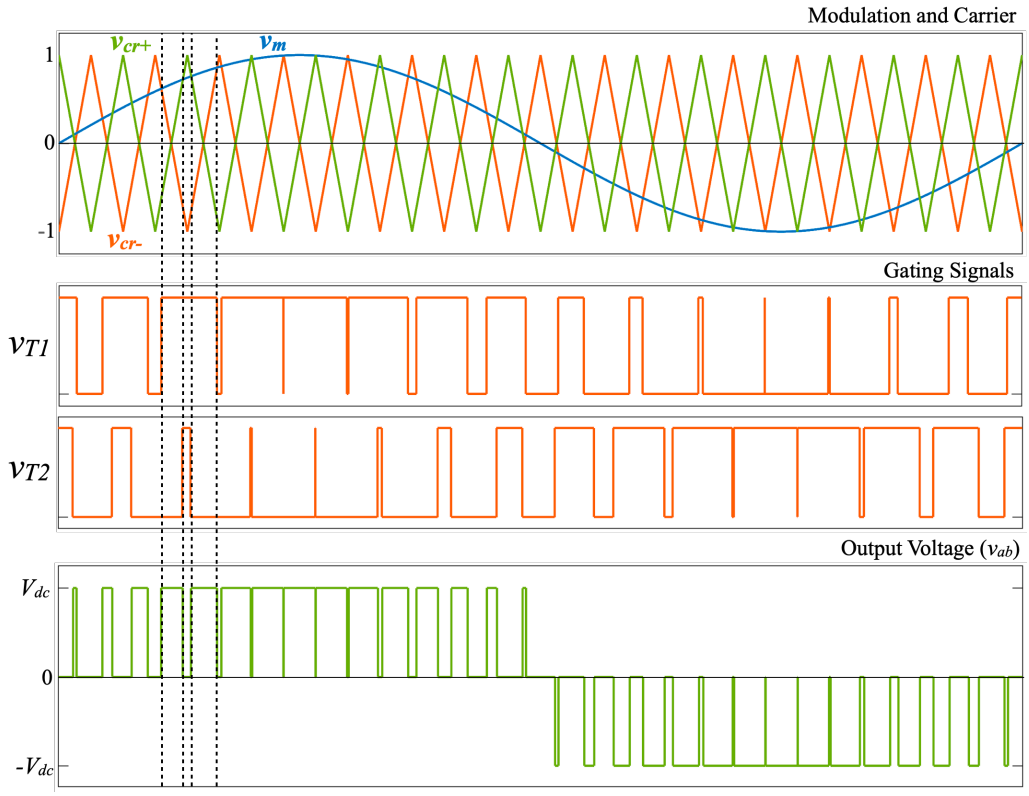

Fig. 2.4. Unipolar Modulation Technique

The main difference between the two types of SPWM is that the bipolar SPWM output voltage switches between $\pm V_{dc}$ while the unipolar SPWM output voltage switches between zero and $\pm V_{dc}$. Unipolar SPWM modulation is preferable because the additional voltage level reduces the output total harmonic distortion (THD). With multiple single-phase H-Bridge inverters connected in series, such as a typical CHB, the phase angles of the triangular carriers are shifted to provide multiple voltage levels. The angle shift in the triangular carriers and multiple voltage levels provide lower THD, Electromagnetic interference, and higher effective switching frequency [3].

For N number of cells, the relationship to the number of line-to-neutral output voltage levels, m, is expressed by (2.1) [3].

$$m = (2N + 1) \tag{2.1}$$

The number of triangular carriers, m_c, with unipolar SPWM is defined by (2.2) [3].

$$m_c = (m - 1) \tag{2.2}$$

The necessary triangular carrier phase shift between the series-connected power cells, based on (2.2), is expressed by (2.3) [3].

$$\theta_{shift} = \frac{360°}{m_c} \tag{2.3}$$

The maximum fundamental RMS voltage, $V_{AB1,\ max}$, in relation to the number of cells utilizing SPWM modulation, is expressed by (2.4) [3].

$$V_{AB1,max} = 1.224 \cdot N \cdot V_{dc} \tag{2.4}$$

Where V_{dc} represents the DC-bus voltage of a power cell.

Based on (2.1) and (2.4), the change in DC voltage and the number of power cells in a CHB drive enables the flexibility to tune three important aspects: desired output voltage, harmonic output content, and cost of the CHB drive. In practice, the utilization of flexibility can be seen in Table. 2.1.

TABLE 2.1. DC VOLTAGE AND TOTAL # OF POWER CELLS OF A CHB [20]

Output Voltage (kV)	DC-bus Voltage (V)	Total # of Power Cells
2.3 / 2.4	650	9
3 / 3.3	920	9
4 / 4.16	848	12
6	976	15
6.3 / 6.6	920	18
6.9	976	18
10	976	24
11	976	27

2.2 Conventional Regenerative CHB MV Drive

In industrial applications such as downhill conveyers, cranes, and hoists, the load can overhaul the motors and operate in braking or regenerative mode [5]. In the ore mining industry, a downhill conveyer transporting ores may generate up to several megawatts of power that cannot be recovered with a traditional non-regenerative CHB drive [21]. Furthermore, utilizing a traditional non-regenerative CHB drive in a braking or regenerative mode of operation can introduce overvoltage of the DC-bus. The energy flowing back into the power cell cannot be dissipated without additional circuitry, such as a braking chopper. A braking chopper circuit dissipates the excess energy through a resistor, mitigating the risk of DC-bus overvoltage [14]. However, this introduces inefficiencies as the excess energy would be wasted as heat.

2.2.1 Structure

A regenerative CHB power cell has been introduced in [15]-[17] to address the unidirectional power capability of the traditional non-regenerative CHB drive. Fig. 2.5 shows the regenerative power cell.

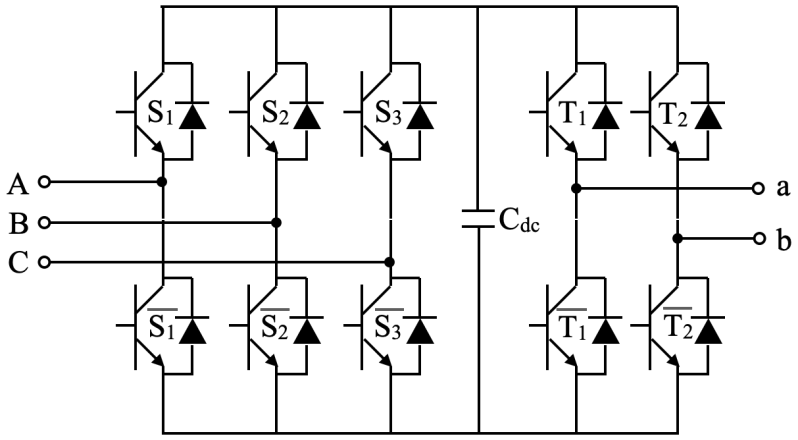

Fig. 2.5. 10-Switch Regenerative Power Cell for CHB [15]-[17]

In the regenerative CHB power cell, the six-pulse diode rectifier is replaced with a 2L-VSI to allow bidirectional power flow between the grid and the load. The replacement of the diode rectifier with a 2L-VSI allows the regenerative power cell to achieve the following [15]-[17]:

- Bi-directional power flow between the grid and the load
- Reactive power compensation
- DC bus voltage regulation in all modes of operation
- DC bus capacitor ripple reduction
- Better harmonic profile, which enables the use of a simpler transformer without phase-shifting

Due to the switching devices on the grid side, the regenerative power cell's rectification stage is referred to as Active Front End (AFE). In contrast, the non-regenerative power cell is called Diode Front End (DFE).

2.2.2 Grid and Motor Side Modulation

The motor side inverter remains unchanged with a conventional regenerative CHB power cell. Therefore, the same modulation and control technique is used on the motor side. On the grid side, a new control scheme must be implemented to control the 2L-VSI. Fig. 2.6 shows the 2L-VSI utilized in the conventional regenerative power cell.

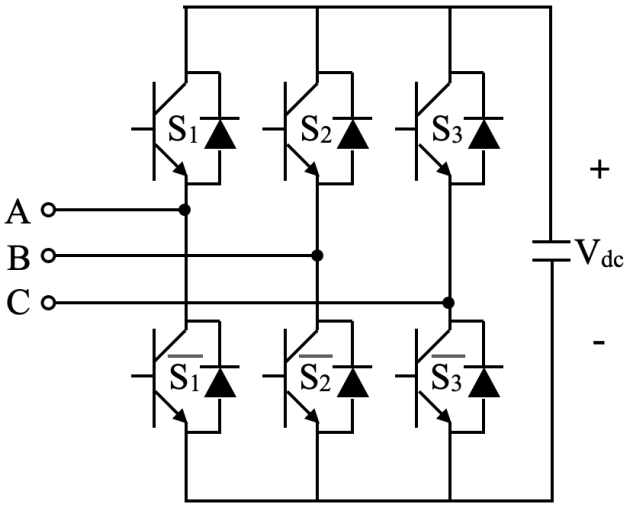

Fig. 2.6. 2L-VSI for Regenerative CHB Power Cell

The 2L-VSI utilizes only two switches per phase to generate a three-phase output voltage. As a result, the bipolar modulation technique synthesizes the necessary output voltage. The carrier shifting technique can be used with the 2L-VSI between different power cells.

2.2.3 AFE Side Control

In a regenerative CHB power cell, the grid side inverter replaces the function of a diode rectifier to enable bidirectional power flow. A typical control scheme for the 2L-VSI, based on a Voltage Oriented Control (VOC), is shown in Fig 2.7 [16].

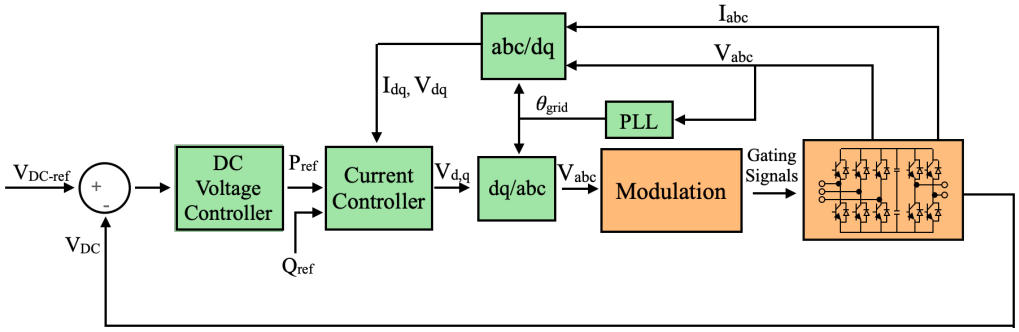

Fig. 2.7. 2L-VSI AFE Control Block Diagram [16]

The function of the control scheme can be summarized as follows:

1) Regulate DC voltage by providing the current controller with a reference active power value (P_{ref})

2) Control the reactive power by the provided reference reactive power value (Q_{ref})

3) Provide modulation signal synchronized with the phase angle of the grid (θ_{grid})

The AFE control scheme utilizes a *d-q* rotating reference frame to control the active and reactive power while maintaining synchronization with the grid. Using a *d-q* reference frame allows the conversion of a three-phase time-varying AC signal to a two-phase, direct (*d*) and quadrature (*q*) signals that rotate at the same angular frequency as the grid. The direct and quadrature component of the *d-q* rotating frame effectively represents any three-phase AC variables into two DC variables, providing a powerful tool to simplify and analyze sophisticated control schemes. The transformation of the three-phase (*abc*) variables to two-phase (*d-q*) variables can be performed by (2.6) [3].

$$\begin{bmatrix} x_d \\ x_q \end{bmatrix} = \frac{2}{3}\begin{bmatrix} \cos\theta & \cos(\theta - 2\pi/3) & \cos(\theta - 4\pi/3) \\ -\sin\theta & -\sin(\theta - 2\pi/3) & -\sin(\theta - 4\pi/3) \end{bmatrix}\begin{bmatrix} x_a \\ x_b \\ x_c \end{bmatrix} \tag{2.6}$$

Conversely, the two-phase (d-q) variables are converted to three-phase (abc) variables by performing (2.7) [3].

$$\begin{bmatrix} x_a \\ x_b \\ x_c \end{bmatrix} = \frac{2}{3} \begin{bmatrix} \cos\theta & -\sin\theta \\ \cos(\theta - 2\pi/3) & -\sin(\theta - 2\pi/3) \\ \cos(\theta - 4\pi/3) & -\sin(\theta - 4\pi/3) \end{bmatrix} \begin{bmatrix} x_d \\ x_q \end{bmatrix} \tag{2.7}$$

Where x represents the current or voltage and θ represent the angular displacement between the a-axis and d-axis of the three-phase and two-phase reference frame, respectively.

In the AFE control scheme seen in Fig. 2.10, the DC-bus voltage is regulated by the DC voltage controller. The DC voltage controller compares the actual DC-bus voltage with the reference DC voltage provided to generate the reference active power (P_{ref}) for the current controller. By adjusting the reference active power provided to the current controller, the DC-bus voltage in the power cell can be increased or decreased. The reference reactive power (Q_{ref}) is typically set to zero for unity power operation.

The current controller regulates the modulating signal to control the active and reactive power of the system. In a balanced three-phase system, the active (P) and reactive (Q) powers in a d-q frame can be expressed as (2.8) [16].

$$\begin{aligned} P &= \frac{3}{2}(v_d i_d + v_q i_q) \\ Q &= \frac{3}{2}(v_q i_d - v_d i_q) \end{aligned} \tag{2.8}$$

Where v_d and v_q are the d-q components of the grid voltage, and i_d and i_q are the d-q components of the cell input current.

The grid voltage is represented as (2.9).

$$V_A = V\cos\omega t$$
$$V_B = V\cos\left(\omega t - \frac{2\pi}{3}\right) \quad (2.9)$$
$$V_C = V\cos\left(\omega t + \frac{2\pi}{3}\right)$$

Where V_A, V_B, and V_C represent the three-phase grid voltages, V represents the magnitude of the grid voltage, and ω represents the angular frequency of the grid voltage.

The grid voltage in (2.9) is represented in cosine terms as aligning the *d-q* reference frame 90° from phase A allows the quadrature component to equal zero when transformation property (2.6) is used. With the quadrature component of voltage equal to zero and (2.8), the active and reactive power is controlled through i_d and i_q. The AFE current controller tracks the *d-q* cell input current to match the reference currents and outputs a modulation signal in a *d-q* frame as v_d and v_q. The resulting modulation signal is transformed from the *d-q* reference frame to *abc* frame through (2.7), and the resulting three-phase AC voltage is sent to the modulation scheme to generate the gating signal for the 2L-VSI. The current controller and the transformation between *d-q* and *abc* frame require a grid angle estimate. As a result, a phase-locked loop (PLL) is required in this control scheme.

2.2.4 Challenges

While the regenerative CHB drive addresses concerns regarding regenerated energy, there are many challenges that the regenerative topology introduces when compared with its non-regenerative topology. The challenges can be categorized as follows:

1) Increase in cost and size

- The conventional regenerative CHB power cell requires ten switching devices.
- The addition of the grid side inverter introduces additional power losses, requiring an advanced heatsink design.
- The number of gate drivers required for the switching devices increases as the regenerative power cell requires six more switching devices than the non-regenerative power cell.

2) Complexity

- The additional gate drivers increase the complexity of the control hardware.
- The AFE control scheme is much more complex to implement than utilizing uncontrolled diode rectifiers.
- With the increase in switching devices, the probability of power device failure increases.

2.3 Summary

The review of the conventional non-regenerative and regenerative CHB motor drives provides the necessary knowledge for the work in this thesis. The structure, modulation, and control techniques are discussed. The benefits of the conventional regenerative CHB motor drive and the regenerated energy concerns are demonstrated through the analysis of the control technique. The drawbacks of implementing the conventional regenerative CHB motor drives are listed.

The introduction of the regenerative power cell demonstrates the overwhelming benefits of utilizing an inverter in the rectification stage of the CHB drive, and the drawbacks reinforce the importance of researching economical versions of the regenerative CHB as switch-count reduction address all the challenges identified.

Chapter 3

Existing Reduced Switch-Count Regenerative CHB Power Cells

3.1 Introduction

The conventional regenerative CHB MV drive introduces many challenges due to its increase in complexity, size, and cost. The gain in the number of switching devices, especially with CHB MV drives with a high power cell count, can dramatically increase these challenges. The research in switch-count reduction of the regenerative CHB drive has been an attractive topic for developing more practical and cost-effective versions of a regenerative CHB [22]-[27].

Many viable reduced switch-count CHB power cells have been proposed [22]-[27] and are listed as follows:

- H-Bridge Input H-Bridge (H-H) Power Cell [22].
- Semi-Reduced Power Cell [23], [24].
- Reduced Power Cell [25].
- Reduced Switch-Count Regenerative Cell [27].

Although each existing reduced switch-count CHB power cell offers a unique design, the reduced switch-count power cells can be categorized into two classifications, as shown in Fig 3.1.

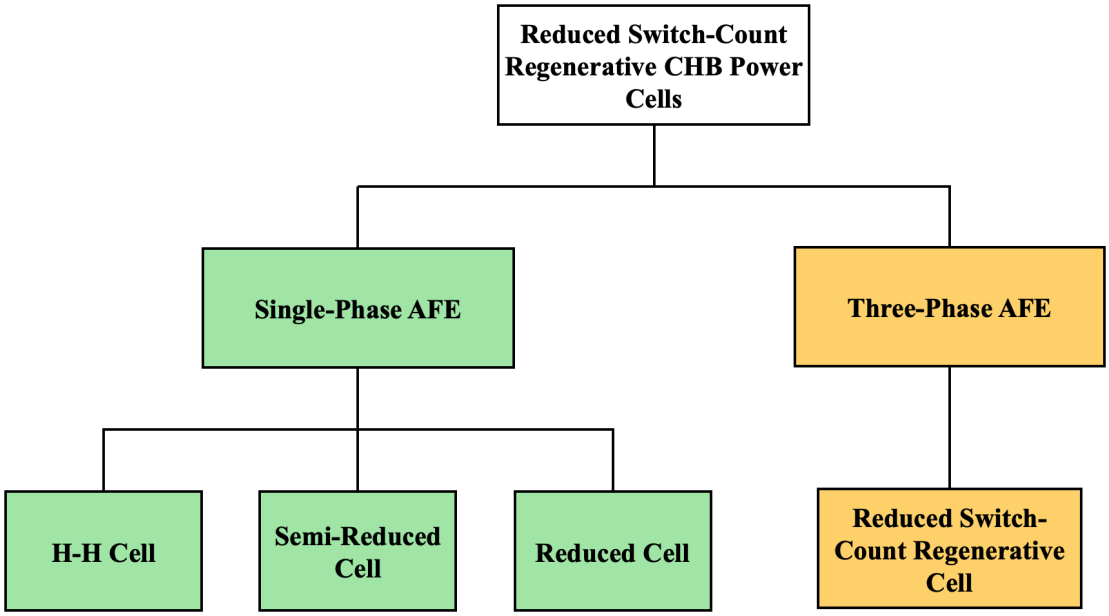

Fig. 3.1. Classification of Reduced Switch-Count Power Cells

Compared to the conventional regenerative CHB power cell, the H-H, Semi-Reduced, and Reduced power cell replaces the grid side three-phase AFE inverter with a single-phase AFE inverter. The Reduced Switch-Count Regenerative Cell maintains a three-phase AFE

inverter. As the conventional non-regenerative and regenerative CHB power cell utilize a three-phase grid interface, it is advantageous to use a three-phase AFE. Nonetheless, a reduced switch-count power cell that aims to replace the conventional regenerative power cell should satisfy the following aspects [22]-[27]:

- Good grid interface design for retrofitting existing power cells
- Easy and simple active front end (AFE) control scheme
- Minimum DC-link voltage ripples
- Compliance with the grid connection standards such as IEEE std. 519-2014
- Good dynamic performance
- Stability against grid side disturbances
- Reactive power compensation capability
- Reasonable voltage and current ratings for switching devices

3.2 Inverter Topologies for Reduced Switch-Count Power Cells

The existing reduced switch-count regenerative CHB power cells minimize the total number of switching devices by replacing the inverter topology in the power cell. Based on the reduced switch-count regenerative power cells proposed in [22]-[27], three alternative AFE inverters and one output inverter are identified.

3.2.1 Active Front End (AFE) Inverter Alternatives

a) Single-Phase Full-Bridge Controlled Rectifier

The single-phase full-bridge controlled rectifier as an alternative AFE inverter is proposed in [22], [26] and utilized in the H-H cell. The single-phase full-bridge rectifier

replaces the three-phase 2L-VSI in the conventional regenerative power cell and is shown in Fig. 3.2.

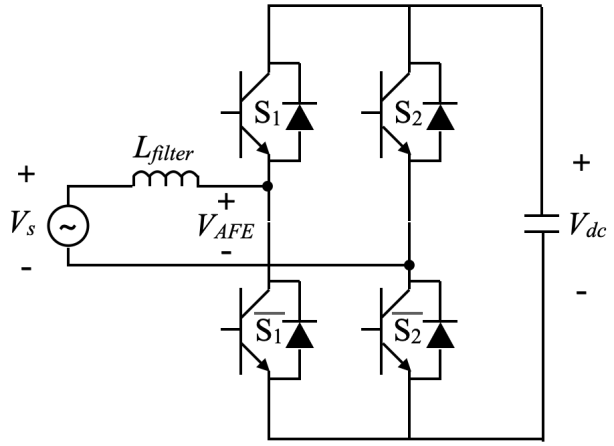

Fig. 3.2. Single-Phase Full-Bridge Controlled Rectifier

The switching states of the single-phase full-bridge controlled rectifier are illustrated in Table 3.1. The bottom switches, $\overline{S_1}$ and $\overline{S_2}$, complement the upper switches, S_1 and S_2.

TABLE 3.1. SINGLE-PHASE FULL-BRIDGE AFE SWITCHING STATES

Switching State	S_1	S_2	V_{AFE}
I	0	0	0
II	0	1	$-V_{dc}$
III	1	0	V_{dc}
IV	1	1	0

The inductor filter voltage, v_L, is expressed by (3.1) [22], [26].

$$v_L = L_{filter}\frac{di_s}{dt} = v_s - v_{AFE} = v_s - kV_{dc} \tag{3.1}$$

Where i_s is the cell input current, L_{filter} is the filter inductance, and k is the switching state constant.

Based on the switching states and inductor voltage, the behavior of the single-phase full-bridge controlled rectifier can be characterized. If the magnitude of the supply voltage is larger than the DC-link voltage, the cell input current cannot be controlled. If $V_{dc} > V_s$, the behavior of the cell input current based on the switching state is shown in Table 3.2 [22], [26].

TABLE 3.2. SINGLE-PHASE FULL-BRIDGE RECTIFIER AFE CHARACTERISTICS

Switching States	v_L	i_s	k
I & IV	Dependent on v_s	Dependent on v_s	0
II	Positive	Increasing	-1
III	Negative	Decreasing	1

As the switching states II and III can control the cell input current, the single-phase full-bridge controlled rectifier can operate as an AFE inverter. The AFE control scheme for the single-phase full-bridge controlled rectifier is shown in Fig 3.3.

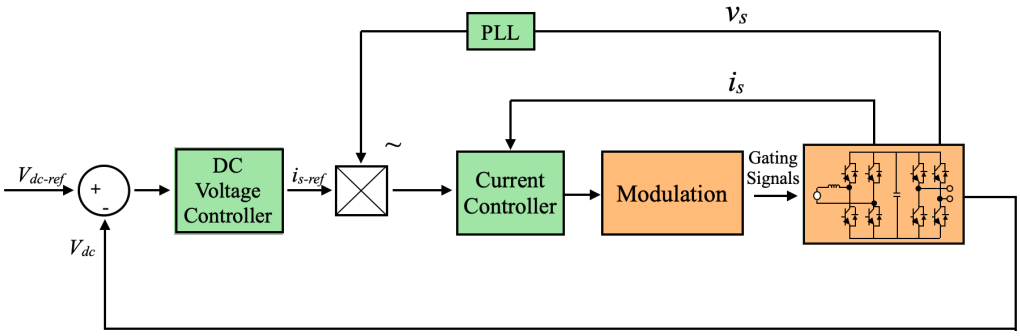

Fig. 3.3. AFE Control for Single-Phase Full-Bridge Controlled Rectifier [22], [26]

Compared to the conventional regenerative CHB power cell AFE control scheme, the single-phase full-bridge controlled rectifier proposes a similar control structure. The DC voltage and cell current control loops generate the necessary modulation signal. However, as a single-phase system cannot utilize a d-q reference frame, the controller requires a single-phase PLL and hysteresis or linear current controller [26].

b) Single-Phase Half-Bridge AFE Inverter

The single-phase half-bridge AFE inverter is utilized in the Semi-Reduced and Reduced regenerative CHB power cell. The half-bridge AFE inverter is shown in Fig. 3.4.

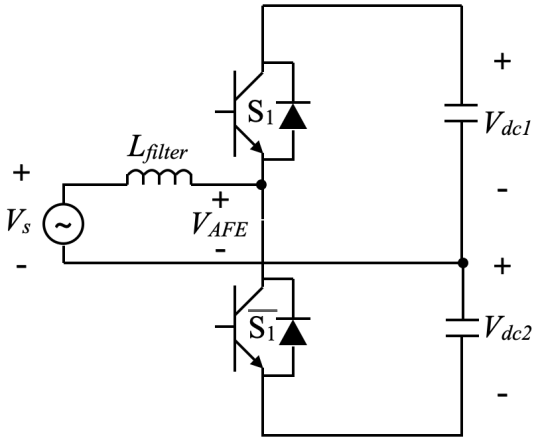

Fig. 3.4. Single-Phase Half-Bridge AFE Inverter

The switching states for the single-phase half-bridge AFE inverter are illustrated in Table 3.3. The bottom switch, $\overline{S_1}$, complements the upper switch, S_1.

TABLE 3.3. SINGLE-PHASE HALF-BRIDGE SWITCHING STATES

Switching States	S_1	V_{AFE}
I	1	$+V_{dc1}$
II	0	$-V_{dc2}$

As each switching state corresponds to the DC-link capacitor voltage, the inductor filter voltage, during state I, is expressed by (3.2) [23]-[25].

$$v_{L-I} = L_{filter}\frac{di_s}{dt} = v_s - v_{AFE} = v_s - V_{dc1} \tag{3.2}$$

The inductor filter voltage, during state II, is expressed by (3.3) [23]-[25].

$$v_{L-II} = L_{filter}\frac{di_s}{dt} = v_s - v_{AFE} = v_s + V_{dc2} \tag{3.3}$$

Based on Table 3.3, (3.2), and (3.3), the half-bridge AFE inverter is characterized by Table 3.4. With the half-bridge AFE inverter, both V_{dc1} and V_{dc2} must be higher than v_s to operate as an AFE inverter as the output voltage, V_{AFE}, is limited to the individual capacitor voltage [23]-[25].

TABLE 3.4. SINGLE-PHASE HALF-BRIDGE AFE INVERTER

Switching States	$\boldsymbol{v_L}$	$\boldsymbol{i_s}$
I	Negative	Decreasing
II	Positive	Increasing

As the capacitor midpoint is utilized in the half-bridge AFE inverter, the capacitor charging current must be considered. During state I, the capacitor charging current is expressed by (3.4) [23]-[25].

$$\begin{aligned} i_{c1} &= i_s - i_l \\ i_{c2} &= -i_l \end{aligned} \tag{3.4}$$

During state II, the capacitor charging current is expressed by (3.5) [23]-[25].

$$\begin{aligned} i_{c1} &= -i_l \\ i_{c2} &= -i_s - i_l \end{aligned} \tag{3.5}$$

Where i_{c1} and i_{c2} represent the upper and lower capacitors' current, i_s represents the cell input current, and i_l represents the input current to the load side inverter.

Based on (3.4) and (3.5), the charging and discharging conditions for the half-bridge AFE inverter are summarized in Table 3.5.

TABLE 3.5. HALF-BRIDGE AFE INVERTER CAPACITOR CHARGING CONDITIONS

Switching States	C_1	C_2
I	Charging: $(i_s - i_l) > 0$ Discharging: $(i_s - i_l) < 0$	Dependent on i_l
II	Dependent on i_l	Discharging: $(i_s + i_l) < 0$ Charging: $(i_s + i_l) > 0$

As the half-bridge AFE inverter operation is similar to the single-phase full-bridge AFE inverter, the control scheme from the full-bridge inverter can be used with the half-bridge inverter. However, due to the complexities of the capacitor charging conditions, the control scheme must be supplemented with a capacitor voltage balancing controller. The AFE control scheme for the half-bridge AFE inverter is shown in Fig. 3.5.

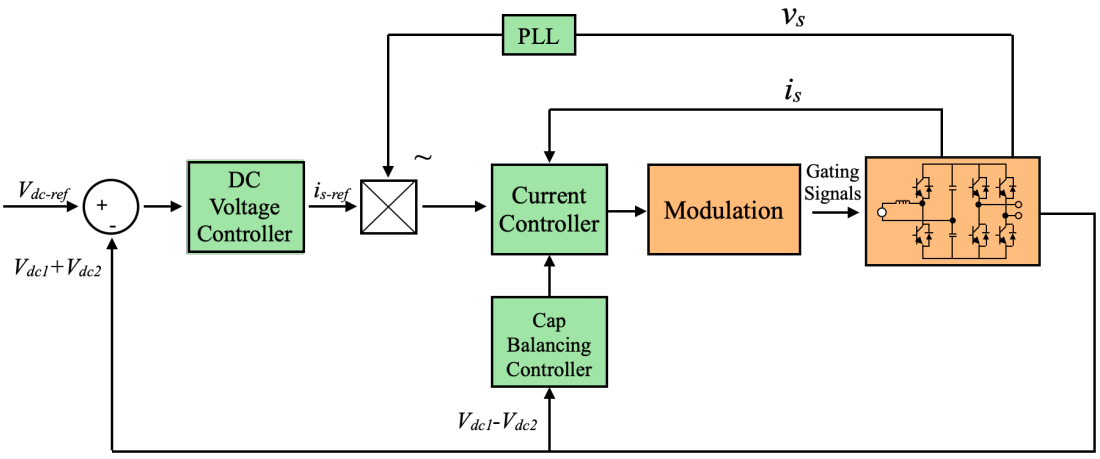

Fig. 3.5. AFE Control for Half-Bridge AFE Inverter [23]-[25]

c) Four-Switch Three-Phase Inverter AFE

The Four-Switch Three-Phase Inverter (FSTPI) AFE is proposed in [28] and is introduced with the three-phase Reduced Switch-Count CHB power cell [27]. The FSTPI AFE is shown in Fig 3.6.

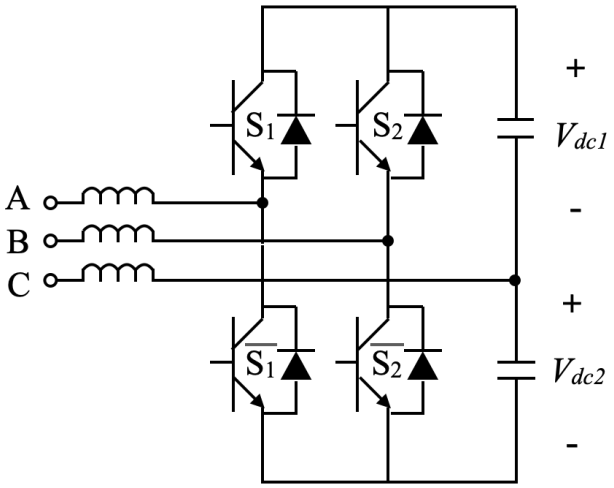

Fig. 3.6. FSTPI AFE [28]

The FSTPI AFE reduces the total number of switches by two compared to the 2L-VSI utilized in the conventional regenerative CHB drive. Out of the alternative AFE inverters proposed, the FSTPI AFE is unique due to its three-phase connection. Maintaining the three-phase interface with the grid allows using a three-phase transformer and three-phase grid filter, making the FSTPI AFE topology more suitable for retrofitting the conventional regenerative CHB power cell. The switching state for the FSTPI AFE is shown in Table 3.6. The bottom switches, $\overline{S_1}$ and $\overline{S_2}$, complement the upper switches, S_1 and S_2.

TABLE 3.6. FSTPI AFE SWITCHING STATES

Switching State		**Voltage Vector**		
S_1	S_2	**Vector**	**Magnitude**	**Angle**
0	0	V_1	$V_{dc}/3$	240°
0	1	V_2	$V_{dc}/\sqrt{3}$	150°
1	0	V_3	$V_{dc}/\sqrt{3}$	−30°
1	1	V_4	$V_{dc}/3$	60°

The resulting output voltage vector for the FSTPI AFE can be expressed by (3.6) [27], [28].

$$\bar{v} = \frac{2}{3}\left(S_1 \cdot V_{dc} + S_2 \cdot V_{dc} \cdot e^{i\frac{2\pi}{3}} + \frac{V_{dc}}{2} \cdot e^{-i\frac{2\pi}{3}}\right) \tag{3.6}$$

Table 3.6 and (3.6) demonstrate the difference in voltage vectors compared to a 2L-VSI. The voltage vectors for the 2L-VSI and the FSTPI are illustrated in Fig. 3.7(a) and (b).

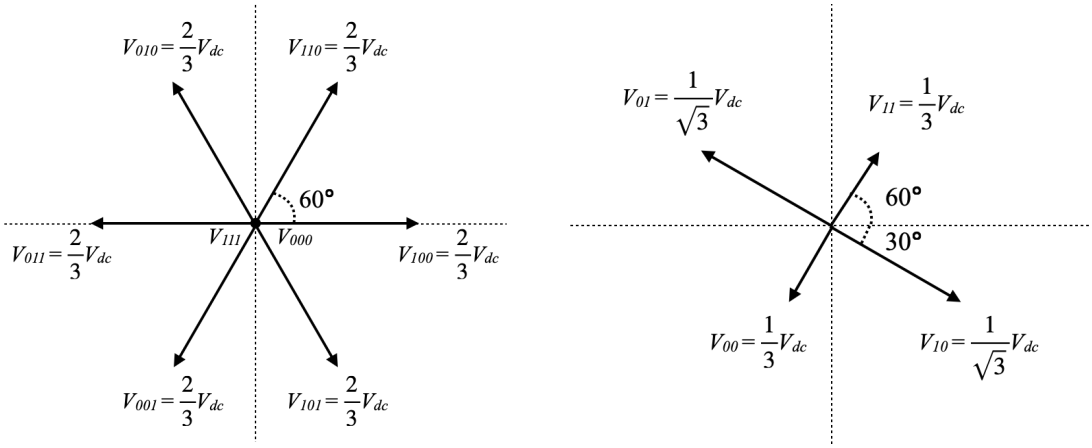

(a) 2L-VSI Voltage Vectors [3] (b) FSTPI Voltage Vectors [27], [28]

Fig. 3.7. Voltage Vectors of the Conventional AFE and FSTPI AFE

The difference in the switching states and the vectors demonstrate the following [27], [28]:

1) No zero-voltage vector exists for the FSTPI. The zero-voltage state is synthesized by applying two complementary voltage vectors for an equal time.

2) The output voltage is reduced by a factor of $\sqrt{3}$ compared with a 2L-VSI.

3) The reduction in switching states causes increased harmonic content on the output voltage, and a higher switching frequency should be considered.

The FSTPI synthesizes the three-phase output voltage with only four switches and one grid phase connected to the capacitor midpoint. Two modulation schemes can be used: Space Vector Modulation (SVM) and SPWM. Many implementations of SVM for the FSTPI are provided in the literature [29]-[32]. Due to the absence of a zero-voltage vector with an FSTPI, the SVM technique must be modified the synthesize the zero-voltage vector. Alternatively, the FSTPI can use a modified SPWM proposed in [27], [28]. The modified SPWM shifts the reference point to the capacitor midpoint to modulate the desired output voltage. The technique can be derived by an FSTPI connected to a three-phase load, as shown in Fig. 3.8.

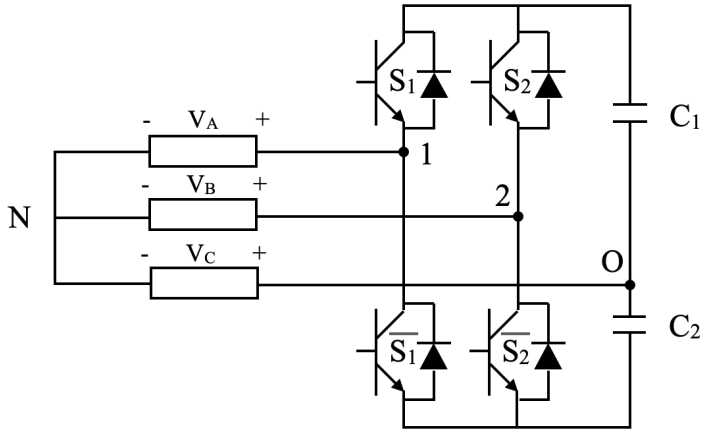

Fig. 3.8. FSTPI with a Three-Phase Load

The FSTPI with a three-phase load is characterized by (3.7) if point *O* is considered a reference point.

$$\begin{aligned} V_{AN} &= V_{1O} - V_{NO} \\ V_{BN} &= V_{2O} - V_{NO} \\ V_{CN} &= -V_{NO} \\ V_{NO} &= \frac{V_{1O} + V_{2O}}{3} = -V_{CN} \end{aligned} \tag{3.7}$$

If the desired output voltages are defined by V_{AN}, V_{BN}, and V_{CN}, the necessary modulating signal, V_{1O}, and V_{2O}, is expressed by (3.8).

$$\begin{aligned} V_{1O} &= V_{AN} - V_{CN} \\ V_{2O} &= V_{BN} - V_{CN} \end{aligned} \tag{3.8}$$

The desired output voltage for the FSTPI is defined as (3.9).

$$\begin{aligned} V_{AN} &= V\sin(\omega_{in}t) \\ V_{BN} &= V\sin\left(\omega_{in}t - \frac{2\pi}{3}\right) \\ V_{CN} &= V\sin\left(\omega_{in}t + \frac{2\pi}{3}\right) \end{aligned} \tag{3.9}$$

Where V represents the output voltage magnitude, and ω_{in} is the angular frequency of the FSTPI output voltage.

The modified modulation signal for the FSTPI is then expressed as (3.10) by using the findings from (3.8) [27], [28].

$$\begin{aligned} V_{10} &= V\sin(\omega_{in}t) - V\sin\left(\omega_{in}t + \frac{2\pi}{3}\right) = \sqrt{3}V\sin\left(\omega_{in}t - \frac{\pi}{6}\right) \\ V_{2O} &= V\sin\left(\omega_{in}t - \frac{2\pi}{3}\right) - V\sin\left(\omega_{in}t + \frac{2\pi}{3}\right) = \sqrt{3}V\sin\left(\omega_{in}t - \frac{\pi}{2}\right) \end{aligned} \tag{3.10}$$

As the resulting modulating signal is obtained by the difference of the two grid voltages, the implementation of the modified modulation signal is achieved by a simple modification to the existing three-phase SPWM modulator. Fig 3.9 illustrates the modified modulator used for the FSTPI [27], [28]. In the modified modulator, the reference signal of the FSTPI is divided by $\sqrt{3}$ to ensure that the modulation signal does not exceed the maximum amplitude of the triangular carrier signal.

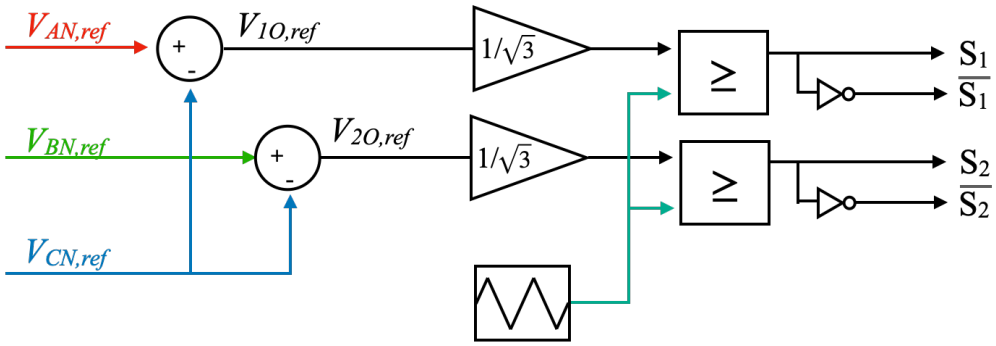

Fig. 3.9. Modified Modulator for FSTPI [27], [28]

As the FSTPI utilizes a capacitor midpoint, the charging and discharging conditions must be considered. However, the charging and discharging conditions should incorporate the whole power cell as the output inverter can impact the capacitor charging conditions. With the modified modulator, the FSTPI AFE can use the same control scheme, as the 2L-VSI as shown in Fig. 3.10.

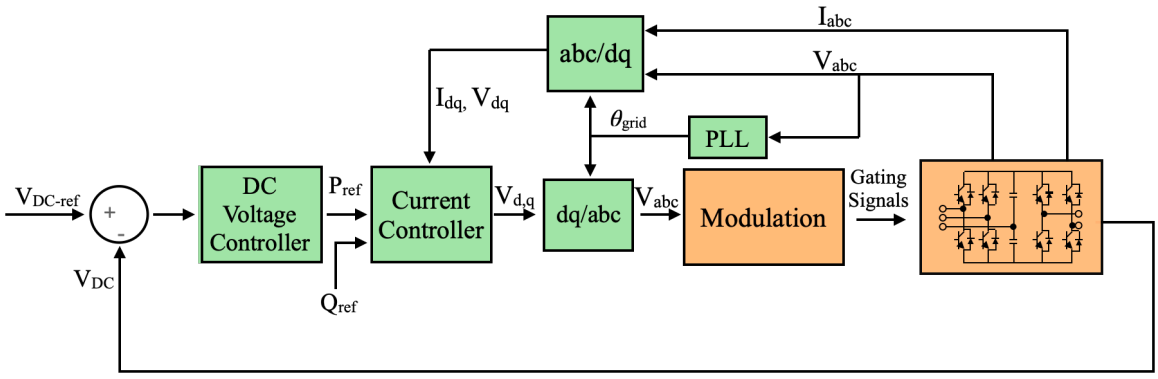

Fig. 3.10. AFE control Scheme for FSTPI AFE [27]

3.2.2 Output Inverter Alternatives

The single-phase half-bridge output inverter, as a replacement of the H-Bridge found in the conventional regenerative CHB power cell, is seen in the Reduced Cell [25]. The half-bridge output inverter can be seen in Fig 3.11.

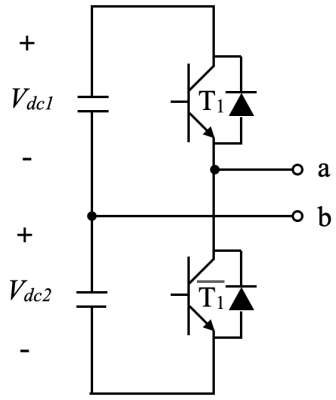

Fig. 3.11. Half-Bridge Output Inverter

The half-bridge output inverter achieves a total switch reduction of two compared to the conventional regenerative power cell. The half-bridge utilizes a capacitor midpoint to reduce the total number of switches, and its switching states are expressed in Table 3.7.

TABLE 3.7. SINGLE-PHASE HALF-BRIDGE OUTPUT INVERTER SWITCHING STATES

Switching States	S_1	V_{AFE}
I	1	$+V_{dc1}$
II	0	$-V_{dc2}$

Compared to an H-Bridge inverter, the following differences are identified:

- The maximum output voltage is reduced by a factor of 2
- Capacitor voltage balancing needs to be considered
- The voltage levels are reduced from three to two as the half-bridge does not have a zero-voltage state.

The half-bridge output inverter in a CHB configuration utilizes the same carrier phase shift to achieve multilevel output voltage. The necessary phase shift is expressed by (3.11).

$$\theta_{shift} = \frac{360°}{m_c} \tag{3.11}$$

Where m_c represents the number of triangular carriers.

The number of triangular carriers is reduced by two in the half-bridge inverter as the number of switching devices decreases. For an *N*-cell CHB, the half-bridge inverter has (*N*+1) voltage levels while the H-Bridge has (2*N*+1) voltage levels due to the reduction in triangular carriers and switching devices.

3.3 H-Bridge Input H-Bridge Output (H-H) Cell

The H-H cell introduced in [22] replaces the 2L-VSI three-phase AFE inverter with a single-phase full-bridge AFE inverter. The H-H cell reduces the total number of switching devices by two per power cell, as shown in Fig. 3.12.

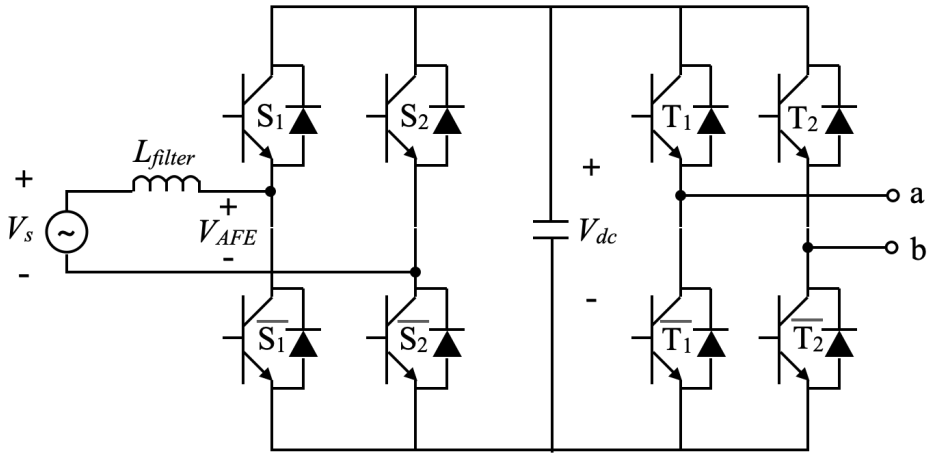

Fig. 3.12. H-H Power Cell [22]

As the H-H cell only changes the AFE inverter in the power cell, in terms of control, the control scheme identified in Section 3.2.1a) needs to be implemented. As a power cell with the new AFE inverter, the H-H cell presents operational and structural differences compared to the conventional regenerative power cell.

a) DC-Link Voltage Ripples

An H-Bridge inverter is utilized in both the AFE and output inverter in the H-H cell. The instantaneous power for the H-bridge inverter is described by (3.12) [22].

$$p(t) = V\sin(\omega t)\cdot I\sin(\omega t-\varphi) = \frac{VI}{2}(\cos\varphi - \cos(2\omega t-\varphi)) \qquad (3.12)$$

Where V is the maximum voltage, I is the maximum current, ω is the angular frequency, and φ is the phase shift between the voltage and current.

The instantaneous power defined by (3.12) demonstrates the effect of the H-Bridge inverter on the DC-link. As the H-Bridge instantaneous power contains a pulsating power that is double the output frequency, the DC-link of the H-H cell will contain voltage ripples that are double the input frequency ($2\omega_{in}$) and double the output frequency ($2\omega_o$).

b) Harmonics on the Cell Input Current

As the DC-link voltage contains ripples, the pulsating component on the DC-link will be reflected on the cell input current. Additionally, the harmonics resulting from the PWM scheme will also be reflected on the input current. With the H-H cell, two lower-order harmonics are identified in the cell input current [22]: ($\omega_{in} \pm 2\omega_o$) and ($3\omega_{in}$). The harmonic spectrum of the H-H cell input current, operating with an input frequency of 50Hz and output frequency of 10Hz, is observed in Fig. 3.13.

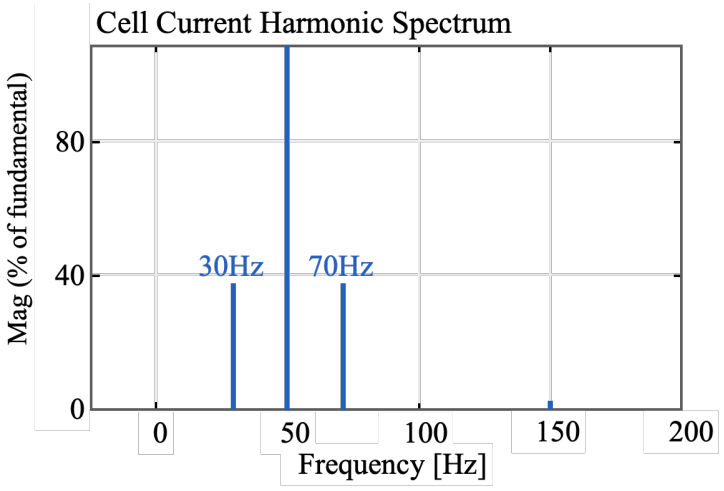

Fig. 3.13. Harmonic Spectrum of the H-H Cell Input Current [22]

c) Grid Connection Standards

The H-H cell needs to eliminate the low order harmonics ($\omega_{in} \pm 2\omega_o$) to satisfy the grid connection standards. The low order harmonic elimination is accomplished by configuring the H-H cell as illustrated in Fig. 3.14.

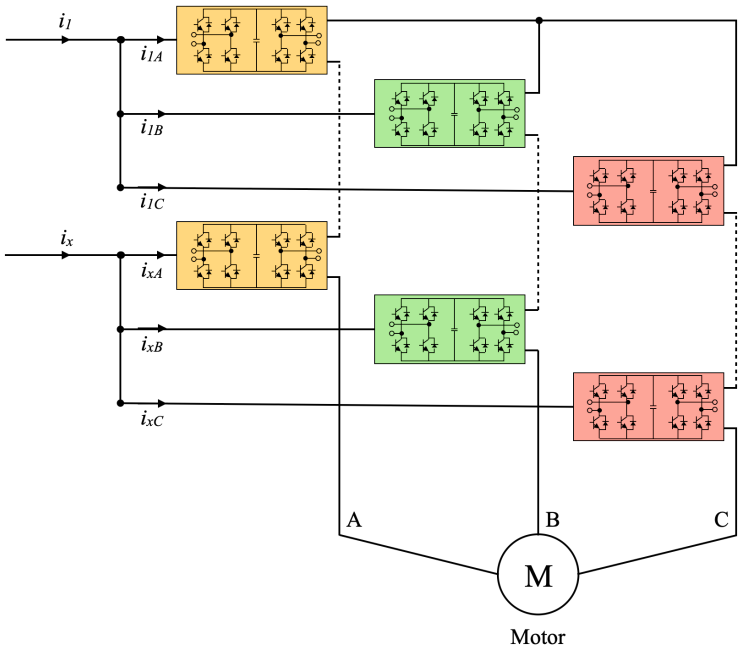

Fig. 3.14. Required Connection for H-H Cell Low Order Harmonic Elimination [22]

In the configuration of the CHB drive seen in Fig 3.14, three H-H cells with different load phases are connected in parallel to the same source. Due to the shared connection, the voltage ripple on the DC-link in each power cell is displaced 120° apart in phase angle. As a result, the low order harmonics caused by the DC-link ripple ($\omega_{in} \pm 2\omega_o$) are eliminated. In addition, the high order harmonics caused by SPWM switching are eliminated by shifting the carriers by 120° between the parallel-connected cells. The proposed low order harmonic elimination method is only effective if the number of cells per phase is a multiple of three [22].

d) Ratings of the Switching Devices

The required voltage and current ratings for the switching devices in the H-H cell are determined by comparing the voltage and current ratings of the switching devices in the conventional regenerative CHB power cell. In the conventional regenerative CHB power cell, the maximum fundamental RMS line-to-line output voltage of the 2L-VSI is expressed by (3.13) [3].

$$V_{l-l,3\emptyset} = 0.707V_{dc} \tag{3.13}$$

If the DC-link voltage between the 2L-VSI and full-bridge AFE inverter is equal, the voltage rating of the switching devices will be equal. The maximum fundamental RMS line-to-line output voltage of the full-bridge AFE inverter with the same DC-link voltage is expressed by (3.14) [3].

$$V_{ph,1\emptyset} = 0.707V_{dc} \tag{3.14}$$

As the 2L-VSI is a three-phase inverter while the full-bridge AFE is a single-phase inverter, the average power for the conventional regenerative power cell and H-H cell is defined by (3.15), respectively.

$$\begin{aligned} P_{in,3\emptyset} &= \sqrt{3} \cdot V_{l-l,3\emptyset} \cdot I_{ph,3\emptyset} \\ P_{in,1\emptyset} &= V_{ph,1\emptyset} \cdot I_{ph,1\emptyset} \end{aligned} \tag{3.15}$$

From (3.13), (3.14), and (3.15), the relationship for the current ratings of the H-H cell is represented by (3.16).

$$I_{1-\emptyset} = 1.73I_{ph,3\emptyset} \tag{3.16}$$

The relationship (3.16) indicates that for the H-H cell with the same power ratings as the conventional regenerative CHB power cell, the current ratings of the AFE switches should be increased by 73%. As the H-bridge output inverter is unchanged, it can be assumed that the voltage and current rating of the switching devices on the output inverter is equal to the conventional regenerative power cell.

3.4 Semi-Reduced Power Cell

The Semi-Reduced Cell replaces the 2L-VSI in the conventional regenerative power cell with a single-phase half-bridge AFE inverter. The replacement allows a switch count reduction of four, as shown in Fig. 3.15.

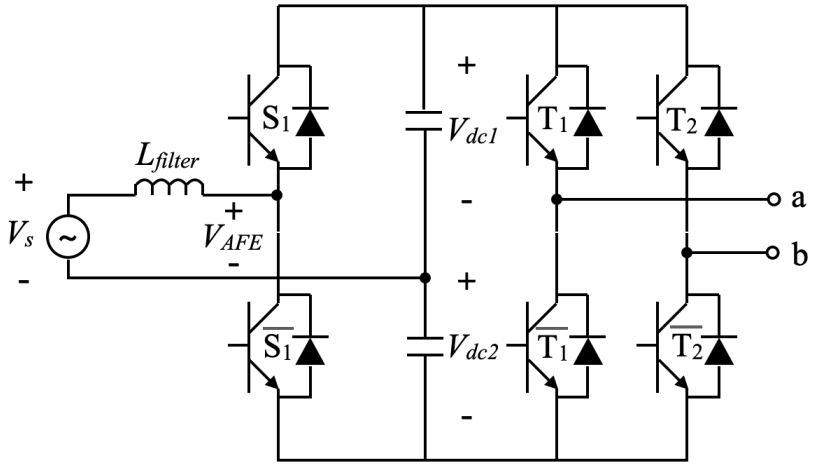

Fig. 3.15. Semi-Reduced Cell [23], [24]

The output inverter in the Semi-Reduced cell remains unchanged. The control scheme identified in Section 3.2.1b) needs to be implemented for the Semi-Reduced cell.

a) DC-Link Voltage Ripples

The analysis of the H-H cell demonstrated that the H-Bridge output inverter introduces second-order voltage ripples in the DC-link capacitors. The Semi-Reduced cell utilizes an H-Bridge output inverter, so the same second-order ripples exist in the DC-link

voltage. In addition to the voltage ripples caused by the H-bridge, the semi-reduced cell experiences voltage ripples from the grid side half-bridge inverter [23], [24]. The half-bridge AFE inverter is represented using an average circuit model in Fig. 3.16.

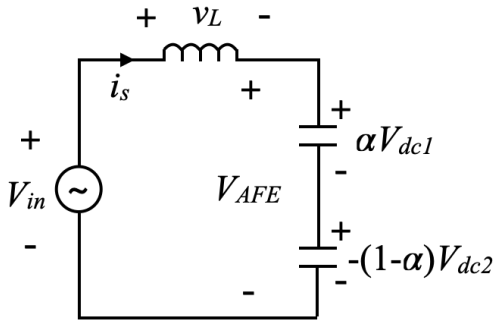

Fig. 3.16. Half-Bridge Average Circuit Model [24]

α is the duty cycle ratio for the upper switch, and (1-α) is the duty cycle ratio for the complimentary switch. The instantaneous active power of each DC-link capacitor is expressed by (3.17) based on the average circuit model and unity power factor operation [23], [24].

$$p_{c1}(t) = \propto V_{dc1} \cdot i_s = \propto V_{dc1} \cdot I_s \sin(\omega_{in} t)$$

$$p_{c1}(t) = V_{dc1}\left(\frac{V_{AFE} I_s}{2V_{dc}}[\cos(\delta) - \cos(2\omega_{in} t - \delta)] + \frac{I_s}{2}\sin(\omega_{in} t)\right) \tag{3.17}$$

$$p_{c2}(t) = -(1-\propto)V_{dc2} \cdot i_s$$

$$p_{c2}(t) = V_{dc2}\left(\frac{V_{AFE} I_s}{2V_{dc}}[\cos(\delta) - \cos(2\omega_{in} t - \delta)] - \frac{I_s}{2}\sin(\omega_{in} t)\right)$$

Where V_{dc1} and V_{dc2} are the average voltage of capacitors c_1 and c_2, V_{AFE} is the magnitude of the AFE output voltage, I_s is the magnitude of the grid current, V_{dc} is the voltage of the DC-link, ω_{in} is the angular frequency of the grid and δ is the phase shift between the AFE output and grid voltage.

The instantaneous active power defined by (3.17) demonstrates the existence of fundamental and second-order voltage ripples in the DC-link capacitors. However, the total DC-link voltage is only subjected to second-order voltage ripples as the fundamental voltage ripples are 180° out of phase in each capacitor.

b) Harmonics on the Cell Input Current

As the Semi-Reduced cell suffers from second-order voltage ripples, the low-order harmonics observed in the H-H cell are observed in the Semi-Reduced cell. In addition, high order harmonics exist in the cell input current due to SPWM switching [23], [24].

c) Grid Connection Standards

The low order harmonics observed on the cell input current must be eliminated for the Semi-Reduced cell to satisfy the grid connection standards. The H-H cell's low order harmonics elimination method can be used with the Semi-Reduced cell. Additionally, a different low order harmonic elimination method is introduced with the Semi-Reduced cell and can be used to eliminate low order harmonics, as shown in Fig. 3.17.

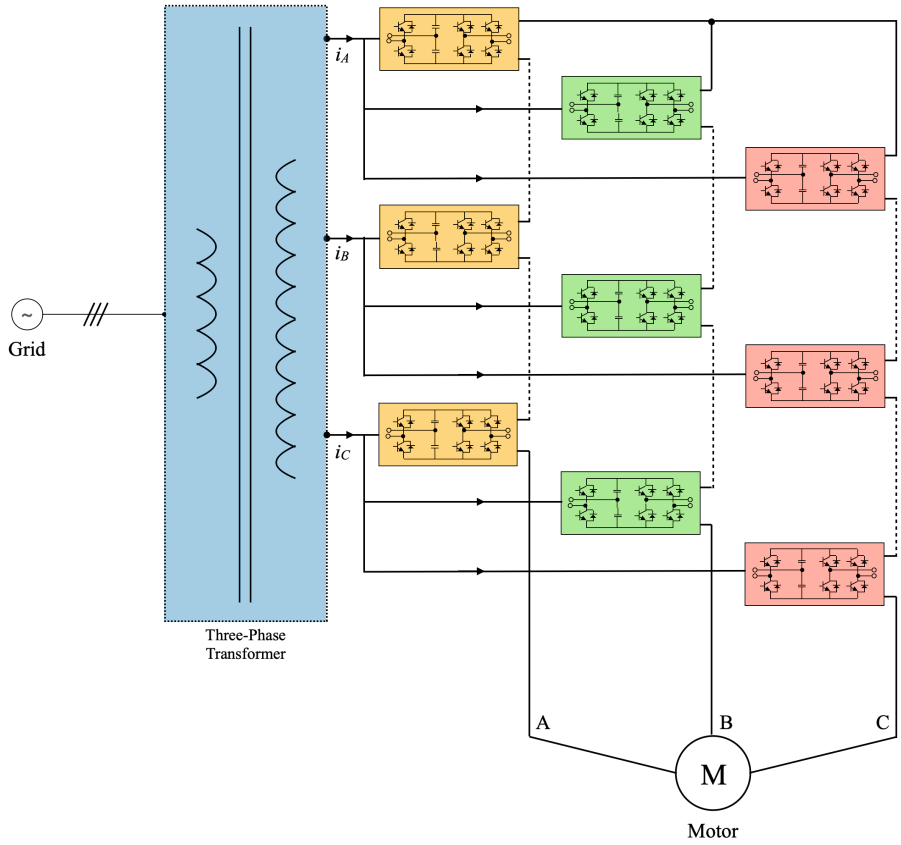

Fig. 3.17. Semi-Reduced Cell Low Order Harmonic Elimination Method [24]

As shown in Fig. 3.17, the low order harmonic elimination method shares a similar technique as the method introduced with the H-H cell. However, the method introduced with the Semi-Reduced cell allows the use of a three-phase transformer. Similarly, the low order harmonic elimination is only effective when the number of power cells is a multiple of three [24]. The high order switching harmonics are eliminated by phase-shifting the carriers of each parallel-connected cell by 120°, similarly to the H-H cell [22], [24].

d) Ratings of Switching Devices

The Semi-Reduced cell only changes the AFE inverter to achieve a reduction in switch count. The maximum fundamental RMS line-to-line output voltage can be expressed as (3.18).

$$V_{ph,1\emptyset} = 0.35V_{dc} \tag{3.18}$$

Given that the DC-link voltage remains unchanged from the conventional regenerative CHB power cell and the Semi-Reduced cell, the required current rating is calculated using (3.15) and is expressed by (3.19).

$$I_{ph,half-bridge} = 3.46I_{ph,3\emptyset} \tag{3.19}$$

Given the same power capabilities, the current ratings of the AFE switching devices in the Semi-Reduced cell must increase by 246%.

3.5 Reduced Cell

The Reduced cell replaces both the grid side AFE inverter and the output inverter in the conventional regenerative CHB power cell with a single-phase half-bridge inverter [25]. The Reduced cell achieves a total switch count reduction of six, making the Reduced cell a regenerative CHB power cell with the least switch count. The Reduced cell is shown in Fig. 3.18.

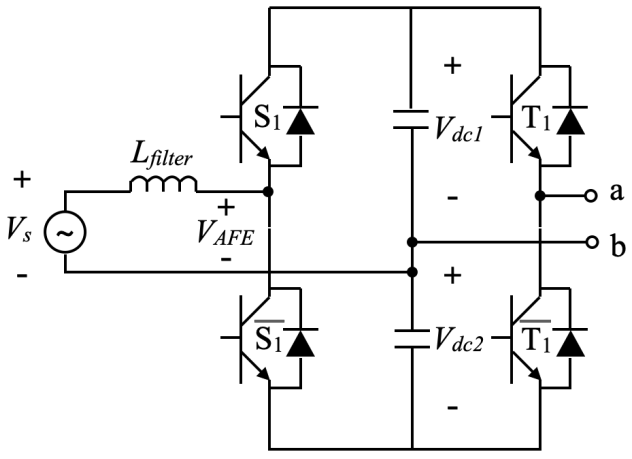

Fig. 3.18. Reduced Cell [25]

The Reduced cell changes both the grid and load side inverter to reduce its switch count. As a result, the control scheme identified in Section 3.2.1b) must be implemented. Additionally, the characteristic of the output inverter can be characterized as defined in Section 3.2.2.

a) DC-Link Voltage Ripples

As the Reduced cell utilizes two half-bridge inverters, the instantaneous power for each capacitor is subject to pulsating power from both inverters. Utilizing the average model illustrated in Fig. 3.16, the instantaneous power for the DC-link capacitors can be expressed by (3.20) [25].

$$p_{c1}(t) = \alpha_{in} V_{dc1} \cdot i_s + \alpha_o V_{dc1} \cdot i_o$$

$$p_{c1}(t) = \left[\left(\frac{V_{AFE} I_s}{2V_{dc}}(\cos(\delta_{in}) - \cos(2\omega_{in} t - \delta_{in})) + \frac{I_s}{2}\sin(\omega_{in} t)\right) + \left(\frac{V_o I_o}{2V_{dc}}(\cos(\emptyset_o) - \cos(2\omega_o t - \emptyset_o)) + \frac{I_o}{2}\sin(\omega_o t)\right)\right] \quad (3.20)$$

$$p_{c2}(t) = (1 - \alpha_{in}) V_{dc2} \cdot i_s - (1 - \alpha_o) V_{dc2} \cdot i_o$$

$$p_{c2}(t) = \left[\left(\frac{V_{AFE} I_s}{2V_{dc}}(\cos(\delta_{in}) - \cos(2\omega_{in} t - \delta_{in})) - \frac{I_s}{2}\sin(\omega_{in} t)\right) + \left(\frac{V_o I_o}{2V_{dc}}(\cos(\emptyset_o) - \cos(2\omega_o t - \emptyset_o)) - \frac{I_o}{2}\sin(\omega_o t)\right)\right]$$

Where α_{in} and α_o are the inverter input and output duty ratios, V_{dc1} and V_{dc2} are the average voltage of c_1 and c_2. V_{AFE} is the magnitude of the AFE output voltage, I_s is the magnitude of the grid current, V_{dc} is the voltage of the DC link, and ω_{in} is the angular frequency of the grid. ω_o is the angular frequency of the output, δ_{in} is the phase shift between the AFE voltage and current, and $\emptyset_o$ is the phase shift between the output voltage and current.

The findings from (3.20) demonstrate the existence of fundamental and second-order harmonic ripples on the DC-link capacitors from both the grid AFE inverter and the output half-bridge inverter. Similar to the Semi-Reduced cell, the fundamental ripple component is phase shifted by $180°$ between the two DC-link capacitors. Only second-order harmonics exist on the total DC-link voltage.

b) Harmonics on the Cell Input Current

As fundamental and second-order ripples exist in the DC-link capacitors, the Reduced cell contains low order harmonics on the cell input current and high order harmonics from the SPWM switching [25].

c) Grid Connection Standards

The low order harmonics observed on the cell input current must be eliminated for the Reduced cell to satisfy the grid connection standards. The low order harmonic elimination method is shown in Fig 3.14 and Fig 3.17 to eliminate the low order harmonics with the Reduced cell. The high order switching harmonics are eliminated by shifting the phase angle of each parallel-connected cell's carriers by 120° [22], [24], [25].

d) Ratings of Switching Devices

The output voltage of the half-bridge output inverter is reduced by a factor of two compared to the H-Bridge. The Reduced cell must double its DC-link voltage to generate an equal output voltage. As a result, the voltage ratings of each switching device in the Reduced cell must be doubled.

With the increase in DC-link voltage, the current rating relationship between the 2L-VSI AFE and the half-bridge AFE is expressed by (3.21).

$$I_{ph,half-bridge} = \frac{3.46}{2} I_{ph,3\emptyset} \tag{3.21}$$

the voltage ratings of the switching devices must be increased by 100% compared to the conventional regenerative CHB power cell. The current ratings of the AFE switching devices must be increased by 73%.

3.6 Reduced Switch-Count Regenerative Cell

The Reduced Switch-Count Regenerative cell replaces the 2L-VSI AFE inverter with an FSTPI AFE compared to the conventional regenerative CHB power cell. The replacement allows a switch count reduction of two while maintaining a three-phase AFE interface with the grid. The Reduced Switch-Count Regenerative cell is shown in Fig. 3.19 [27].

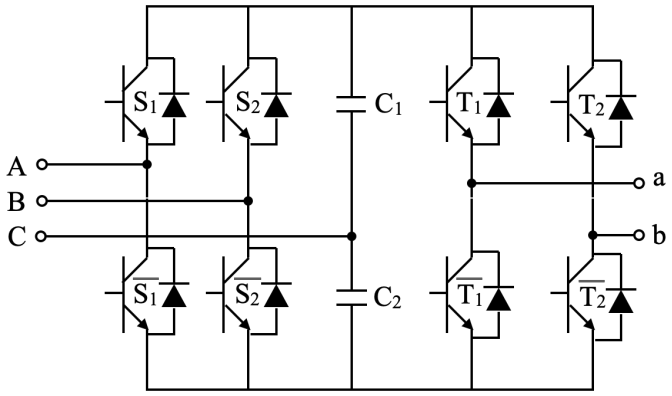

Fig. 3.19. Reduced Switch-Count Regenerative Cell [27]

As the Reduced Switch-Count Regenerative cell maintains the three-phase interface with the grid, the same control scheme for the 2L-VSI can be implemented for the FSTPI with a modification to the SPWM modulator as identified in Section 3.2.1c).

a) DC-link Voltage Ripples

The existence of the DC-link voltage ripples is identified by analyzing the input and output current of the DC-link with the Reduced Switch-Count Regenerative cell. The input and output fundamental currents are expressed as (3.22) [27].

$$\begin{aligned} i_1 &= I_{in}\sin(\omega_{in}t-\theta) \\ i_2 &= I_{in}\sin(\omega_{in}t-\frac{2\pi}{3}-\theta) \\ i_3 &= I_{in}\sin(\omega_{in}t+\frac{2\pi}{3}-\theta) \\ i_o &= I_o\sin(\omega_o t-\emptyset_o) \end{aligned} \tag{3.22}$$

Where i_1, i_2, and i_3 are the three-phase cell input current, i_o is the H-Bridge output current, I_{in} is the fundamental magnitude of the cell input current, and I_o is the fundamental magnitude of the H-bridge output current. ω_{in} and ω_o are the angular frequency of the input and output inverter, θ is the phase shift between the FSTPI phase voltage and current, and $\emptyset_o$ is the phase shift between the H-Bridge voltage and current.

The DC-link input current with regards to (3.22) is expressed by (3.23) [27].

$$\begin{aligned} i_{dc-in1} &= \frac{I_{in}}{2}\sin\left(\omega_{in}t-\theta-\frac{\pi}{3}\right)+\frac{\sqrt{3}}{4}m_{in}\cdot I_{in}\cos\theta \\ i_{dc-in2} &= \frac{I_{in}}{2}\sin\left(\omega_{in}t-\theta-\frac{\pi}{3}\right)-\frac{\sqrt{3}}{4}m_{in}\cdot I_{in}\cos\theta \end{aligned} \tag{3.23}$$

Where i_{dc-in1} and i_{dc-in2} are the current for the upper and lower DC-link capacitors, and m_{in} is the modulation index of the FSTPI inverter.

The DC-link output current with regards to (3.22) is expressed by (3.24) [27].

$$i_o = m_o\cdot I_o[\cos\emptyset_o+\cos(2\omega_o t-\emptyset_o)] \tag{3.24}$$

Where i_o is the DC-link output current, and m_o is the modulation index of the output H-Bridge inverter.

Based on (3.22), (3.23), and (3.24), the capacitor voltages for the Reduced Switch-Count cell are defined by (3.25).

$$V_{dc1} = \frac{1}{C_1}\int i_{c1}dt = \frac{1}{C_1}\int (i_{dc-in1} - i_{dc-o})dt$$
$$V_{dc2} = \frac{1}{C_2}\int i_{c2}dt = \frac{1}{C_2}\int (-i_{dc-in2} - i_{dc-o})dt \quad (3.25)$$

Where the V_{dc1} and V_{dc2} are the upper and lower capacitor voltage, and C_1 and C_2 are the capacitance of the upper and lower capacitor.

The analysis of the capacitor currents in the Reduced Switch-Count cell shows the existence of fundamental voltage ripples from the FSTPI AFE inverter and second-order voltage ripples from the H-Bridge output inverter. The fundamental ripples between the two capacitors are phase-shifted by 180° and do not appear on the total DC-link voltage [27].

b) Harmonics on the Cell Input Current

As the DC-link voltage contains a voltage ripple of $2\omega_o$, the cell input current will contain low order harmonics of $(\omega_{in} \pm 2\omega_o)$. The three-phase interface of the FSTPI allows the low-order harmonics to be eliminated for any number of cells per phase. The power cell configuration utilized with the 2L-VSI and the conventional regenerative CHB is shown in Fig. 3.20.

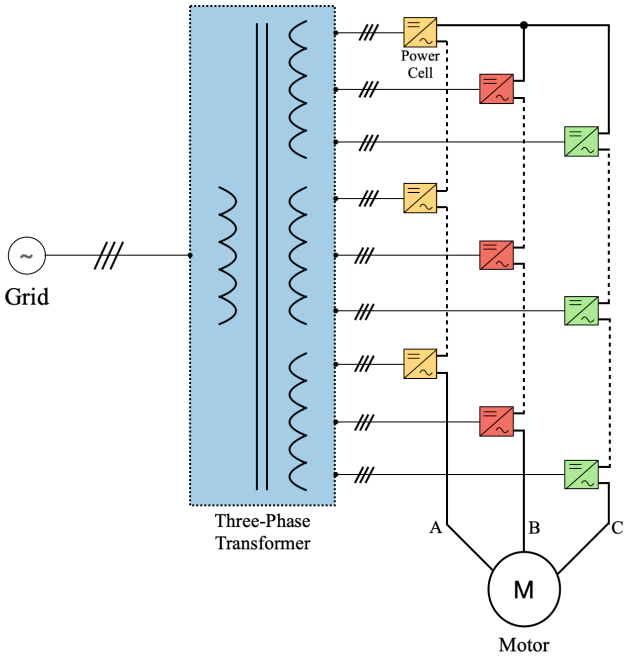

Fig. 3.20. Power Cell Configuration for Reduced Switch-Count Cell

The three-phase power cell configuration, shown in Fig. 3.20, is distinct from the single-phase configurations utilized with the single-phase reduced switch count power cells. The low-order harmonics are injected into all three phases of the grid current rather than only one phase of the grid. As a CHB drive has three output phases that are 120° apart in phase angle, each phase of the grid current contains three sets of low order harmonics that are 120° apart in phase angle. As a result, the low order harmonics are eliminated, and the primary grid current will not contain low order harmonics for any number of power cells per phase. The high order switching harmonics are eliminated by shifting the phase angle of the carrier signals by 120° between the group of series-connected power cells [27].

c) Grid Connection Standards

The three-phase Reduced Switch-Count Regenerative Power cell does not require any low order harmonic elimination method to satisfy the grid connection standards. However, with the FSTPI AFE inverter, the cell input current is unbalanced due to the

fundamental voltage ripples between the two DC-link capacitors. Therefore, the cell input current unbalance needs to be addressed to satisfy the grid connection standards.

Analyzing (3.23), (3.24), and (3.25), the instantaneous voltage difference can be isolated to the fundamental voltage ripples seen in the DC-link input current. The DC-link capacitors experience the other current components equally. The fundamental ripple component between the two DC-link capacitors is equal except for the 180° phase shift, and the fundamental ripple component corresponds to the midpoint-connected grid phase. The phase alternation method is proposed with the Reduced Switch-Count power cell to address the current unbalance and is shown in Fig. 3.21 [27].

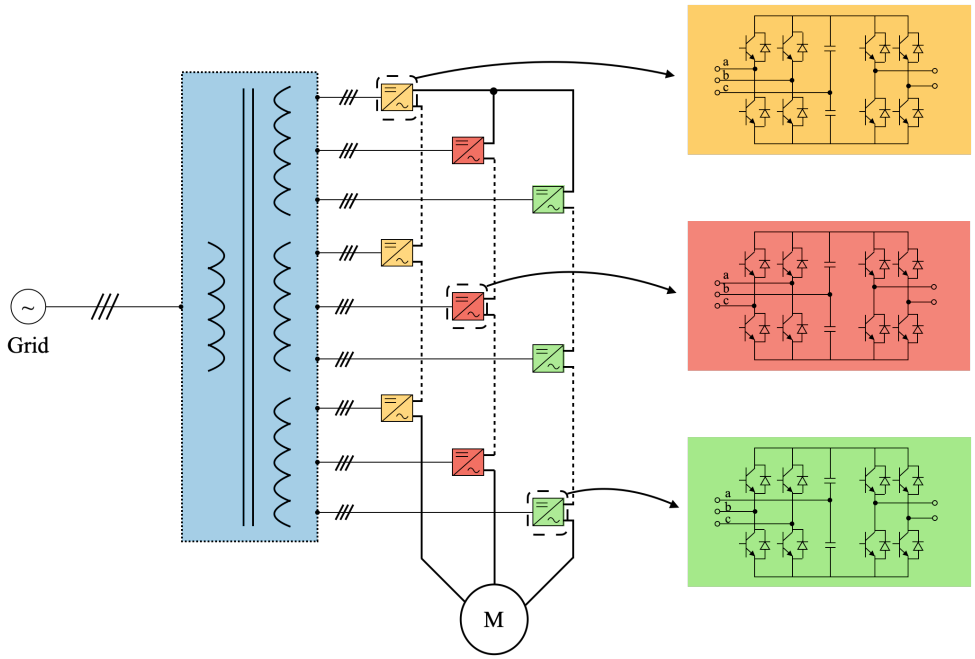

Fig. 3.21. Phase Alternation Method for Current Unbalance [27]

In the phase alternation method, the midpoint-connected grid phase alternate between the group of series-connected power cell. The alternation of the midpoint applies a 120° phase shift to the fundamental voltage ripple between the group of power cells, enabling

the grid current to be balanced. However, the cell current input will remain unbalanced with the phase alternation method [27].

With the absence of low order harmonics, elimination of high order switching harmonics, and balanced grid current, the Reduced Switch-Count Regenerative cell satisfies the grid connection standards.

d) Ratings of Switching Devices

As the Reduced Switch-Count Regenerative cell utilizes an H-Bridge output inverter, the DC-link voltage is equal to the conventional regenerative CHB power cell for the device rating analysis. The voltage rating of the switching devices remains equal as a result. The maximum output voltage of the FSTPI utilizing SPWM is expressed by (3.26).

$$V_{l-l,FSTPI} = 0.353V_{dc} \tag{3.26}$$

The current relationship between the 2L-VSI and the FSTPI, utilizing (3.26), is defined as (3.27).

$$I_{FSTPI} = 2I_{ph,3\emptyset} \tag{3.27}$$

The relationship expressed by (3.27) implies that the current ratings for the switching devices must be increased by 100% [27].

3.7 Challenges

The existing reduced switch-count power cell topologies successfully reduce switch count while adhering to the requirements to replace the conventional regenerative CHB power cell. However, the switch count reduction proposes many challenges [22]-[27]:

a) Challenges of Single-phase Reduced Switch Count Power Cells

- More complex AFE control as rotating *d-q* reference cannot be used.
- Low order harmonic elimination is only possible when the number of power cells per phase is a multiple of three.
- Additional voltage ripples on the DC-link Capacitors and potential voltage imbalance with the Semi-Reduced and Reduced cell.
- The Reduced cell output voltage levels are reduced to ($N + 1$).
- The current ratings of the AFE switching devices need to increase, and for the reduced cell, the voltage rating of all switching devices needs to increase.

b) Challenges of the Three-Phase Reduced Switch Count Power Cell

- Additional voltage ripples on the DC-link Capacitors and potential voltage imbalance.
- Different power cell configurations per output phase to eliminate the current unbalance observed on the grid current.
- The current rating of the AFE switching devices needs to double.

3.8 Summary

The existing reduced switch-count regenerative CHB power cells are discussed to demonstrate the current state of switch-count reduction in a regenerative CHB. The alternative inverters that minimize switch count are analyzed, and each power cell is reviewed in detail. The operation, control, modulation, and configuration differences show how each configuration achieves switch-count reduction and analyzes the challenges.

The three-phase Reduced Switch-Count Regenerative Cell demonstrates the benefit of utilizing a three-phase grid interface while successfully reducing the switch count. The three-phase grid connection allows cancellation of harmonics for any cells per phase and allows the power cell to maintain the same configuration as the conventional regenerative CHB drive.

The comparison of the existing reduced switch-count regenerative CHB power cell is shown in Table 3.8.

TABLE 3.8. COMPARISON OF EXISTING REDUCED SWITCH-COUNT REGENERATIVE CHB POWER CELLS WITH THE CONVENTIONAL REGENERATIVE CELL FOR AN *N*-CELL CHB [27]

Cell Configuration	**Three-Phase AFE**		**Single-Phase AFE**		
	Conventional Regenerative Cell [15]-[17]	**Reduced Switch-Count Regenerative Cell [27]**	**H-H Cell [22]**	**Semi-Reduced Cell [23], [24]**	**Reduced Cell [25]**
# of Switches	10	8	8	6	4
Output Voltage Levels	$2N+1$	$2N+1$	$2N+1$		$N+1$
AFE Control Frame	Rotating *d-q*		Stationary *abc* (more complex)		
Low order harmonic elimination	Effective for any number of cells/phase		Effective only if number of cells/phase is multiple of three		
Low order DC-link ripples	Output 2nd order		Output and input 2nd order		
Capacitor ripples	Output 2nd order	Output 2nd order	Output and input 2nd order		
		Input fundamental		Input Fundamental	
			Output fundamental		
AFE Switches current rating	I_{in}	$2I_{in}$	$1.73I_{in}$	$3.46I_{in}$	$1.73I_{in}$
Switches voltage ratings	V_{dc}		V_{dc}		$2V_{dc}$

Chapter 4

Proposed Six-Switch Regenerative Power Cell Topology I for a CHB Motor Drive

4.1 Introduction

The review, analysis, and challenges of the existing reduced switch count power cells indicate the importance of utilizing a three-phase AFE inverter to minimize the challenges of replacing the conventional regenerative CHB power cell. The single-phase reduced switch-count power cells provide the insight to achieve the most switch count reduction. In contrast, the three-phase Reduced Switch-Count Regenerative cell demonstrates the possibility of reducing switch count utilizing a three-phase grid connection.

With the advancement in the multipack IGBT modules, such as a six-pack Infineon 1200V IGBT module [33], a reduced switch-count regenerative power cell with a switch count of six or less can be beneficial in terms of cost, size, and complexity.

This chapter proposes a new three-phase reduced switch-count regenerative power cell to reduce the number of switching devices by four compared to the conventional regenerative CHB power cell. The new reduced switch-count regenerative power cell utilizes a Four-Switch Three-Phase Inverter (FSTPI) and an H-Bridge inverter to achieve the reduction.

4.2 Proposed Power Cell

The new three-phase reduced switch-count regenerative power cell is shown in Fig 4.1. In the new configuration, the 2L-VSI is replaced with an FSTPI AFE while maintaining the single-phase H-Bridge inverter. The switch reduction is achieved by implementing an FSTPI and sharing a common inverter leg between the FSTPI and H-Bridge. As another six-switch power cell is proposed in the later chapter, this topology is referred to as a Six-Switch Regenerative H-Bridge Power Cell.

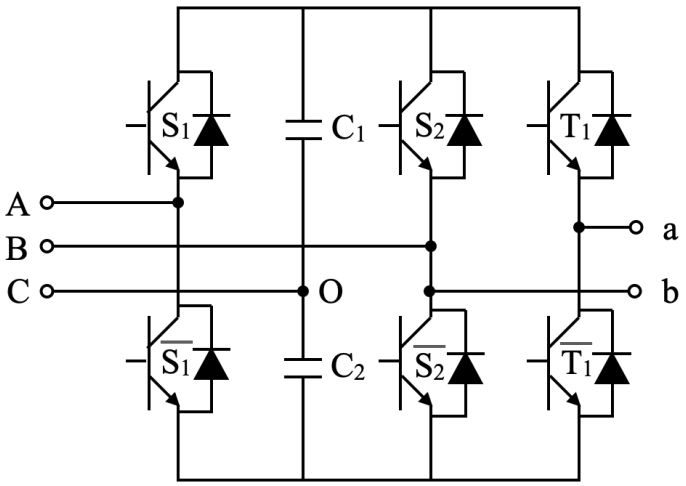

Fig. 4.1. Six-Switch Regenerative H-Bridge Power Cell

4.2.1 Structure

The proposed Six-Switch Regenerative H-Bridge Power Cell structure utilizes the same three-phase grid and single-phase load connection as the conventional regenerative CHB power cell. The control scheme of the FSTPI AFE and modulation of the H-Bridge inverter do not require changes. However, the modulator for the system requires modification to account for the shared common leg of the proposed topology. In addition, one of the grid phases is connected to the midpoint of the DC-link capacitors, introducing challenges such as capacitor voltage balancing, current unbalance, and harmonics on the cell input current.

4.2.2 Grid Side Modulation

Based on the existing alternative inverters that can be used for switch reduction, the FSTPI AFE utilizes the least number of switching devices to modulate a three-phase output voltage. As discussed in the previous chapter, the modulation signals for a grid phase C midpoint connected FSTPI are represented by (4.1).

$$\begin{aligned} V_{AO} &= V_A - V_C = \sqrt{3}V \sin\left(\omega_{in}t - \frac{\pi}{6}\right) \\ V_{BO} &= V_B - V_C = \sqrt{3}V \sin\left(\omega_{in}t - \frac{\pi}{2}\right) \end{aligned} \tag{4.1}$$

As the operation principle of the FSTPI confines the modulation signal of the two legs, the two grid-connected inverter legs only have the amplitude of the modulating signals as a degree of freedom. In the power cell configuration shown in Fig. 4.1, the modulation of the shared leg between the FSTPI AFE and the H-Bridge inverter is confined to the modulating signal defined by V_{BO}.

4.2.3 Motor Side Modulation

The output voltage of the H-Bridge inverter is defined by the voltage difference between the two legs of the inverter, V_{ab}. As the proposed power cell shares a common connection with the grid, the H-bridge inverter utilizing SPWM modulation can be modeled as two half-bridge inverters to simplify the analysis. Fig 4.2 shows the H-Bridge inverter isolated from the proposed power cell.

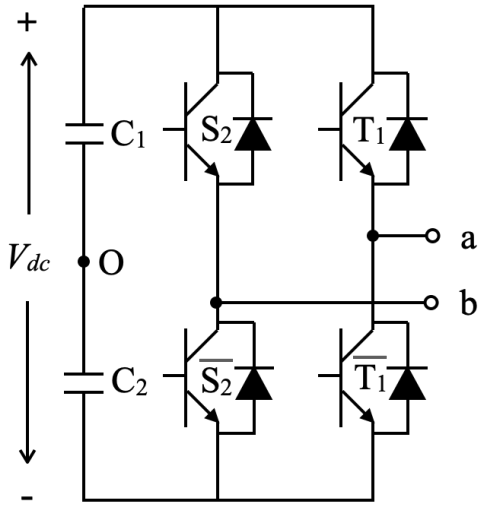

Fig. 4.2. H-Bridge Inverter from the Six-Switch Regenerative H-Bridge Power Cell

In a typical single-phase H-Bridge inverter in a CHB, the output voltage of the two individual legs, in reference to point "O", is modeled by (4.2).

$$V_{aO} = \frac{V_{dc}}{2} m_o v_{ref}$$

$$V_{bO} = -\frac{V_{dc}}{2} m_o v_{ref} \tag{4.2}$$

$$V_{ab} = V_{aO} - V_{bO} = V_{dc} m_o v_{ref}$$

Where V_{dc} is the total DC-link voltage, m_o is the modulation index of the output inverter, and v_{ref} is the modulating signal of the output inverter.

The model of the H-Bridge inverter as two half-bridge inverters in (4.2) shows that each leg of the H-Bridge produces an output based on the reference modulating signal opposing in sign. The maximum output voltage of each leg is half of the DC-link voltage, but the difference between the two inverters allows the utilization of the total DC-link voltage in the output voltage. Based on the findings with the FSTPI AFE from the previous section, the output voltage of the shared leg in the H-Bridge inverter, V_{bO}, is confined to the FSTPI modulating signal V_{BO}. As the output voltage of the H-Bridge inverter, V_{ab}, is the difference between the two legs of the H-Bridge, the modulation of the H-Bridge must be modified to ensure correct motor side modulation.

4.2.4 Proposed Modulation Technique for the Six-Switch H-Bridge Regenerative Power Cell

The FSTPI and H-Bridge inverter analysis imply that the two inverters cannot work independently. The output voltage of the non-shared output inverter leg, V_{aO}, is solely responsible for producing the output voltage for the load side while canceling the output voltage produced in the common leg. The condition to ensure proper modulation and operation of the FSTPI and H-Bridge is defined by (4.3).

$$\begin{aligned} m_{in} + m_o &= 1 \\ 0 \leq m_{in} &\leq 1 \\ 0 \leq m_o &\leq 1 \end{aligned} \tag{4.3}$$

Where m_{in} is the modulation index of the FSTPI.

The output voltage of the two individual legs, in reference to point "O", for the proposed power cell is then defined by (4.4).

$$V_{aO} = \frac{V_{dc}}{2}\left(m_{in}\frac{v_{BO}}{2\sqrt{3}} + m_o\frac{v_{ref}}{2}\right)$$
$$V_{bO} = \frac{V_{dc}}{2}\left(m_{in}\frac{v_{BO}}{2\sqrt{3}}\right) \quad (4.4)$$

The modulation techniques of the FSTPI and H-Bridge inverter in the proposed power cell demonstrate the changes required to ensure the interoperability of the two inverters with the common leg. Based on the operation principle of the FSTPI, (4.1) and (4.4), the FSTPI modulation signal is redefined as (4.5).

$$V_{AO-ref} = \frac{m_{in}}{2}\sin\left(\omega_{in}t - \frac{\pi}{6}\right)$$
$$V_{BO-ref} = \frac{m_{in}}{2}\sin\left(\omega_{in}t - \frac{\pi}{2}\right) \quad (4.5)$$

The modulation signal for the leg without the common point is defined as (4.6).

$$V_{aO-ref} = V_{BO-ref} + \frac{m_o}{2}v_{ref} \quad (4.6)$$

Fig. 4.3 shows the proposed power cell and modulation signals based on (4.5) and (4.6). Although the output inverter in the proposed power cell is an H-Bridge configuration, due to the limitation imposed by the FSTPI AFE, the output inverter operates as a half-bridge inverter with a neutral point defined by V_{BO}.

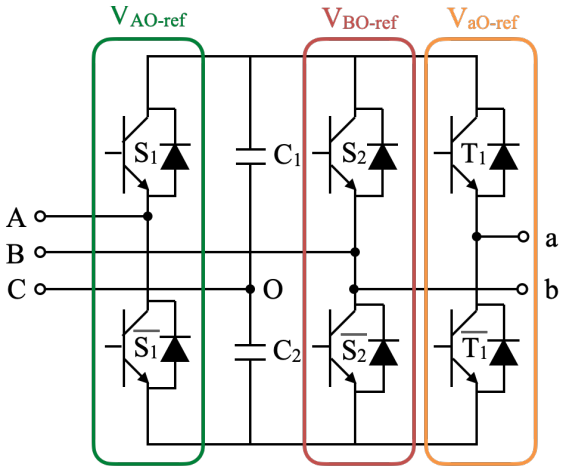

Fig. 4.3. Modulation Signals for the Six-Switch Regenerative H-Bridge Power Cell

The proposed Six-Switch Regenerative H-Bridge Power cell maintains the three-phase grid connection as the conventional regenerative CHB power cell. As a result, the same AFE control scheme is used with the proposed power cell, shown in Fig 4.4.

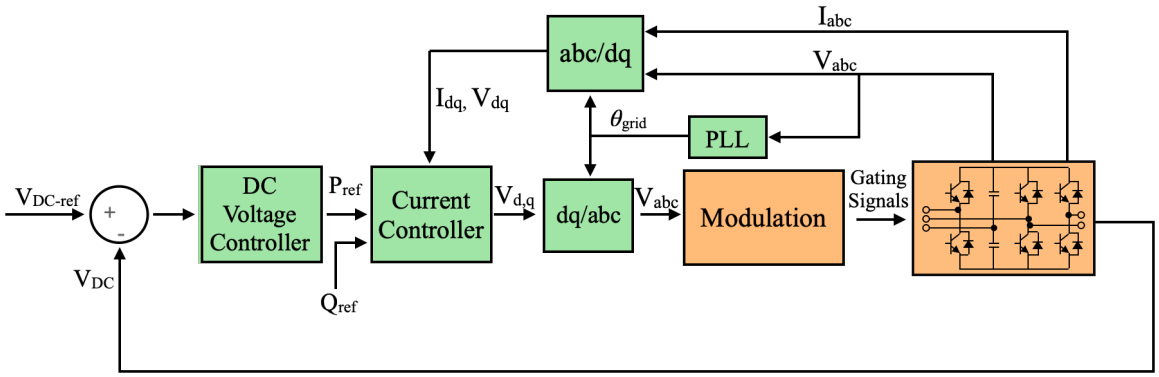

Fig. 4.4 AFE Control Scheme for the Proposed Six-Switch Regenerative H-Bridge Power Cell

The changes in the modulation scheme are implemented through a modified modulator for the FSTPI and H-Bridge output inverter. Fig 4.5 shows the modified modulator for the proposed power cell.

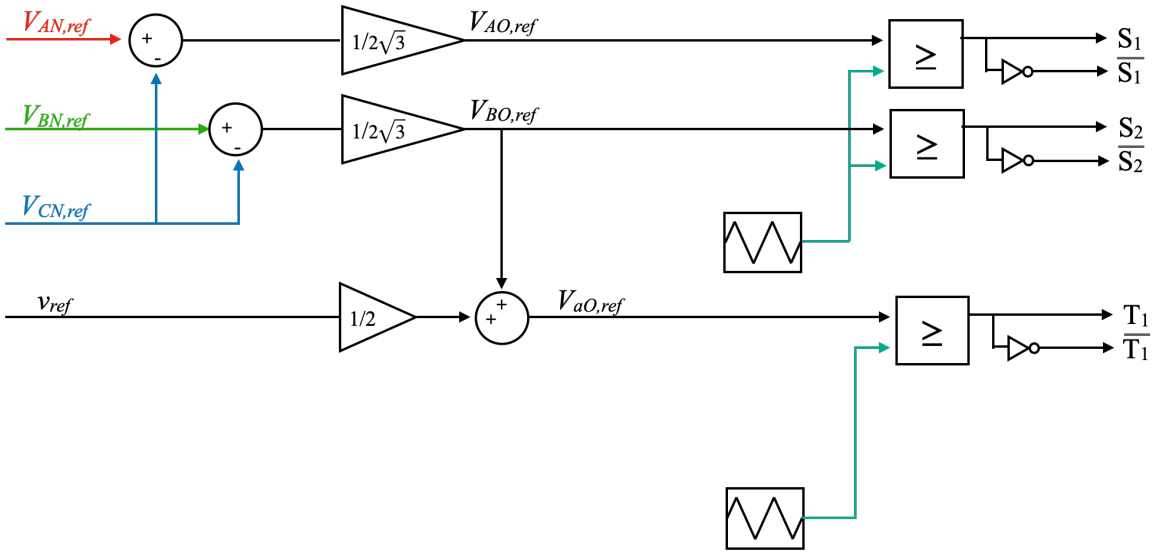

Fig. 4.5. Modified Modulator for Proposed Six-Switch Regenerative H-Bridge Power Cell

4.3 Limitations

The proposed Six-Switch Regenerative H-Bridge power cell poses limitations due to the inverters' common leg. The limitations are categorized and listed as follows:

1) Limitations as a Power Cell

- The changes in modulation technique for interoperability of the two inverters cause low DC-link utilization for the grid and output inverters.
- The modulation technique of the H-Bridge can increase switching harmonic if the triangular carriers differ between the grid and load side inverters.
- The capacitor midpoint connection introduces cell input current unbalance and increased harmonic content, as seen in the previous chapter.

2) Limitations as a Replacement for Conventional Regenerative CHB power cell

- The DC-link voltage must be increased to achieve an equal output voltage compared to the conventional regenerative CHB power cell.
- The reduction in modulation index with the output inverter leads to the loss of output voltage levels and increased harmonic content.
- The reduction in the modulation index with the FSTPI leads to higher harmonic content in the grid voltage and current, affecting compliance with grid connection standards.
- The loss of freedom in the triangular carriers between the grid and output inverters complicates switching harmonic elimination.
- The use of FSTPI and H-Bridge with a modified modulation scheme can introduce capacitor voltage balancing issues that need to be explored.

4.4 Voltage and Current Ratings of Switching Devices

The proposed Six-Switch Regenerative H-Bridge power cell only employs an alternative inverter for the AFE inverter. However, due to the operational changes in the output inverter, the voltage and current ratings of all switching devices must be evaluated. In the proposed power cell, the DC-link voltage increases by a factor of four due to the reduction in output voltage with the H-Bridge inverter. With the increased DC-link voltage, the maximum output voltage of the FSTPI utilizing SPWM is expressed by (4.7).

$$V_{l-l,FSTPI} = 0.177V_{dc} \tag{4.7}$$

The maximum output voltage for the 2L-VSI utilizing SPWM and third order harmonic injection is expressed by (4.8) [3].

$$V_{l-l,2L-VSI} = 0.707V_{dc} \tag{4.8}$$

The current rating for the FSTPI is determined by the power equation expressed by (4.9).

$$\begin{gathered} P_{2L-VSI} = P_{FSTPI} \\ \sqrt{3}V_{l-l,2L-VSI}I_{2L-VSI} = \sqrt{3}V_{l-l,FSTPI}I_{FSTPI} \end{gathered} \tag{4.9}$$

The required current rating is expressed by (4.10), considering the DC-link voltage increase.

$$I_{FSTPI} = I_{2L-VSI} \tag{4.10}$$

Conducting the same analysis for the H-Bridge inverter, the maximum output voltage of the H-Bridge inverter in the conventional regenerative CHB, utilizing SPWM modulation and third order harmonic injection, is expressed by (4.11) [3].

$$V_{Conv,H-Bridge} = 0.707V_{dc} \tag{4.11}$$

The maximum output voltage of the H-Bridge inverter in the proposed power cell, utilizing SPWM modulation is expressed by (4.12).

$$V_{Reduced,H-Bridge} = 0.177V_{dc} \tag{4.12}$$

The current rating for the H-Bridge inverter in the proposed power cell is determined by the power equation expressed by (4.13).

$$\begin{gathered} P_{Conv,H-Bridge} = P_{Reduced,H-Bridge} \\ V_{Conv,H-Bridge}I_{Conv,H-Bridge} = V_{Reduced,H-Bridge}I_{Reduced,H-Bridge} \end{gathered} \tag{4.13}$$

The required current rating for the H-Bridge inverter in the proposed power cell is expressed by (4.14), considering the increase in the DC-link voltage.

$$I_{Reduced,H-Bridge} = I_{Conv,H-Bridge} \tag{4.14}$$

For the proposed Six-Switch Regenerative H-Bridge power cell, the current ratings of the switching devices remain equal to the 2L-VSI in the conventional regenerative CHB power cell. However, the voltage ratings of all switching devices need to increase by a factor of four.

4.5 Implementation Feasibility of the Proposed Power Cell

The control, modulation, limitations, and device ratings analysis show a successful switch count reduction with the Six-Switch Regenerative H-Bridge power cell. However, the overwhelming limitations, especially with the increase in DC-link voltage by a factor of four, can hinder the ability of the proposed power cell to be a replacement for a regenerative CHB power cell.

The proposed power cell cannot utilize the DC-link efficiently with the common leg between the grid and motor side inverters in the given configuration. Additionally, the control of the common leg complicates the elimination of switching harmonics if the carrier

phase-shifting method is used. Without addressing the output voltage of the grid inverter induced on one phase of the output inverter, the feasibility of the Six-Switch Regenerative H-Bridge power cell as a replacement power cell for the conventional regenerative CHB power cell needs to be considered. An alternative control or modulation technique of the Six-Switch Regenerative H-Bridge power cell is a great topic for future research.

4.6 Simulation Studies

The verification of the modified modulation of the proposed Six-Switch Regenerative H-Bridge power cell is conducted with a simulation model. A 9-cell CHB model is developed with the proposed Six-Switch Regenerative H-Bridge power cell. The system parameters are shown in Table 4.1. The load side of the CHB is connected to an induction motor.

TABLE 4.1. SYSTEM PARAMETERS FOR THE PROPOSED SIX-SWITCH REGENERATIVE H-BRIDGE POWER CELL IN A 9-CELL CHB

9-Cell Regenerative CHB Simulation Parameters	
Grid Voltage	3 [kV]
Rated Output Current	160 [A]
Nominal Frequency	60 [Hz]
Switching Frequency	1980 [Hz]
Grid-Connecting Filter	3 [mH]
Cell Input Voltage	450 [V]
DC Reference Voltage	3400 [V]
Capacitor Value	8000 [μF]
Number of Motor Pole Pairs	3
Motor Rated Speed	1192 [RPM]

The simulation model is conducted with a motor speed and torque profile shown in Fig. 4.6. The profile subjects the motor load in both motoring and regenerative conditions.

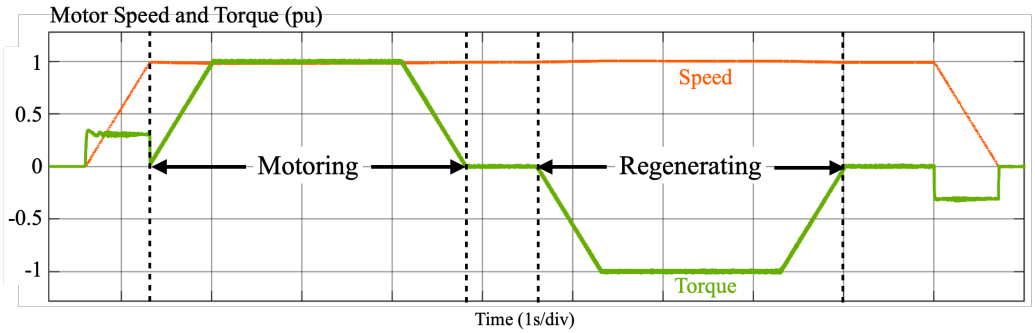

Fig. 4.6. Motor Speed and Torque Profile for the Six-Switch Regenerative H-Bridge Cell

Fig. 4.7 show the motor voltage and current under the dynamic profile shown in Fig. 4.6.

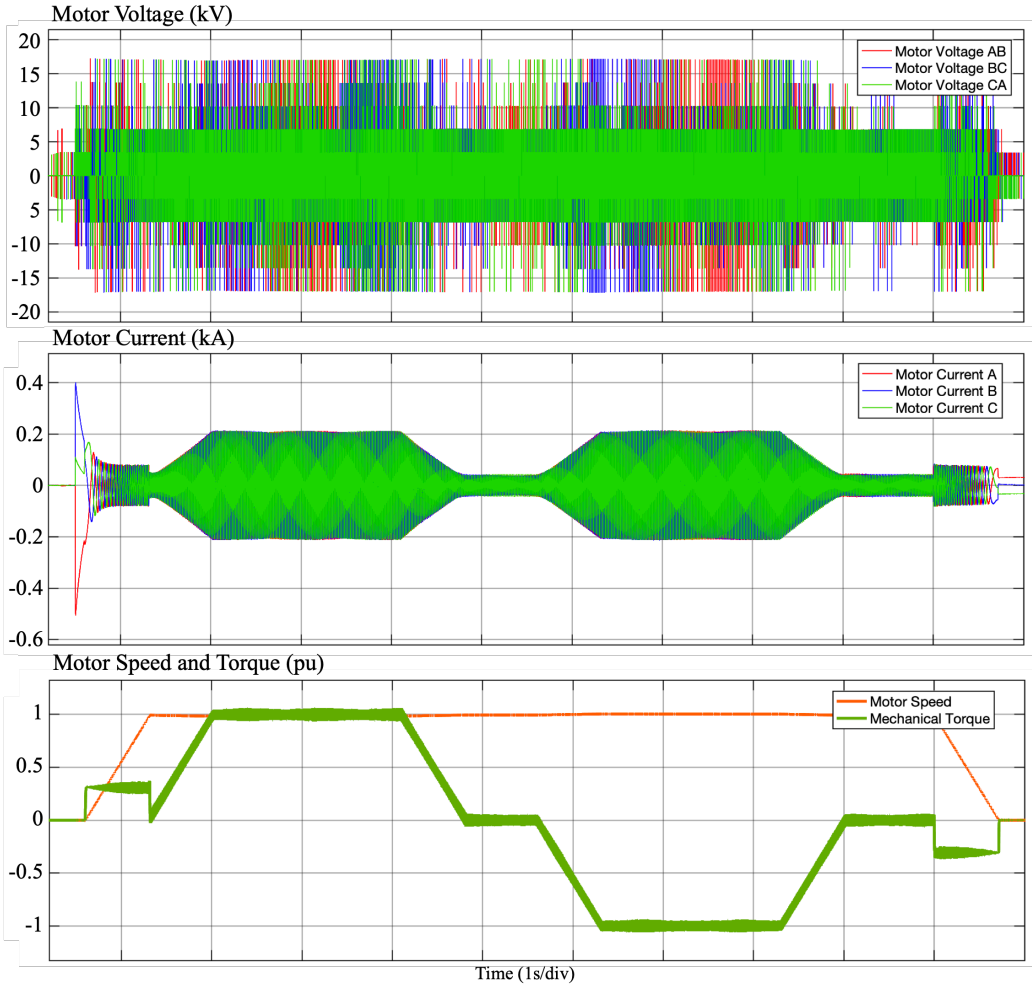

Fig. 4.7. Motor Voltage and Current of the Six-Switch Regenerative H-Bridge Cell

The motor voltage and current demonstrate the ability of the proposed power cell to operate under motoring and regenerative conditions. Due to the low DC-link utilization of the Six-Switch H-Bridge power cell, a DC-link of 3400V is required for the 3kV motor load of the simulation model. Although the fundamental output line-to-line voltage for the output inverter is controlled to 3kV, the motor is subjected to higher voltage levels with the proposed modulation technique. Fig 4.8 shows the capacitor voltages in both modes of operations.

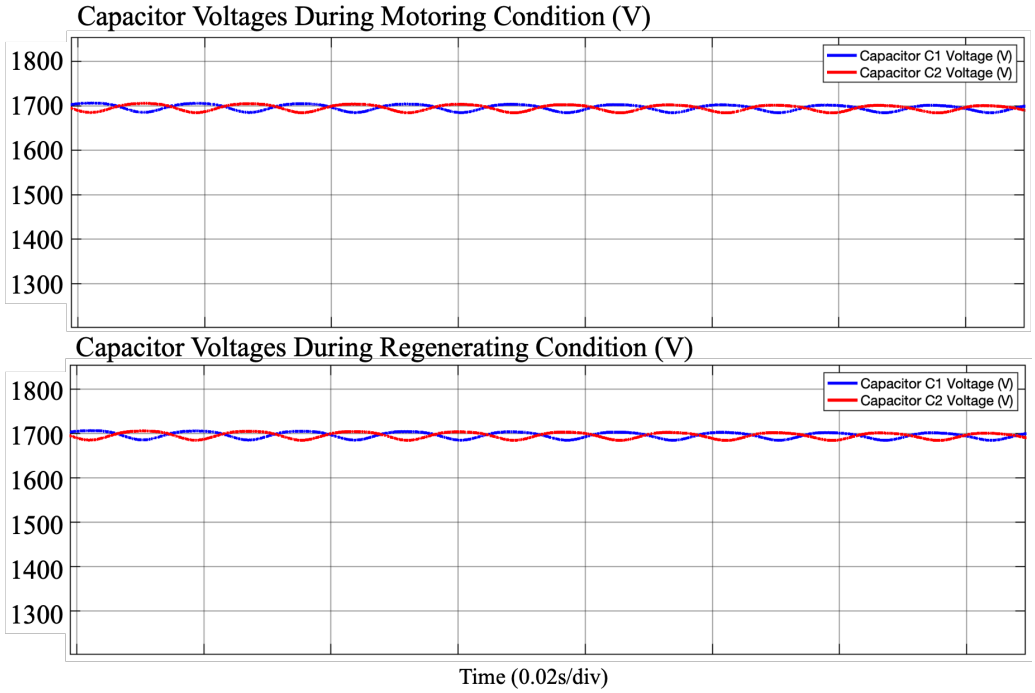

Fig. 4.8. Capacitor Voltages of the Six-Switch Regenerative H-Bridge Cell

Fig 4.9 shows the grid current, and its harmonic spectrum.

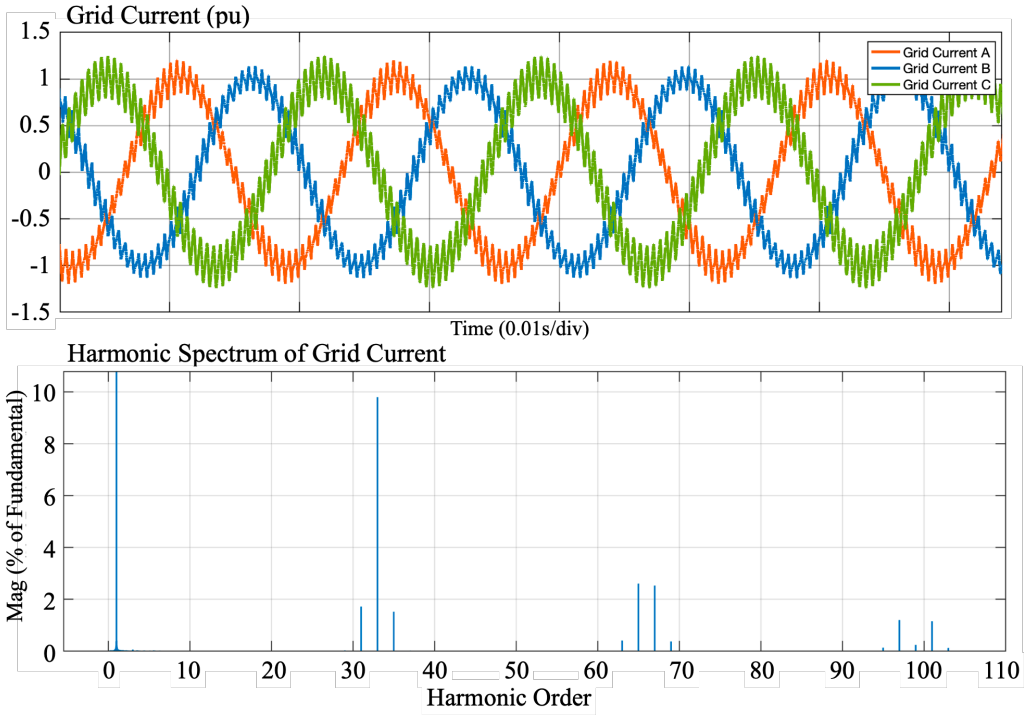

Fig. 4.9. Grid Current and Harmonic Spectrum of the Six-Switch Regenerative H-Bridge Cell

The capacitor voltages in both modes of operations show that the AFE inverter and control scheme maintains a stable DC-link voltage. Both DC-link capacitors maintain an average voltage based on their reference value. The grid current and harmonic spectrum show high switching harmonics present on the grid side. The limitation in the modulation index of the grid inverter contributes to the switching harmonics. The total THD of the grid current is 10.96%.

4.7 Summary

A new reduced switch-count regenerative power cell for a regenerative CHB is proposed. The proposed power cell configuration utilizes a shared inverter leg between the FSTPI and H-Bridge inverter to achieve the switch count reduction of four compared to the conventional regenerative CHB power cell. A new modulation technique is proposed

to ensure proper operation and control of the proposed power cell configuration. The power cell structure, control, and characteristics with a common leg are analyzed and verified through a simulation model.

The proposed Six-Switch Regenerative H-Bridge power cell demonstrates a successful switch count reduction. However, the analysis and limitations identify an area of concern with the proposed power cell that impacts the feasibility of the power cell. In the following chapter, a new reduced switch-count regenerative power cell is proposed that addresses the area of concern.

Chapter 5

Proposed Six-Switch Regenerative Power Cell Topology II for a CHB Motor Drive

5.1 Introduction

The analysis and limitations of the Six-Switch Regenerative H-Bridge power cell show the impact of sharing a common inverter leg between the grid and motor side inverter. While the Six-Switch Regenerative H-Bridge power cell introduced many challenges that need to be explored and addressed, the power cell configuration demonstrates three important aspects. The Six-Switch Regenerative H-Bridge power cell reduces the total

switch count by four, allowing a power cell design with a single multipack IGBT module. The proposed power cell configuration maintains a three-phase grid connection, and the proposed cell is a three-phase reduced switch-count regenerative power cell with the least switch count.

This chapter proposes a new reduced switch-count regenerative power cell configuration that maintains the three important aspects of the previous Six-Switch Regenerative H-Bridge power cell while addressing the common inverter leg that introduced many limitations. The new reduced switch-count regenerative power cell utilizes a Four-Switch Three-Phase Inverter (FSTPI) and a single-phase half-bridge inverter to achieve the reduction. As discussed in the previous chapter, a switch-count reduction proposes challenges that need to be addressed, and the new proposed reduced switch-count power cell has three challenges:

- Capacitor voltage balancing
- Cell input current harmonics and unbalance
- Switching frequency harmonics

This chapter analyzes and addresses the challenges that arise with the new proposed power cell. The solutions to the challenges are verified with simulation studies and experimental results. The results from the simulation and experimental studies are promising and demonstrate the ability to replace the conventional regenerative power cell while reducing the required number of switches from ten to six.

5.2 Proposed Power Cell Configuration

The new three-phase reduced switch-count regenerative power cell is shown in Fig. 5.1. Comparing the conventional regenerative CHB power cell, the 2L-VSI AFE is replaced with an FSTPI AFE. The H-Bridge output inverter is replaced with a half-bridge inverter. The control, modulation, and the number of output voltage levels change, compared to the conventional regenerative CHB power cell, since the grid and output side inverters are replaced with alternative topologies. As another six-switch power cell is proposed in the previous chapter, this topology is referred to as a Six-Switch Regenerative I-Bridge power cell.

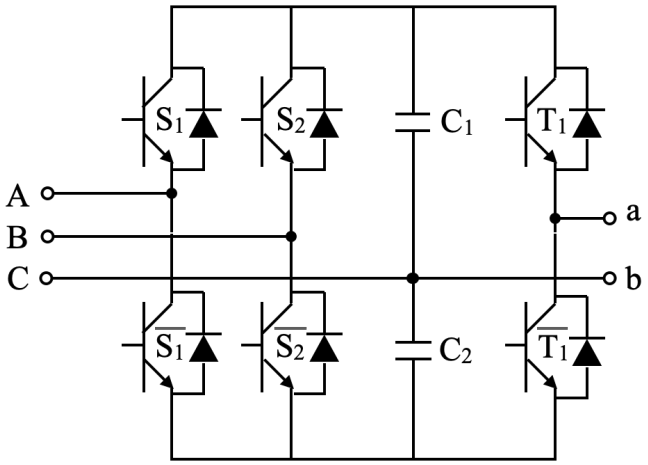

Fig. 5.1. Proposed Six-Switch Regenerative I-Bridge Power Cell.

5.2.1 Structure

The existing three-phase Reduced Switch-Count Regenerative cell utilizes an FSTPI AFE to reduce the number of switches with the grid side inverter. The proposed Six-Switch Regenerative I-Bridge power cell utilizes the same grid side inverter to reduce switch count. The capacitor midpoint is the power cell's neutral point, and one of the grid phases is connected to the midpoint. The operational principles remain unchanged with the new

proposed power cell and utilize the same control scheme and modified modulator as discussed in the previous chapter and shown in Fig 5.2.

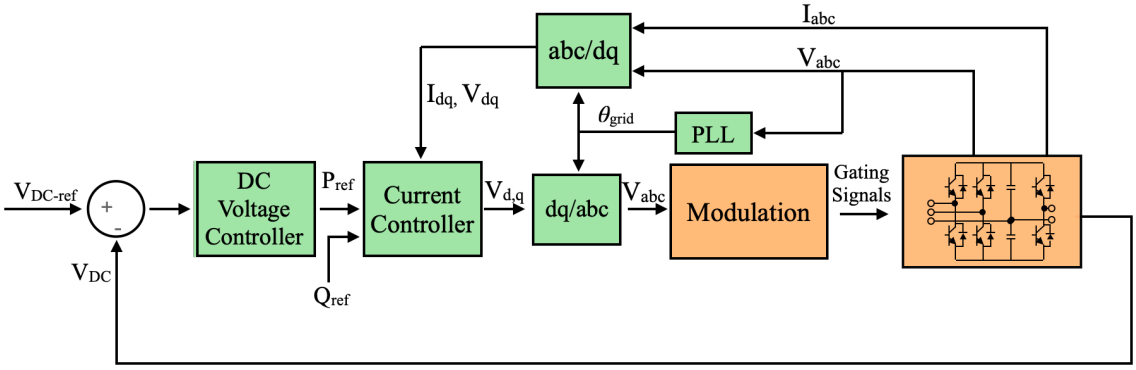

(a) AFE Control Scheme for the Proposed Power Cell

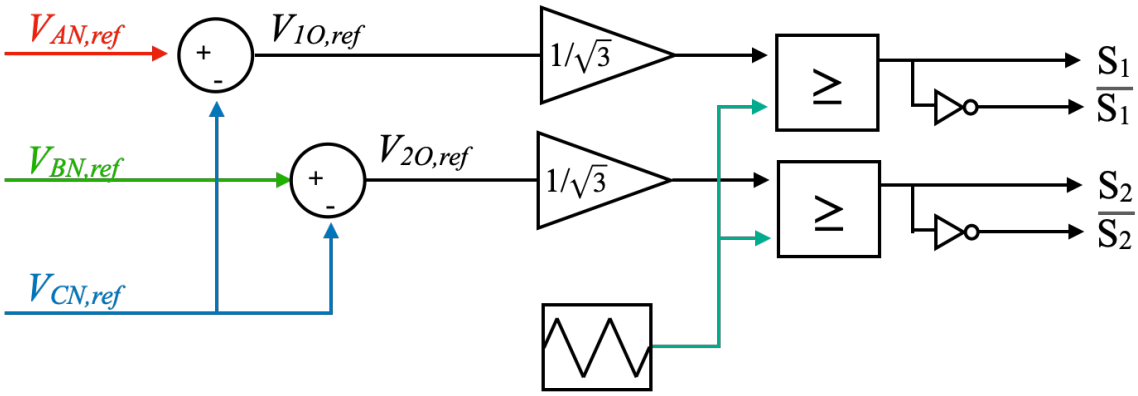

(b) Modulator for the Proposed Power Cell [27], [28]

Fig. 5.2. AFE Control for the Proposed Power Cell

The characteristic of the single-phase half-bridge output inverter is discussed in the previous chapter. The half-bridge output inverter reduces switch count by utilizing the capacitor midpoint. By reducing the total switch count on the output inverter, the DC-link voltage and switching frequency need to increase as the half-bridge inverter reduces output voltage and the number of output voltage levels.

5.2.2 DC-Link Voltage Ripples

The analysis of the DC-link capacitor current must be conducted to understand the characteristics of harmonics, capacitor voltage balancing, and the input current unbalance with the proposed reduced switch-count power cell. The proposed power cell with the current paths identified is shown in Fig. 5.3.

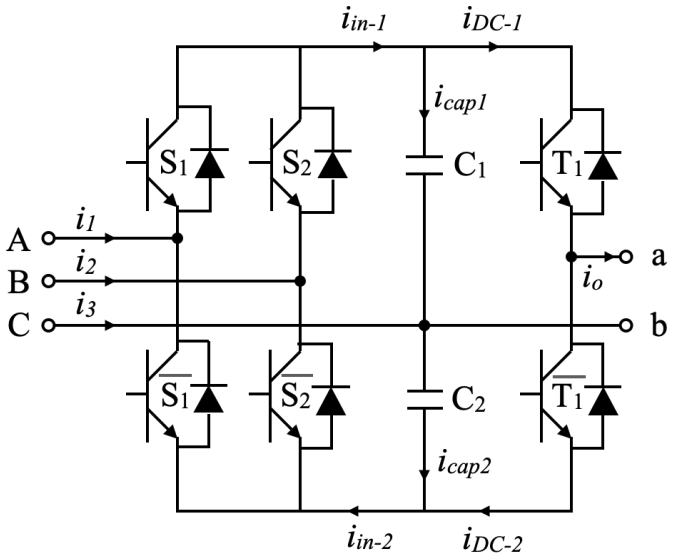

Fig. 5.3. Proposed Six-Switch Regenerative I-Bridge Power Cell with Current Paths

Based on the identified current paths, the impact of the FSTPI AFE inverter on the DC-link capacitors is analyzed. The DC-link voltage of each capacitor is assumed to be half of the total DC-link voltage in the analysis. The output voltage of the FSTPI based on switching states, S, is represented by (5.1) [27], [28].

$$\begin{bmatrix} V_{An} \\ V_{Bn} \end{bmatrix} = \begin{bmatrix} S_1 & \overline{S_1} \\ S_2 & \overline{S_2} \end{bmatrix} \begin{bmatrix} V_{C1} \\ -V_{C2} \end{bmatrix} \tag{5.1}$$

Where V_{An} and V_{Bn} represent the line-to-midpoint output voltage of the FSTPI, and V_{C1} and V_{C2} represent the capacitor voltages of C_1 and C_2.

The previous analysis of the FSTPI expresses the line-to-neutral output voltage of the FSTPI as (5.2).

$$V_{An} = \sqrt{3}V_{in}\sin\left(\omega_{in}t - \frac{\pi}{6}\right)$$
$$V_{Bn} = \sqrt{3}V_{in}\sin\left(\omega_{in}t - \frac{\pi}{2}\right) \quad (5.2)$$

Where V_{in} represents the output voltage magnitude and ω_{in} is the angular frequency of the FSTPI output voltage.

The switching function, S, equals 1 to indicate that the switching device is in an on state and 0 to indicate that the switching device is in the off state. As a result, the conditions for the switching function of the FSTPI are defined by (5.3) [27], [28].

$$S_1 + \bar{S_1} = 1$$
$$S_2 + \bar{S_2} = 1 \quad (5.3)$$
$$0 \le S_x \le 1, \quad x = 1,2 \ldots$$

The switching states, *S*, is expressed by (5.4), given (5.1), (5.2) and (5.3) [27], [28].

$$S_1 = 0.5\left[1 + a_{in}\sin(\omega_{in}t - {}^{\pi}/_{6})\right]$$
$$\bar{S_1} = 0.5\left[1 - a_{in}\sin(\omega_{in}t - {}^{\pi}/_{6})\right]$$
$$S_2 = 0.5\left[1 + a_{in}\sin(\omega_{in}t - {}^{\pi}/_{2})\right] \quad (5.4)$$
$$\bar{S_2} = 0.5\left[1 - a_{in}\sin(\omega_{in}t - {}^{\pi}/_{2})\right]$$
$$where\ a_{in} = 2\sqrt{3}\frac{V_{in}}{V_{dc}}, \qquad |a_o| \le 1$$

Where V_{in} is the output voltage of the FSTPI, and V_{dc} is the DC-link voltage.

The relationship between the switching states, cell input, and FSTPI DC-link current is expressed by (5.5) [27], [28].

$$\begin{bmatrix} i_{in-1} \\ i_{in-2} \end{bmatrix} = \begin{bmatrix} S_1 & S_2 \\ \bar{S_1} & \bar{S_2} \end{bmatrix} \begin{bmatrix} i_1 \\ i_2 \end{bmatrix} \tag{5.5}$$

The cell input current is expressed as (5.6)

$$\begin{aligned} i_1 &= I_{in} \sin(\omega_{in} t - \theta) \\ i_2 &= I_{in} \sin(\omega_{in} t - \frac{2\pi}{3} - \theta) \\ i_3 &= I_{in} \sin(\omega_{in} t + \frac{2\pi}{3} - \theta) \end{aligned} \tag{5.6}$$

Where I_{in} is the fundamental magnitude of the cell input current and θ is the phase shift between the FSTPI voltage and current.

Substituting (5.4) and (5.6) into (5.5), the DC-link input current is defined as (5.7) [27], [28].

$$\begin{aligned} i_{in-1} &= \frac{I_{in}}{2} \sin\left(\omega_{in} t - \theta - \frac{\pi}{3}\right) + \frac{\sqrt{3}}{4} a_{in} \cdot I_{in} \cos\theta \\ i_{in-2} &= -\frac{I_{in}}{2} \sin\left(\omega_{in} t - \theta - \frac{\pi}{3}\right) + \frac{\sqrt{3}}{4} a_{in} \cdot I_{in} \cos\theta \end{aligned} \tag{5.7}$$

The analysis conducted with the FSTPI can be repeated for the half-bridge inverter to obtain the output DC-link current. The output of the half-bridge inverter based on switching states, *T*, is defined by (5.8).

$$[V_{ab}] = [T_1 \quad \bar{T_1}] \begin{bmatrix} V_{C1} \\ -V_{C2} \end{bmatrix} \tag{5.8}$$

The output voltage of the half-bridge inverter is defined by (5.9).

$$V_{ab} = V_o \sin(\omega_o t) \tag{5.9}$$

Where V_o is the output voltage of the half-bridge inverter, and ω_o is the angular frequency of the half-bridge output voltage.

The condition described by (5.3) is applied to the analysis of the half-bridge output inverter, and the switching states, *T*, is expressed by (5.10).

$$\begin{aligned} T_1 &= 0.5[1 + a_o \sin(\omega_o t)] \\ \overline{T_1} &= 0.5[-1 + a_o \sin(\omega_o t)] \\ where\ a_o &= 2\frac{V_o}{V_{dc}}, \qquad |a_o| \le 1 \end{aligned} \tag{5.10}$$

Considering (5.10), the relationship between the switching states, half-bridge output current and DC-link output current is characterized by (5.11).

$$\begin{aligned} I_{DC-1} &= [T_1] \cdot i_o \\ I_{DC-2} &= [\overline{T_1}] \cdot i_o \end{aligned} \tag{5.11}$$

The output current is expressed as (5.12).

$$i_o = I_o \sin(\omega_o t - \emptyset) \tag{5.12}$$

Where I_o is the fundamental magnitude of the half-bridge output current and $\emptyset$ is the phase shift between the half-bridge output voltage and current.

Substituting (5.11) with (5.10) and (5.12), the DC-link output current is expressed as (5.13).

$$\begin{aligned} i_{DC-1} &= \frac{I_o}{2}\sin(\omega_o t - \emptyset) + \frac{a_o I_o}{4}[\cos\emptyset - \cos(2\omega_o t - \emptyset)] \\ i_{DC-2} &= -\frac{I_o}{2}\sin(\omega_o t - \emptyset) + \frac{a_o I_o}{4}[\cos\emptyset - \cos(2\omega_o t - \emptyset)] \end{aligned} \tag{5.13}$$

The capacitor currents, i_{cap1} and i_{cap2}, for the new proposed power cell is described by (5.14).

$$i_{cap1} = i_{in-1} - i_{DC-1}$$

$$i_{cap1} = \frac{I_{in}}{2}\sin\left(\omega_{in}t - \theta - \frac{\pi}{3}\right) + \frac{\sqrt{3}}{4}a_{in}\cdot I_{in}\cos\theta - \frac{I_o}{2}\sin(\omega_o t - \emptyset) - \frac{a_o I_o}{4}[\cos\emptyset - \cos(2\omega_o t - \emptyset)] \quad (5.14)$$

$$i_{cap2} = i_{in-2} - i_{DC-2}$$

$$i_{cap2} = -\frac{I_{in}}{2}\sin\left(\omega_{in}t - \theta - \frac{\pi}{3}\right) + \frac{\sqrt{3}}{4}a_{in}\cdot I_{in}\cos\theta + \frac{I_o}{2}\sin(\omega_o t - \emptyset) - \frac{a_o I_o}{4}[\cos\emptyset - \cos(2\omega_o t - \emptyset)]$$

The voltage across the two DC-link capacitors, C_1 and C_2, in terms of current, is defined by (5.15).

$$V_{C1} = \frac{1}{C_1}\int i_{cap1}dt$$
$$V_{C2} = \frac{1}{C_2}\int i_{cap2}dt \quad (5.15)$$

The analysis of the DC-link currents (5.14) and (5.15) demonstrates the following:

- Input fundamental (ω_{in}) ripples are present in the DC-link capacitors.
- Output fundamental (ω_o) and second order ($2\omega_o$) ripples are present in the DC-link capacitors.
- The fundamental components from the AFE and output inverter are 180° apart between each capacitor and are not present in the whole DC-link voltage.
- The DC-link voltage ripple causes cell input current unbalance.
- The DC-link voltage ripple is present on the output voltage of the power cell as the voltage of each capacitor determines the half-bridge output voltage.

5.3 Capacitor Voltage Balancing of the Proposed Six-Switch Regenerative I-Bridge Power Cell

As the proposed power cell utilizes the midpoint of the capacitor as a neutral point, the voltage balancing between the DC-link capacitors is crucial. Any deviation in the average voltages between the DC-link capacitors must be addressed to ensure proper operation and control of the power cell. The proposed power cell connected to the grid and operating with an RL load is shown in Fig 5.4. The FSTPI operates as an AFE inverter, and the half-bridge inverter operates as an output inverter.

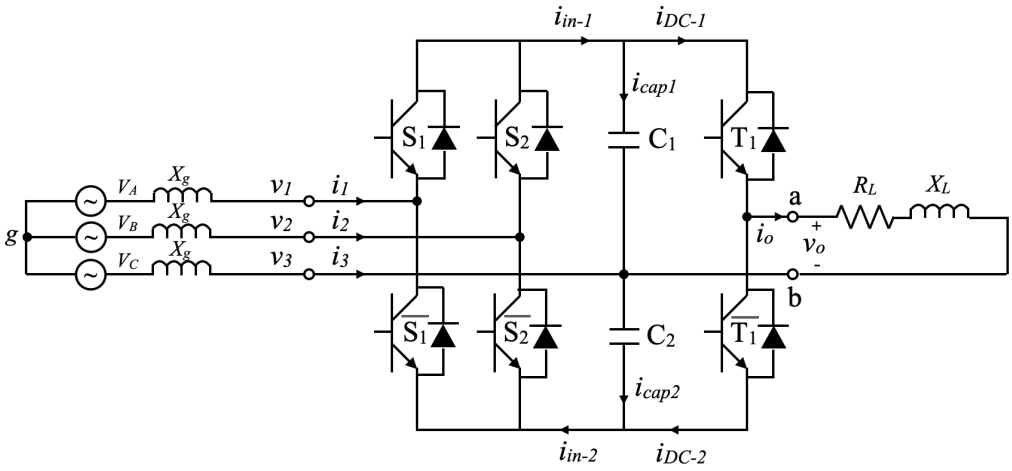

Fig. 5.4. Grid-Connected Six-Switch Regenerative I-Bridge Power Cell with RL load

The analysis of the capacitor currents with a grid-connected power cell with a load can show the individual DC-link capacitor voltage characteristics. If the capacitor voltages are assumed to be different from their reference value, the capacitor current analysis can show whether a voltage balancing mechanism is required. The effect of FSTPI and half-bridge inverter on the DC-link capacitors can be analyzed individually to determine the voltage balancing characteristics.

5.3.1 Impact of the FSTPI AFE on DC-link Capacitors

The FSTPI output line voltage is expressed by (5.16) [27], [28].

$$\begin{aligned} v_{13} &= S_1 \cdot V_{C1} - \overline{S_1} \cdot V_{C2} \\ v_{23} &= S_2 \cdot V_{C1} - \overline{S_2} \cdot V_{C2} \\ v_{12} &= v_{13} - v_{23} \end{aligned} \tag{5.16}$$

Where V_{C1} and V_{C2} represent the voltage of capacitors, C_1 and C_2.

For the analysis of capacitor voltage balancing, the voltage of the capacitors, V_{C1} and V_{C2}, are expressed by (5.17) [27].

$$\begin{aligned} V_{C1} &= \frac{V_{dc}}{2} + \Delta V_{C1} \\ V_{C2} &= \frac{V_{dc}}{2} + \Delta V_{C2} \end{aligned} \tag{5.17}$$

Where V_{dc} represents the total DC-link voltage, ΔV_{C1} represents the deviation from the average voltage in capacitor C_1, and ΔV_{C2} represents the deviation from the average voltage in capacitor C_2.

As the AFE inverter controls the total DC-link voltage, any deviation between the capacitor's voltage will be confined between the DC-link capacitors. Therefore, the relationship between the voltage deviation is expressed by (5.18) [27].

$$\Delta V_{C1} = -\Delta V_{C2} \tag{5.18}$$

The line current for the FSTPI is expressed by (5.19) [27].

$$i_1 = \frac{V_{Ag} - v_{1g}}{X_g}$$
$$i_2 = \frac{V_{Bg} - v_{2g}}{X_g} \tag{5.19}$$

The phase voltage of the FSTPI, v_{1g} and v_{2g}, is expressed by (5.20) [27].

$$v_{1g} = \frac{V_{12} + v_{13}}{3} = \frac{1}{3}[(2S_1 - S_2)V_{C1} + (\bar{S_2} - 2\bar{S_1})V_{C2}]$$
$$v_{2g} = \frac{V_{23} + v_{12}}{3} = \frac{1}{3}[(2S_2 - S_1)V_{C1} + (\bar{S_1} - 2\bar{S_2})V_{C2}] \tag{5.20}$$

Substituting (5.19) with (5.17) and (5.20), the phase current of the FSTPI with the capacitor voltage deviation is represented by (5.21) [27].

$$i_1 = I_{in}\sin(\omega_{in}t + \emptyset) - K_t\Delta V_{C1}$$
$$i_2 = I_{in}\sin\left(\omega_{in}t + \emptyset - \frac{2\pi}{3}\right) - K_t\Delta V_{C2} \tag{5.21}$$

Where *I* represent the maximum magnitude of the phase current, $\emptyset$ is an arbitrary current phase angle, and K_t is a constant that depends on the line filter inductor's internal resistance.

The DC-link input currents, i_{in-1} and i_{in-2}, with the FSTPI current, (5.21), are expressed by (5.22) [27].

$$i_{in-1} = \frac{I_{in}}{2}\sin\left(\omega_{in}t - \theta - \frac{\pi}{3}\right) + \frac{\sqrt{3}}{4}a_{in}\cdot I_{in}\cos\theta - K_t\Delta V_{C1}$$
$$i_{in-2} = -\frac{I_{in}}{2}\sin\left(\omega_{in}t - \theta - \frac{\pi}{3}\right) + \frac{\sqrt{3}}{4}a_{in}\cdot I_{in}\cos\theta - K_t\Delta V_{C2} \tag{5.22}$$

The DC-link input current represented by (5.22) demonstrates that any deviation in capacitor voltage from its reference value will cause a negative DC component that is

proportional to the deviation voltage value. The negative DC component in the DC-link input current will allow the capacitor to return to its reference voltage value and balance the voltage between the two DC-link capacitors [27].

5.3.2 Impact of the Half-Bridge Inverter on DC-link Capacitors

Similar to the capacitor current analysis for the FSTPI, the analysis is conducted on the half-bridge inverter. The output voltage of the half-bridge inverter is expressed by (5.23).

$$v_{ab} = T_1 \cdot V_{C1} - \overline{T_1} \cdot V_{C2} \tag{5.23}$$

The phase current of the half-bridge inverter is expressed by (5.24).

$$i_o = \frac{V_{ab}}{Z_L} \tag{5.24}$$

Considering the (5.17), (5.23), and (5.24), the current for the half-bridge inverter is expressed by (5.25).

$$i_o = I_o \sin(\omega_o t + \delta) + K_L \Delta V_{C1} \tag{5.25}$$

Where I_o is the magnitude of the output current, δ is an arbitrary current phase angle, and K_L is a constant that depends on the load resistance and the internal resistance of the inductor.

Utilizing (5.18), an identical expression for current for the half-bridge inverter is expressed by (5.26).

$$i_o = I_o \sin(\omega_o t + \delta) - K_L \Delta V_{C2} \tag{5.26}$$

The output DC-link current is represented by (5.27).

$$i_{DC-1} = \frac{I_o}{2}\sin(\omega_o t - \emptyset) + \frac{a_o I_o}{4}[\cos\emptyset - \cos(2\omega_o t - \emptyset)] + \frac{K_L \Delta V_{C1} m_o}{2}\sin(\omega_o t) + K_L \Delta V_{C1}$$

$$i_{DC-2} = -\frac{I_o}{2}\sin(\omega_o t - \emptyset) + \frac{a_o I_o}{4}[\cos\emptyset - \cos(2\omega_o t - \emptyset)] + \frac{K_L \Delta V_{C2} m_o}{2}\sin(\omega_o t) + K_L \Delta V_{C2} \quad (5.27)$$

The output DC-link current represented by (5.23) demonstrates that for any deviation in DC-link capacitor voltage, the half-bridge inverter applies a DC component proportional to its reference value and an AC component.

5.3.3 Impact of the Proposed Six-Switch Regenerative I-Bridge Configuration on the DC-link Capacitors

The capacitor current analysis of the FSTPI and half-bridge inverter reveals the characteristics of the two inverters if any voltage deviation occurs between the two DC-link capacitors. The capacitor voltage balancing capability of the proposed power cell can be assessed through the current of the capacitors with both inverters present. From the analysis completed for the DC-link voltage ripples, the capacitor's current in the proposed cell can be expressed by (5.28).

$$i_{cap1} = i_{in-1} - i_{DC-1}$$

$$\begin{aligned} i_{cap1} = {} & \frac{I_{in}}{2}\sin\left(\omega_{in}t - \theta - \frac{\pi}{3}\right) + \frac{\sqrt{3}}{4}a_{in}\cdot I_{in}\cos\theta \\ & - \frac{I_o}{2}\sin(\omega_o t - \emptyset) - \frac{a_o I_o}{4}[\cos\emptyset - \cos(2\omega_o t - \emptyset)] \\ & - K_t\Delta V_{C1} - \frac{K_L\Delta V_{C1} m_o}{2}\sin(\omega_o t) - K_L\Delta V_{C1} \end{aligned} \tag{5.28}$$

$$i_{cap2} = i_{in-2} - i_{DC-2}$$

$$\begin{aligned} i_{cap2} = {} & -\frac{I_{in}}{2}\sin\left(\omega_{in}t - \theta - \frac{\pi}{3}\right) + \frac{\sqrt{3}}{4}a_{in}\cdot I_{in}\cos\theta \\ & + \frac{I_o}{2}\sin(\omega_o t - \emptyset) - \frac{a_o I_o}{4}[\cos\emptyset - \cos(2\omega_o t - \emptyset)] \\ & - K_t\Delta V_{C2} - \frac{K_L\Delta V_{C2} m_o}{2}\sin(\omega_o t) - K_L\Delta V_{C2} \end{aligned}$$

The capacitor voltage deviation values in (5.28) are composed of two components. The negative DC component proportional to its reference value signifies the inherent capacitor voltage balancing capabilities as any deviation in voltage applies a negative DC component that is in opposition to its deviation value. The negative AC component demonstrates that the capacitor with the lower DC voltage will experience a higher fundamental current draw in the case of a voltage deviation. In any case, the AC component does not impact the capacitor voltage balancing of the power cell, and it can be concluded that the proposed power cell does not require any capacitor voltage balancing.

5.4 Low Order Harmonics and Cell Input Current Unbalance Analysis

The DC-link voltage ripple analysis demonstrates the existence of fundamental and second order voltage ripples on the two DC-link capacitors. The voltage ripples that appear on the DC-link capacitors are reflected on the output of the FSTPI and half-bridge inverter. Consequently, the DC-link capacitor voltage ripples pose two different challenges:

- Low order harmonics caused by output inverter's DC-link fundamental and second order voltage ripples.
- Cell input current unbalance and output inverter low order harmonics caused by the FSTPI's fundamental DC-link voltage ripples.

Additionally, the operation and modulation of the FSTPI introduces triplen harmonics in the cell input current, which is not caused by the DC-link voltage ripples but due to the topology of the FSTPI.

5.4.1 Low Order Harmonics

In the DC-link capacitor voltages of the proposed power cell, three voltage ripple components are identified, and the low order harmonics are generated by the DC-link voltage ripples. The low order harmonics are present on the output of both inverters.

a) Grid Side Low Order Harmonics

The grid side voltage and current components do not require a low order harmonic elimination method as the three-phase transformer connection eliminates low order harmonics. The low order harmonics will be eliminated on the grid current for any number of cells per phase. The inherent low order harmonic elimination can be observed with the proposed power cell in the configuration as seen in Fig. 5.5 [27].

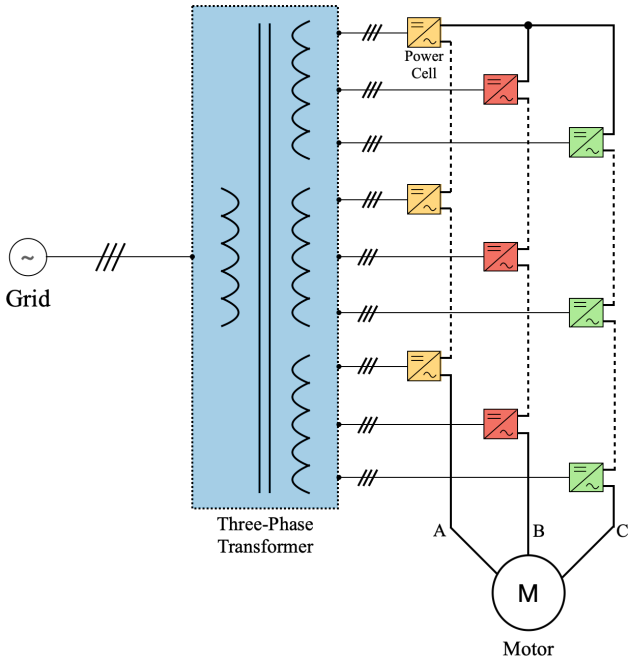

Fig. 5.5. Typical *N*-Cell CHB Drive Configuration

The current observed on the primary side of the transformer is expressed as (5.29)

$$I_{P-abc} = \frac{N_s}{N_p} \sum I_{S-abc} \tag{5.29}$$

Where I_{P-abc} is the three-phase current of the primary side, I_{s-abc} is the three-phase currents of the secondary side, N_P and N_s are the number of turns on the primary and secondary side, respectively.

In the CHB configuration seen in Fig. 5.5, for any number of cells per phase, three distinct DC-link voltage ripples exist as three groups of power cells are responsible for each phase of the load. The DC-link analysis demonstrates a direct correlation between the voltage ripples and the output voltage of the FSTPI and half-bridge inverter. The output voltage modulation of the half-bridge in each power cell group is phase shifted by 120° apart. The low order harmonics caused by the half-bridge inverter, reflecting on the primary

side of the transformer, are canceled as the primary side grid current is defined by (5.29). The FSTPI only causes fundamental low order harmonics, presenting as cell input current unbalance.

b) Load Side Low Order Harmonics

The half-bridge inverter cannot benefit from the inherent low order harmonic cancellation seen on the grid side. As a result, low order harmonics caused by the DC-link voltage ripple exist on the load side without a method of cancellation.

5.4.2 Cell Input Current Unbalance and Load-Side Low Order Harmonics

The cell input current with the proposed power cell is modulated by the FSTPI utilizing a capacitor midpoint, as shown in Fig. 5.6.

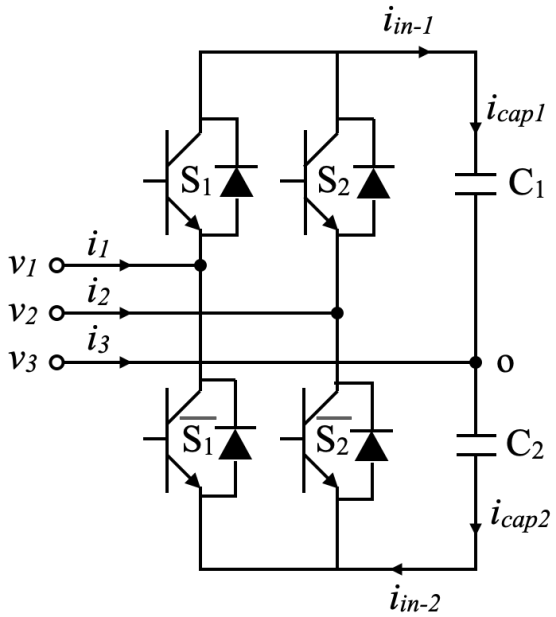

Fig. 5.6. FSTPI AFE in the Proposed Six-Switch Regenerative I-Bridge Power Cell

The capacitor midpoint, *o*, is the neutral point of the FSTPI, and the phase voltages, v_{1o} and v_{2o}, are synthesized using the voltage of the DC-link capacitor. The voltage of the upper capacitor, C_1, provides the positive voltage for the phase voltages, while the

voltage of the lower capacitor, C_2, provides the negative voltage for the phase voltages. As each DC-link capacitor contains input, output fundamental, and second order voltage ripples, the voltage ripple of each capacitor will be reflected on the output phase voltage of the FSTPI.

Considering the input and output fundamental voltage ripple as $v_{dc-ripple}$, the actual output phase voltage of the FSTPI is expressed by (5.29).

$$\begin{aligned} V_{1o} &= V_{max} \sin\left(\omega_{in} t - \frac{\pi}{6}\right) + v_{dc-ripple} \\ V_{2o} &= V_{max} \sin\left(\omega_{in} t - \frac{\pi}{2}\right) + v_{dc-ripple} \end{aligned} \tag{5.29}$$

Where V_{max} is the magnitude of the FSTPI output phase voltage.

The reflection of the voltage ripples on the FSTPI output phase voltage causes the FSTPI to synthesize three-phase voltages that are different in magnitude, causing the cell input current to be unbalanced. Similarly, the half-bridge output inverter operates on the same principle, and the reflection of the voltage ripples is present on the output voltage. The actual output voltage for the half-bridge inverter is expressed as (5.30).

$$V_{ab} = V_{out} \sin(\omega_o t) + v_{dc-ripple} \tag{5.30}$$

Where V_{ab} is the output line voltage of the half-bridge and V_{out} is the magnitude of the output line voltage.

In both cases, addressing the impact of the fundamental ripples is crucial in the proposed power cell as the current unbalance will hinder grid connection compliance, and low order harmonics are undesirable on the load side.

5.4.3 Triplen Harmonics on the Cell Input Current

In a typical three-phase inverter such as the 2L-VSI, the line-to-line voltage share a phase shift of 120° between its output legs. In a balanced system, the phase shift of 120° allows the three phases to share the same triplen harmonic, which are added up and canceled with the neutral point. The two legs of the FSTPI modulate line-to-line voltages that share a phase shift of 60°. The change in phase shift between the modulating legs impacts the triplen harmonic components with the FSTPI, and the triplen harmonic components of the FSTPI are expressed by (5.30) [27].

$$\begin{aligned} v_{13-triplen} &= \sum_{k=3,9,15\ldots} V_k \sin(k(\omega_{in}t + \phi_{13})) \\ v_{23-triplen} &= \sum_{k=3,9,15\ldots} V_k \sin(k(\omega_{in}t + \phi_{13}) - \pi) \\ v_{12-triplen} &= \sum_{k=3,9,15\ldots} 2V_k \sin(k(\omega_{in}t + \phi_{13})) \end{aligned} \tag{5.30}$$

Where k is the triplen harmonic order, V_k is the maximum triplen order line-to-line voltage, and ϕ_{13} is the fundamental phase-shift of the first line-to-line voltage.

The triplen order harmonic phase voltage utilizing (5.30) is expressed by (5.31) [27].

$$\begin{aligned} v_{1g-triplen} &= \sum_{k=3,9,15\ldots} V_k \sin(k(\omega_{in}t + \phi_{13})) \\ v_{2g-triplen} &= \sum_{k=3,9,15\ldots} V_k \sin(k(\omega_{in}t + \phi_{13}) - \pi) \\ v_{3g-triplen} &= 0 \end{aligned} \tag{5.31}$$

The triplen order harmonic phase voltages in the FSTPI demonstrate that the phase connected to the DC-link will not contain any triplen harmonics. For the two voltage-

controlled legs, the triplen harmonic phase voltage and current will be equal in magnitude but in opposing directions [27]. As a result, triplen harmonics will be present in the grid current using an FSTPI.

5.5 Proposed Solutions for Grid Connection Compliance

The IEEE std. 519-2014 standard outlines the maximum current harmonic distortion limit for systems rated from 120V to 69kV and is shown in Table 5.1 [34].

TABLE 5.1. CURRENT DISTORTION LIMITS FOR SYSTEMS RATED 120V THROUGH 69KV [34]

	$3 \leq h < 11$	$11 \leq h < 17$	$17 \leq h < 23$	$23 \leq h < 35$	$35 \leq h < 50$	TDD
Maximum % from fundamental	4.0	2.0	1.5	0.6	0.3	5
h: individual odd harmonic order TDD: Total demand distortion (THD of maximum demand load current)						

Even harmonics for the ranges shown in Table 4.1 must be 25% of the limits given for the odd order harmonics. For the proposed power cell to interface with the grid and operate as a regenerative CHB, the grid side current must satisfy the IEEE std. 519-2014 standard. The challenges identified with the proposed power cell are addressed to ensure compliance with the grid connection standard.

5.5.1 Voltage Injection Method for Cell Input Current Unbalance and Half-Bridge Low Order Harmonics

This work proposes a voltage injection method to address the cell input current unbalance with the FSTPI and low order harmonics with the half-bridge output inverter. In [28], the ripple component of the DC-link capacitors is extracted as (5.32).

$$v_{ripple} = \frac{(V_{C1} - V_{C2})}{2} \tag{5.32}$$

As the unbalance and harmonics caused by the DC-link voltage are due to the reflection of the capacitor voltage ripples on the output voltages, the ripple component expressed by (5.32) is subtracted from the modulation signals to address the unbalance with the FSTPI. The new modified output voltage utilizing (5.31) is expressed by (5.33).

$$\begin{aligned} V_{1O} &= V_{max} \sin\left(\omega_{in} t - \frac{\pi}{6}\right) + v_{dc-ripple} - v_{ripple} \\ V_{2o} &= V_{max} \sin\left(\omega_{in} t - \frac{\pi}{2}\right) + v_{dc-ripple} - v_{ripple} \end{aligned} \tag{5.33}$$

The modified modulation signals allow the inverter to cancel the effect of the DC-link voltage ripple on the output of the FSTPI, effectively canceling the impact of the fundamental voltage ripples applied to the DC-link capacitors. In the proposed power cell, a similar method is proposed to address the unbalance with the FSTPI and address the impact of the fundamental ripples on the half-bridge inverter. The DC-link voltage balancing analysis shows that the capacitor voltage will be inherently balanced for a pure sinusoidal waveform modulated on the FSTPI and half-bridge inverter. However, if a DC offset is introduced in the modulation signal, the inherent voltage balancing of the capacitor is no longer valid and can lead to capacitor voltage balancing issues. The ripple component defined by (5.32) provides an adequate solution for extracting the ripple components in the case where the average voltage of the DC-link capacitors is always equal. However, if any deviations are present in the voltage of the DC-link capacitors, (5.32) introduces DC offset in the modulation signal. The voltage ripple is extracted using an alternate equation to address this challenge for the proposed power cell. The new DC-link ripple voltage is expressed by (5.34).

$$V_{ripple} = \frac{\left[\left(V_{C1} - V_{C1(avg)}\right) - \left(V_{C2} - V_{C2(avg)}\right)\right]}{2} \tag{5.34}$$

Where $V_{C1(avg)}$ and $V_{C2(avg)}$ are the average DC voltage of the DC-link capacitors, C_1 and C_2.

The additional average capacitor voltage terms in (5.34) allow the extracted voltage ripple component to be purely composed of AC components, even in the case of any deviation in average voltage between the two DC-link capacitors. The proposed voltage injection method maintains the inherent voltage balancing capability of the proposed power cell while correcting cell input current unbalance for the FSTPI and low order harmonics for the half-bridge output inverter. The new modulators for the FSTPI and the half-bridge inverter are shown in Fig. 5.7.

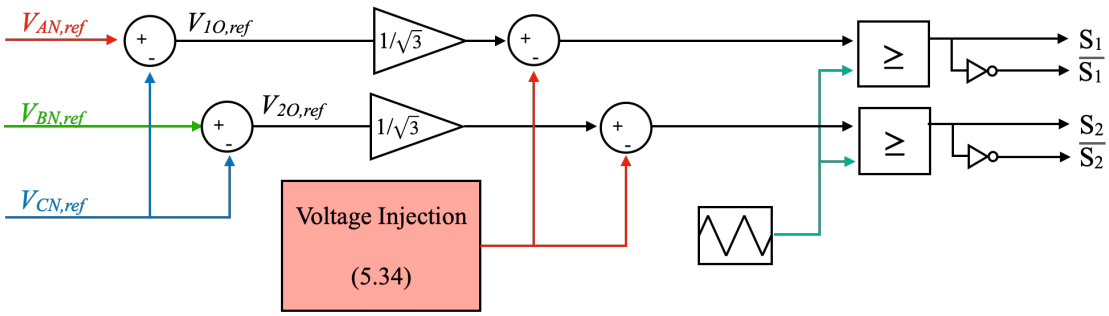

(a) Modulator for the FSTPI AFE utilizing Voltage Injection.

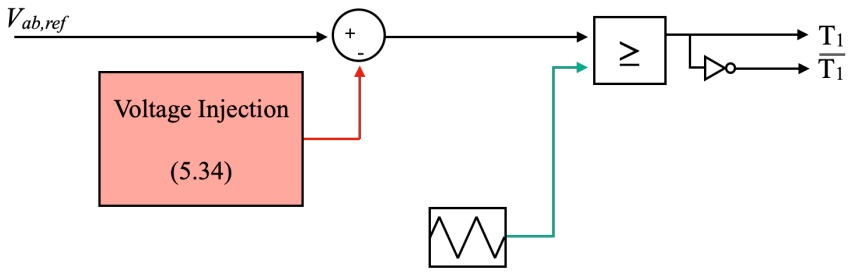

(b) Modulator for the Half-Bridge Output Inverter utilizing Voltage Injection

Fig. 5.7. Modified Modulators for Proposed Voltage Injection Method

5.5.2 Triplen Harmonic Elimination

The three-phase grid connection and the voltage injection method with the proposed power cell eliminate the grid current's low order harmonics caused by the voltage ripples in the DC-link capacitors. The FSTPI, however, introduces triplen harmonics due to its modulation voltages. The triplen harmonics introduced in the grid current are low and do not impact the ability to meet the grid connection standards but can be addressed. The three-phase Reduced Switch-Count Regenerative cell in [27] proposes a phase alternation method to eliminate the grid current unbalance, switching, and triplen harmonics caused by the FSTPI. The phase alternation method is shown in Fig. 5.8 and is used to eliminate the triplen harmonics with the proposed power cell.

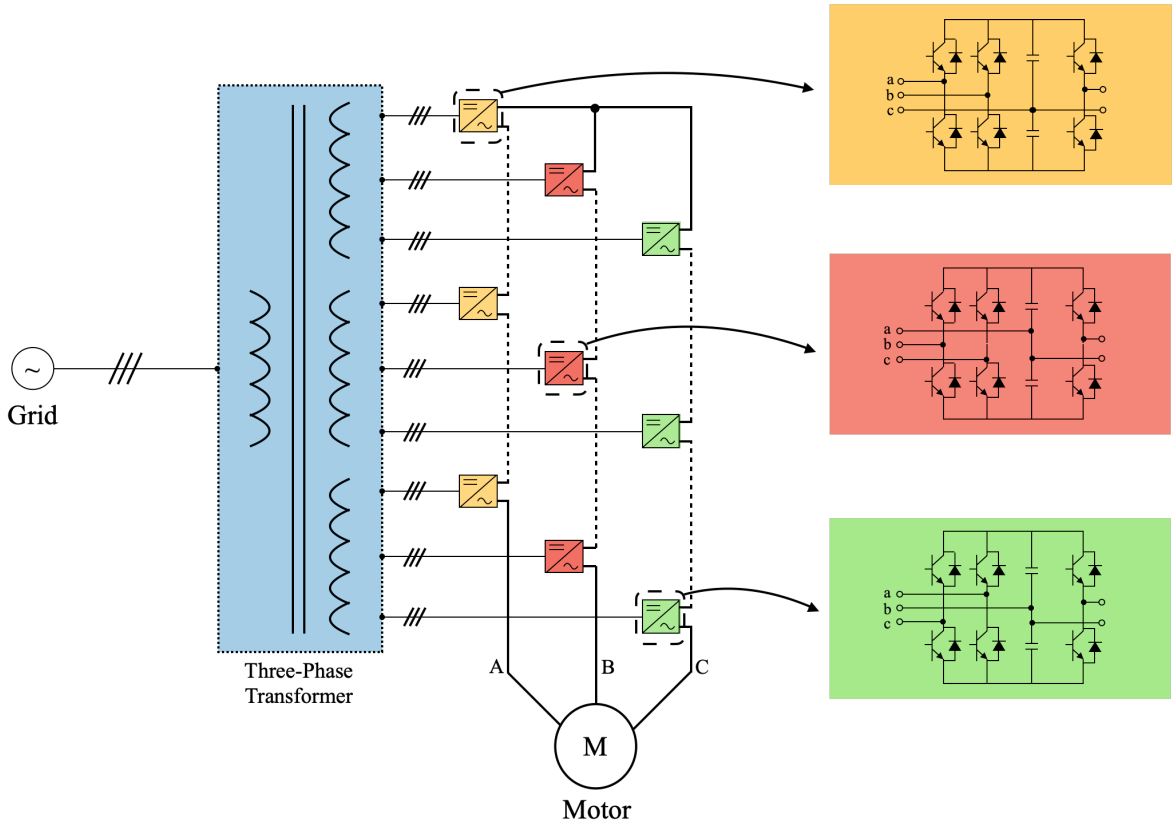

Fig. 5.8. Phase Alternation Method for Triplen Harmonic Elimination [27]

The phase alternation method proposes alternating the grid phase of the phase-connected capacitor midpoint per output phase. The phase alternation method in Fig. 5.8 shows a grid phase C midpoint with the group of output phase A power cells, grid phase A and B with the group of output phase B and C power cells, respectively. The alternation of the grid phases changes the triplen harmonic phase voltage observed on the output of the FSTPI.

The triplen order harmonic phase voltage for grid phase A midpoint connection is expressed by (5.35) [27].

$$\begin{aligned} v_{1g-triplen} &= 0 \\ v_{2g-triplen} &= \sum_{k=3,9,15\ldots} V_k \sin(k(\omega_{in}t + \phi_{13})) \\ v_{3g-triplen} &= \sum_{k=3,9,15\ldots} V_k \sin(k(\omega_{in}t + \phi_{13}) - \pi) \end{aligned} \tag{5.35}$$

The triplen order harmonic phase voltage for grid phase B midpoint connection is expressed by (5.36) [27].

$$\begin{aligned} v_{1g-triplen} &= \sum_{k=3,9,15\ldots} V_k \sin(k(\omega_{in}t + \phi_{13}) - \pi) \\ v_{2g-triplen} &= 0 \\ v_{3g-triplen} &= \sum_{k=3,9,15\ldots} V_k \sin(k(\omega_{in}t + \phi_{13})) \end{aligned} \tag{5.36}$$

The triplen order harmonic phase voltage for grid phase C midpoint connection is expressed by (5.37) [27].

$$v_{1g-triplen} = \sum_{k=3,9,15\ldots} V_k \sin(k(\omega_{in}t + \phi_{13}))$$

$$v_{2g-triplen} = \sum_{k=3,9,15\ldots} V_k \sin(k(\omega_{in}t + \phi_{13}) - \pi) \tag{5.37}$$

$$v_{3g-triplen} = 0$$

As the current relationship with the primary and secondary side of the three-phase transformer is represented by (5.29), the phase alternation method ensures that the triplen harmonics from the power cells will be canceled on the primary side of the transformer for any number of cells per phase.

5.5.3 Switching Harmonics Elimination

The output voltage for one leg of an inverter utilizing SPWM is defined by (5.38) [35].

$$\begin{aligned} v_{leg} = V_1 \sin(\omega_f t + \theta_f) + \sum_{m_c=1}^{\infty} V_{m_c} \sin\left(m_c \frac{\pi}{2}\right) \cos[m_c(\omega_c t + \theta_c)] \\ + \sum_{m_c=1}^{\infty} \sum_{\substack{n_c=-\infty \\ n_c \neq 0}}^{\infty} V_{m_c n_c} \sin\left[(m_c + n_c)\frac{\pi}{2}\right] \cos\big[m_c(\omega_c t + \theta_c) \\ + n_c(\omega_f t + \theta_f)\big] \end{aligned} \tag{5.38}$$

Where ω_f and ω_c are the angular frequencies of the fundamental and carrier, θ_f and θ_c are the phase angles of the fundamental and carrier, and m_c and n_c are carriers and sideband indices.

The output voltage represented by (4.38) can be separated into three components. The first component is the fundamental output voltage, the second component is the carrier harmonics, and the third component is the sideband harmonics. The carrier and sideband

harmonics are the terms in interest to eliminate or minimize the high frequency switching harmonics. The proposed power cell in a regenerative CHB has two different high order harmonic profiles depending on the use of phase alternation method. As a result, two methods are proposed to eliminate switching harmonics.

a) Proposed Switching Harmonics Elimination without Phase Alternation Method

Without the phase alternation method, the proposed power cell in a regenerative CHB shares the same grid phase C midpoint connection. As the FSTPI does not change between the power cells, the grid side high frequency switching harmonics are equal across all power cells in the CHB. The relation between the leg voltages and the output phase voltage of the FSTPI is defined by (5.39).

$$\begin{aligned} V_{AN} &= V_{1O} - V_{NO} \\ V_{BN} &= V_{2O} - V_{NO} \\ V_{CN} &= -V_{NO} = -\left(\frac{V_{1O} + V_{2O}}{3}\right) \end{aligned} \tag{5.39}$$

Where V_{AN}, V_{BN}, and V_{CN} are the output phase voltages and V_{1O} and V_{2O} are the first and second leg voltages.

Based on (5.38) and (5.39), the carrier harmonic voltages are defined by (5.40).

$$\begin{aligned} v_{m_c-A} &= \sum_{m_c=1}^{\infty} \frac{V_{m_c}}{3} \cos(m_c(\omega_c t + \theta_c)) \\ v_{m_c-B} &= \sum_{m_c=1}^{\infty} \frac{V_{m_c}}{3} \cos(m_c(\omega_c t + \theta_c)) \\ v_{m_c-C} &= \sum_{m_c=1}^{\infty} \frac{-2V_{m_c}}{3} \cos(m_c(\omega_c t + \theta_c)) \end{aligned} \tag{5.40}$$

The sideband harmonic leg voltages of the FSTPI are expressed by (5.41).

$$\begin{aligned} v_{1O-m_c n_c} &= \sum_{m_c=1}^{\infty} \sum_{\substack{n_c=-\infty \\ n_c \neq 0}}^{\infty} V_{m_c n_c} \sin\left[(m_c + n_c)\frac{\pi}{2}\right] \cos\left[m_c(\omega_c t + \theta_c) \right. \\ &\qquad \left. + n_c(\omega_f t + \theta_{13})\right] \\ v_{2O-m_c n_c} &= \sum_{m_c=1}^{\infty} \sum_{\substack{n_c=-\infty \\ n_c \neq 0}}^{\infty} V_{m_c n_c} \sin\left[(m_c + n_c)\frac{\pi}{2}\right] \cos\left[m_c(\omega_c t + \theta_c) \right. \\ &\qquad \left. + n_c(\omega_f t + \theta_{13} - 60°)\right] \end{aligned} \tag{5.41}$$

Where θ_{13} is the fundamental angle of the first leg.

The voltage and current of the proposed power cell without the phase alternation method consist of three sideband harmonics groups that can be eliminated [27]:

- $m_c = 1$ and $n_c = \pm 2$
- $m_c = 2$ and $n_c = \pm 1$
- $m_c = 3$ and $n_c = \pm 2$

The phase harmonic voltages of the sideband group ($m_c = 1$ and $n_c = \pm 2$), using (5.41), are expressed as (5.42).

$$\begin{aligned} v_{AN-1,\pm 2} &= \frac{\sqrt{7}}{3} V_{1,\pm 2} \cos\left[(\omega_c \pm 2\omega_f)t + \theta_c \mp 40.9°\right] \\ V_{BN-1,\pm 2} &= \frac{\sqrt{7}}{3} V_{1,\pm 2} \cos\left[(\omega_c \pm 2\omega_f)t + \theta_c \mp 199.1°\right] \\ V_{CN-1,\pm 2} &= \frac{1}{3} V_{1,\pm 2} \cos\left[(\omega_c \pm 2\omega_f)t + \theta_c \pm 60°\right] \end{aligned} \tag{5.42}$$

The phase harmonic voltages of the sideband group ($m_c = 2$ and $n_c = \pm 1$) are defined by (5.43).

$$V_{AN-2,\pm1} = \frac{1}{\sqrt{3}} V_{2,\pm1} \cos\left[\left(2\omega_c \pm \omega_f\right)t + 2\theta_c\right]$$

$$V_{BN-2,\pm1} = \frac{1}{\sqrt{3}} V_{2,\pm1} \cos\left[\left(2\omega_c \pm \omega_f\right)t + 2\theta_c \mp 120°\right] \quad (5.43)$$

$$V_{CN-2,\pm1} = \frac{1}{\sqrt{3}} V_{2,\pm1} \cos\left[\left(2\omega_c \pm \omega_f\right)t + 2\theta_c \pm 120°\right]$$

The phase harmonic voltages of the sideband group ($m_c = 3$ and $n_c = \pm 2$) are defined by (5.44).

$$V_{AN-3,\pm2} = \frac{\sqrt{7}}{3} V_{3,\pm2} \cos\left[\left(3\omega_c \pm 2\omega_f\right)t + 3\theta_c \pm 139.1°\right]$$

$$V_{BN-3,\pm2} = \frac{\sqrt{7}}{3} V_{3,\pm2} \cos\left[\left(3\omega_c \pm 2\omega_f\right)t + 3\theta_c \mp 19.1°\right] \quad (5.44)$$

$$V_{CN-3,\pm2} = \frac{1}{3} V_{3,\pm2} \cos\left[\left(3\omega_c \pm 2\omega_f\right)t + 3\theta_c \mp 120°\right]$$

Based on (5.40), (5.42), (5.43), and (5.44), phase shifting the carrier angle is the only degree of freedom that can minimize or eliminate the high frequency switching harmonics. As the transformer current is a summation of all the secondary side currents, as represented by (5.29), the carrier phase angle of one or a group of power cells can be changed to eliminate the carrier and sideband harmonics. The carrier and the first two sideband harmonic groups can be eliminated by introducing a phase shift of $\left(\frac{360°}{k}\right)$ between each row of power cells, where *k* represents the total number of rows in one phase [27]. The carrier phase angle configuration can be seen in Fig. 5.9. The phase shift of the rows ensures that the summation of the carrier and first two sideband harmonic groups is equal to zero on the primary side. However, the proposed phase shift cannot cancel the third sideband harmonic group due to the $3\theta_c$ term in (5.44).

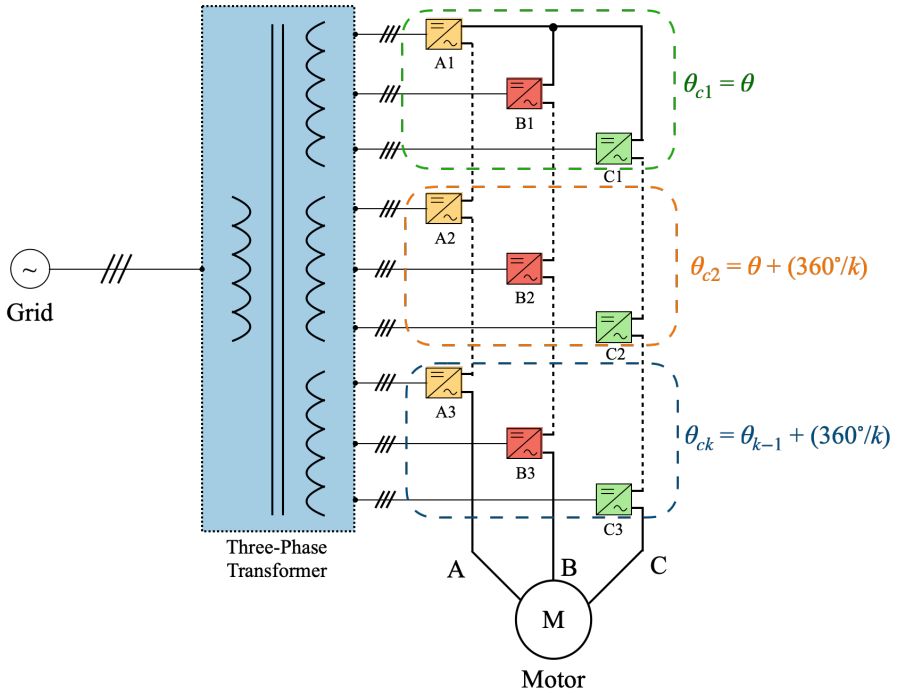

Fig. 5.9. Carrier Shifting Technique for Carrier and Two Sidebands Elimination [27]

In [36], an asymmetric carrier shifting strategy is proposed to reduce the filter size of a conventional regenerative CHB drive using a phase-shifting transformer. The same concept can be applied to eliminate the third sideband harmonic group with the proposed power cell configuration. The carrier phase angles are separated into two categories to address two separate sideband harmonics groups:

- Phase shift between rows of power cells (Different output phases).
- Phase shift between columns of power cells (Same output phases).

The proposed method to eliminate carrier and two sideband harmonic groups with the proposed power cell address the first category of phase shift between rows. However, the $3\theta_c$ term in the third sideband harmonic group negates the effect of the phase shift to cancel the third sideband term on the primary side of the transformer. The condition that cancels the third sideband group is expressed by (5.45).

$$\sum V_{AN-3,\pm2} = 0$$
$$\sum V_{BN-3,\pm2} = 0 \qquad (5.45)$$
$$\sum V_{CN-3,\pm2} = 0$$

The expression (5.44) and condition (5.45) dictate that for the elimination of the third sideband group, a phase shift of $\left(\frac{360°}{3j}\right)$ is required, where j represents the total number of output phases. The phase shift can be applied to the columns of the power cell in addition to the previous phase shift between the rows of the power cell to eliminate all high frequency switching harmonics identified with the proposed power cell without the phase alternation method. The carrier phase angle configuration using asymmetric carrier shifting is shown in Fig 5.10.

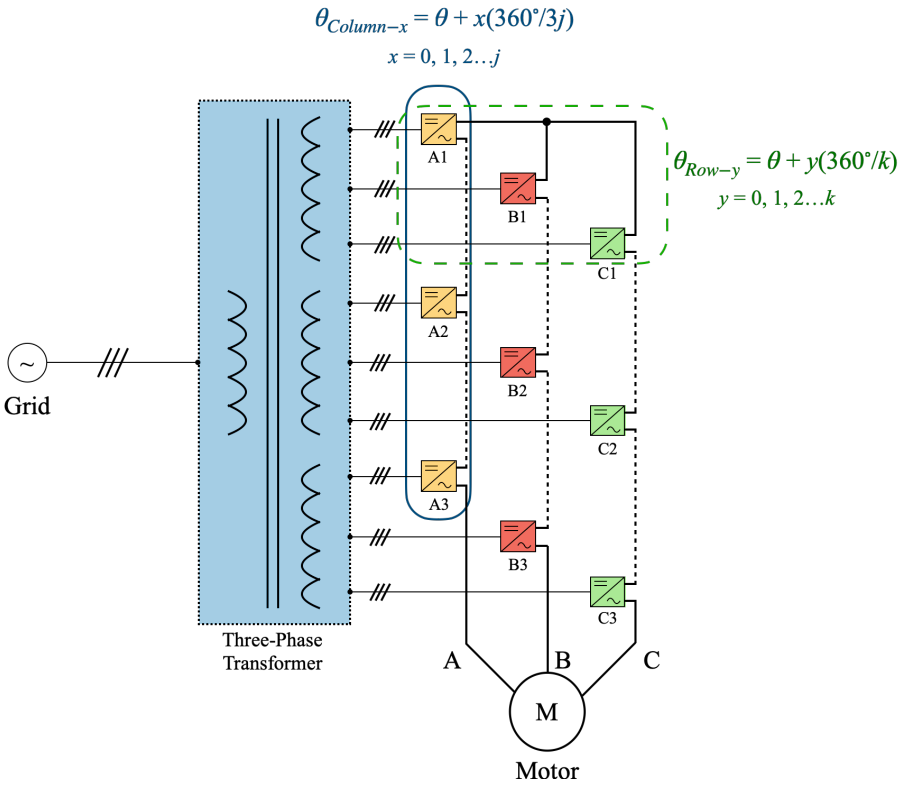

Fig. 5.10. Asymmetric Carrier Shifting for Switching Harmonics Elimination

In a regenerative CHB with three power cells per phase, as seen in Fig 5.10, the proposed method would result in the carrier phase angles shown in Table 5.2.

TABLE 5.2. PROPOSED CARRIER PHASE ANGLE FOR SWITCHING HARMONICS ELIMINATION WITHOUT PHASE ALTERNATION METHOD

	θ_{A1}	θ_{A2}	θ_{A3}	θ_{B1}	θ_{B2}	θ_{B3}	θ_{C1}	θ_{C2}	θ_{C2}
Phase Angle (°)	0	120	240	40	160	280	80	200	320

b) Proposed Switching Harmonics Elimination with Phase Alternation Method

The phase alternation method alternates the grid phase midpoint connection with each column of the power cells or with each output phase. The alternation of the midpoint also changes the output leg voltage of the FSTPI, proposing a different harmonic profile than an FSTPI in a regenerative CHB without phase alternation.

Based on (5.38) and (5.39), the carrier harmonic voltages for grid phase A midpoint connection are expressed by (5.46) [27].

$$v_{m_c-A} = \sum_{m_c=1}^{\infty} \frac{-2V_{m_c}}{3} \cos(m_c(\omega_c t + \theta_c)$$

$$v_{m_c-B} = \sum_{m_c=1}^{\infty} \frac{V_{m_c}}{3} \cos(m_c(\omega_c t + \theta_c) \tag{5.46}$$

$$v_{m_c-C} = \sum_{m_c=1}^{\infty} \frac{V_{m_c}}{3} \cos(m_c(\omega_c t + \theta_c)$$

The carrier harmonic voltages for grid phase B midpoint connection are expressed by (5.47) [27].

$$v_{m_c-A} = \sum_{m_c=1}^{\infty} \frac{V_{m_c}}{3} \cos(m_c(\omega_c t + \theta_c)$$

$$v_{m_c-B} = \sum_{m_c=1}^{\infty} \frac{-2V_{m_c}}{3} \cos(m_c(\omega_c t + \theta_c) \quad (5.47)$$

$$v_{m_c-C} = \sum_{m_c=1}^{\infty} \frac{V_{m_c}}{3} \cos(m_c(\omega_c t + \theta_c)$$

The carrier harmonic voltages for grid phase C midpoint connection are expressed by (5.48) [27].

$$v_{m_c-A} = \sum_{m_c=1}^{\infty} \frac{-2V_{m_c}}{3} \cos(m_c(\omega_c t + \theta_c)$$

$$v_{m_c-B} = \sum_{m_c=1}^{\infty} \frac{V_{m_c}}{3} \cos(m_c(\omega_c t + \theta_c) \quad (5.48)$$

$$v_{m_c-C} = \sum_{m_c=1}^{\infty} \frac{V_{m_c}}{3} \cos(m_c(\omega_c t + \theta_c)$$

Without altering any carrier phase angles, the summation of the carrier harmonic voltages is equal to zero with the phase alternation method. As a result, only the sideband harmonics need to be eliminated for high frequency switching harmonic elimination. The voltage and current of the proposed power cell with the phase alternation method consist of three sideband harmonics groups that can be eliminated [27]:

- $m_c = 1$ and $n_c = \pm 2$
- $m_c = 2$ and $n_c = \pm 1$
- $m_c = 3$ and $n_c = \pm 2$

The phase alternation method alone cannot eliminate any sideband harmonic groups, and the alternation of grid phases proposes a limitation in shifting the phase angle of the carriers. The limitation can be realized using the regenerative CHB configuration in Fig 5.10. The summation of a single cell input phase current consists of sideband harmonic voltages from the first leg of the FSTPI, the second leg of the FSTPI, and harmonic voltages from the midpoint connection. In contrast, the proposed regenerative CHB configuration without phase alternation would be confined to one set of harmonic voltages out of the three. As a result, the asymmetric carrier shifting technique cannot be used for the proposed power cell in a regenerative CHB with the phase alternation method.

Nonetheless, the first two sideband groups can still be eliminated by introducing a phase shift of $\left(\frac{360°}{k}\right)$ between each row of the power cell groups. The proposed method for switching harmonics elimination with the phase alternation method results in a configuration shown in Fig 5.9 and carrier angles shown in Table 5.3 [27].

TABLE 5.3. PROPOSED CARRIER PHASE ANGLE FOR SWITCHING HARMONICS ELIMINATION WITHOUT PHASE ALTERNATION METHOD [27]

	θ_{A1}	θ_{A2}	θ_{A3}	θ_{B1}	θ_{B2}	θ_{B3}	θ_{C1}	θ_{C2}	θ_{C2}
Phase Angle (°)	0	120	240	0	120	240	0	120	240

5.5.4 Proposed Power Cell Configurations Based on Grid Standards Compliance

The analysis of the challenges and solutions of the proposed Six-Switch Regenerative I-Bridge power cell configuration allows two configurations for use in a regenerative CHB. The capability of each configuration is summarized in Table 5.4.

TABLE 5.4. TWO CONFIGURATIONS OF THE PROPOSED POWER CELL IN A REGENERATIVE CHB

	Cell Input Current Unbalance	Low Order Harmonics Elimination	Triplen Harmonics Elimination	Carrier Harmonics Elimination	Sideband Harmonics Elimination ($m_c \leq 2$)	Sideband Harmonics Elimination ($m_c = 3$)
Proposed Power Cell using Phase Alternation	✓	✓	✓	✓	✓	✗
Proposed Power Cell without Phase Alternation	✓	✓	✗	✓	✓	✓

✓ = Addressed ✗ = Not addressed

5.6 Voltage and Current Ratings of Switching Devices

The proposed Six-Switch Regenerative I-Bridge power cell employs alternative inverters for both the AFE and output inverters. When comparing against the conventional regenerative CHB power cell, both ratings are determined with power rating as a fixed parameter. In the proposed power cell, the DC-link voltage doubles due to the reduction in output voltage with the half-bridge inverter. With the increased DC-link voltage, the FSTPI output voltage utilizing SPWM is expressed by (5.43).

$$V_{l-l,FSTPI} = 0.353V_{dc} \tag{5.43}$$

The output voltage for the 2L-VSI utilizing SPWM and third order harmonic injection is expressed by (5.44) [3].

$$V_{l-l,2L-VSI} = 0.707V_{dc} \tag{5.44}$$

The current rating for the FSTPI is determined by the power equation expressed by (5.45).

$$P_{2L-VSI} = P_{FSTPI}$$
$$\sqrt{3}V_{l-l,2L-VSI}I_{2L-VSI} = \sqrt{3}V_{l-l,FSTPI}I_{FSTPI} \tag{5.45}$$

Considering the increase in the DC-link voltage, the required current rating is expressed by (4.46).

$$I_{FSTPI} = I_{2L-VSI} \tag{5.46}$$

With the increase in DC-link voltage, the current ratings for the switching devices remain the same as the 2L-VSI. The same conclusion can be reached for the current ratings of the output inverter switching devices, conducting the same analysis for the half-bridge output inverter. The current ratings for the output inverter are expressed by (5.47).

$$I_{half-bridge} = I_{H-Bridge} \tag{5.47}$$

5.7 Simulation Studies

The verification of the proposed Six-Switch Regenerative I-Bridge power cell and its proposed methods for elimination of harmonics are conducted with a simulation model. A 9-cell regenerative CHB simulation model is developed with the proposed Six-Switch Regenerative I-Bridge power cell to verify its operation and proposed methods in a regenerative CHB. The system parameters are shown in Table 5.5. The load side of the CHB is connected to an induction motor.

TABLE 5.5. SYSTEM PARAMETERS FOR THE PROPOSED POWER CELL IN A 9-CELL CHB

9-Cell Regenerative CHB Simulation Parameters	
Grid Voltage	3 [kV]
Rated Output Current	160 [A]
Nominal Frequency	60 [Hz]
Switching Frequency	1980 [Hz]
Grid-Connecting Filter	3 [mH]
Cell Input Voltage	450 [V]
DC Reference Voltage	1700 [V]
Capacitor Value	8000 [μF]
Number of Motor Pole Pairs	3
Motor Rated Speed	1192 [RPM]

The verification is conducted with three different models. The first model is a baseline model without any proposed methods and demonstrates the inherent capabilities, harmonics, and other challenges of the proposed power cell in a regenerative CHB configuration. The other two simulation models are the two possible configurations identified in the previous section. Each simulation model is subjected to a motor load undergoing motoring and regenerative mode of operation, as shown in Fig. 5.11.

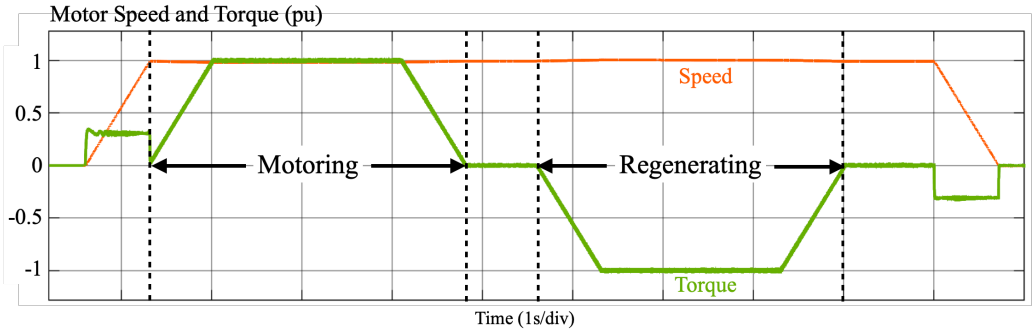

Fig. 5.11. Motor Speed and Torque Profile for Simulation Models

5.7.1 Baseline Model

The motor voltage and current for the baseline model is shown in Fig 5.12.

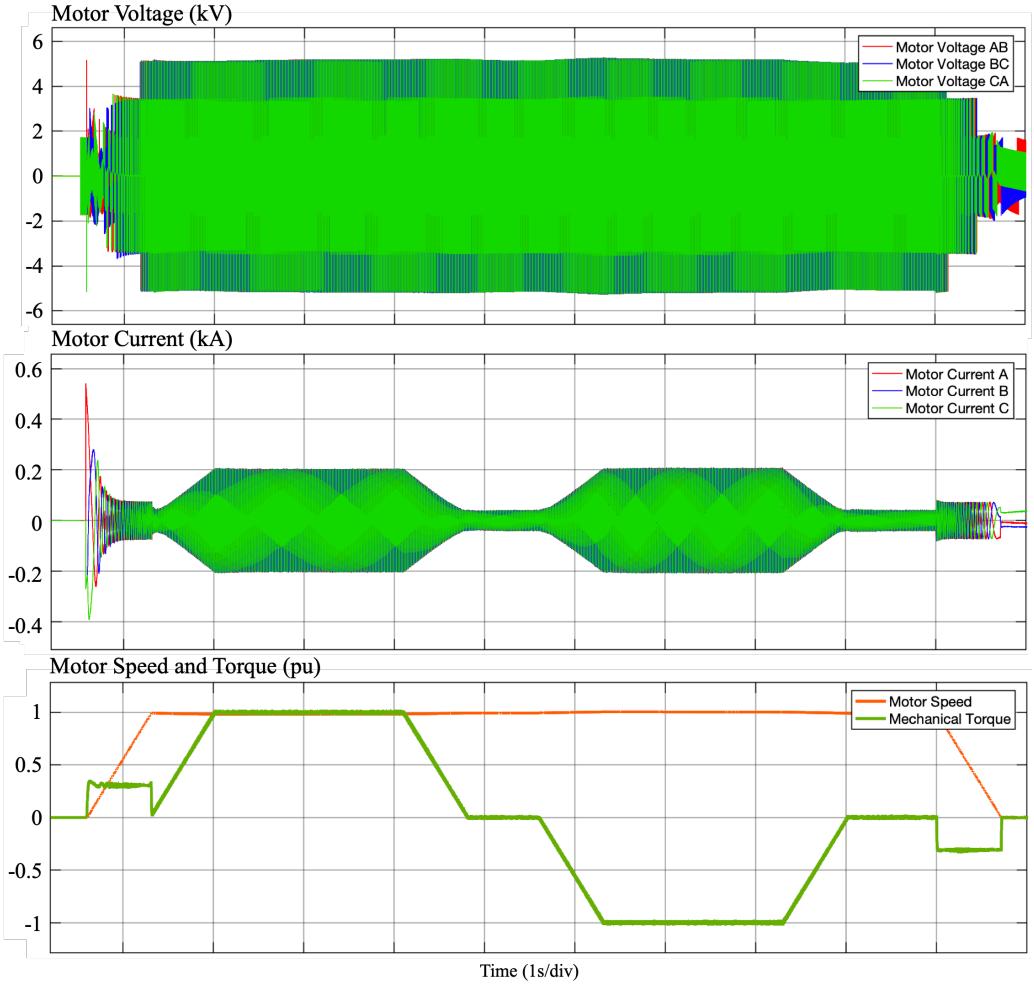

Fig. 5.12. Baseline Simulation Model Motor Voltage and Current

The motor voltage and current demonstrate the motoring and regeneration capability of the proposed power cell in a regenerative CHB. Based on the motor output voltage and current in both modes of operation, the proposed regenerative power cell maintains a stable DC-link voltage and demonstrates a good dynamic response. Fig. 5.13 shows the capacitor voltages during motoring and regenerating conditions.

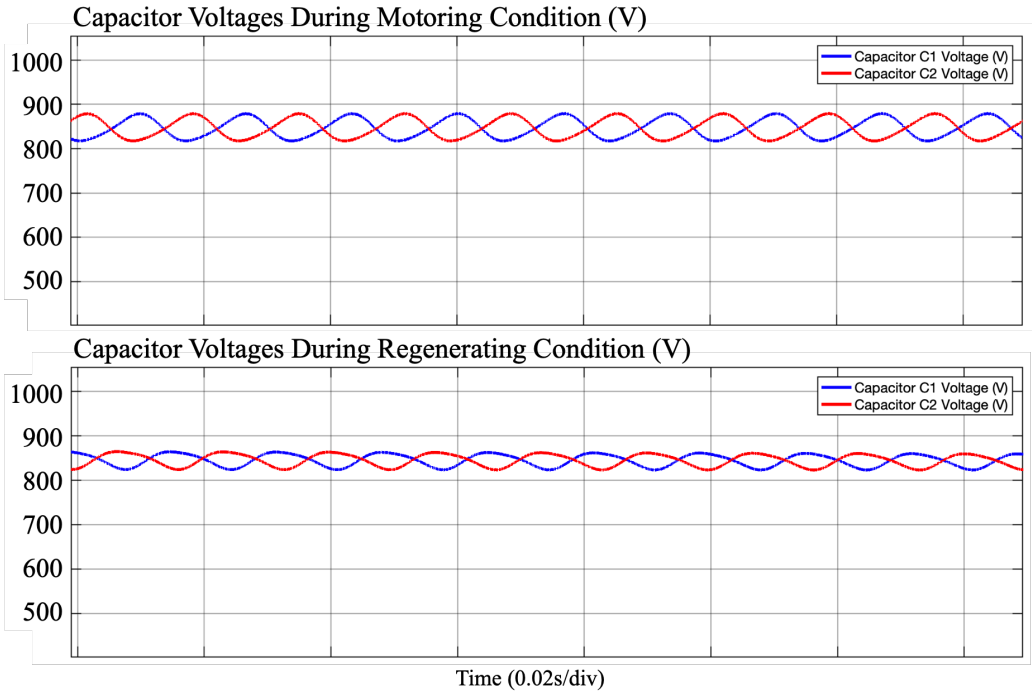

Fig. 5.13. Baseline Simulation Model DC-link Capacitor Voltages

The capacitor voltages in Fig. 5.13 demonstrate the voltage ripples analyzed in the previous section. In the individual DC-link capacitors, fundamental ripple components are expected from the grid and load side inverters, while the fundamental component between the DC-link capacitors will be 180° apart. In both modes of operations, the ripple component and the phase shift are observed. Additionally, the average DC-link voltage of the two capacitors remains equal in both conditions, and the FSTPI AFE has good control over the total DC-link voltage. Fig 5.14 shows the total DC-link voltage in motoring and regenerating conditions.

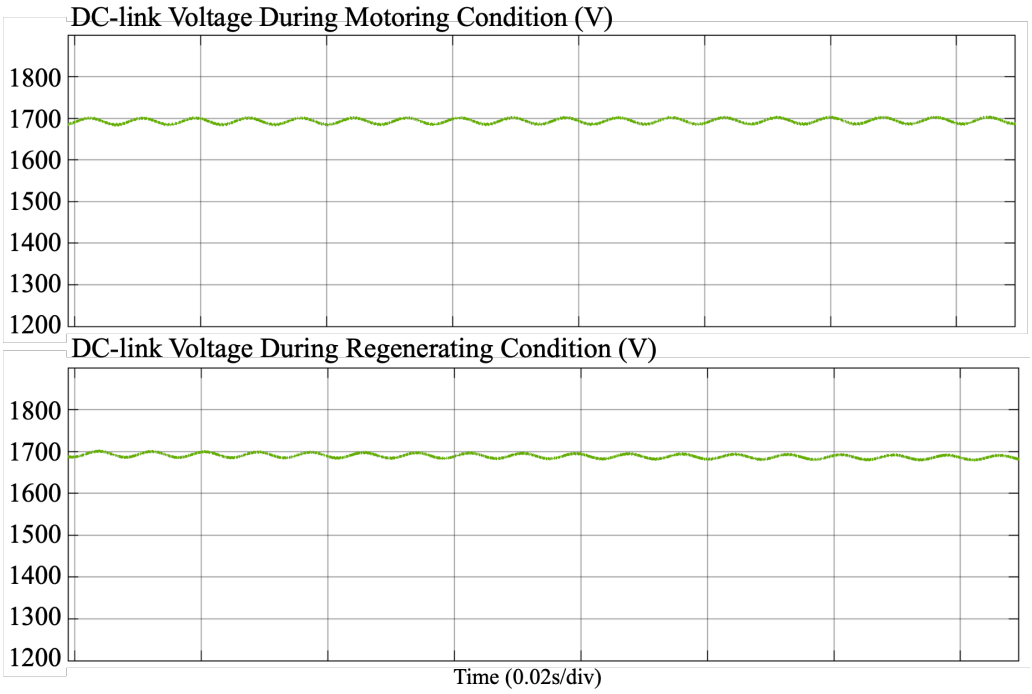

Fig. 5.14. Baseline Simulation Model DC-link Voltage

Fig 5.14 shows the fundamental component cancellation on the whole DC-link and only the second order component from the output inverter remains. The output inverter operates at 60Hz, and a 120Hz voltage ripple is observed on the DC-link. Fig. 5.15 shows the harmonic spectrum of the individual DC-link capacitor and the total DC-link.

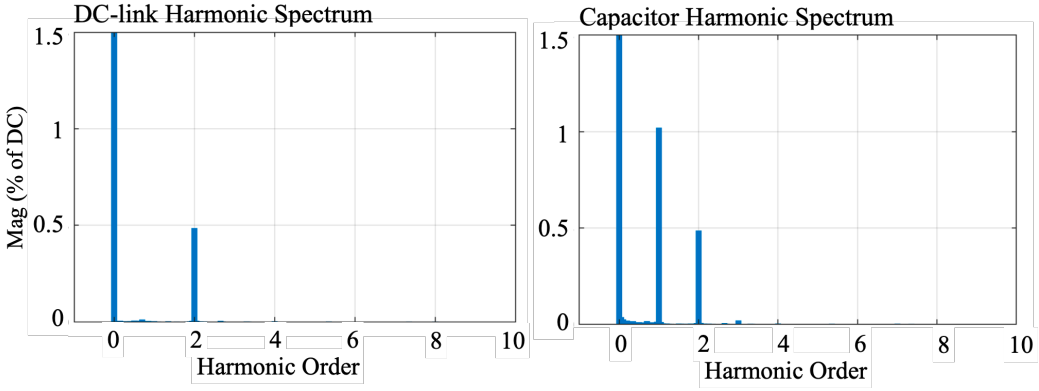

Fig. 5.15. Harmonic Spectrum of the Capacitor Voltages with the Baseline Simulation Model

Fig 5.16 shows the grid and cell input current of the baseline model. As no harmonic or unbalance correction is implemented, triplen harmonics, current unbalance, and switching harmonics are expected in the current waveform.

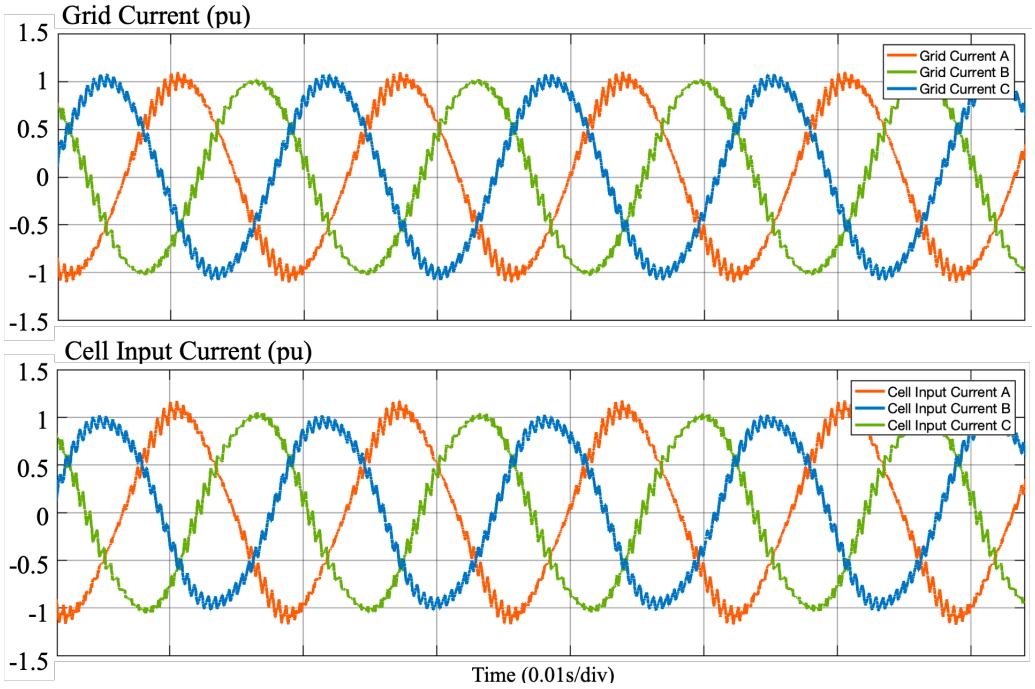

Fig. 5.16. Grid and Motor Current of the Baseline Simulation Model

Fig 5.17 shows the harmonic spectrum of the grid current to identify the harmonics present in the current. Triplen and switching harmonics are seen in Fig. 5.17. The Total Harmonic Distortion (THD) is 5.94%.

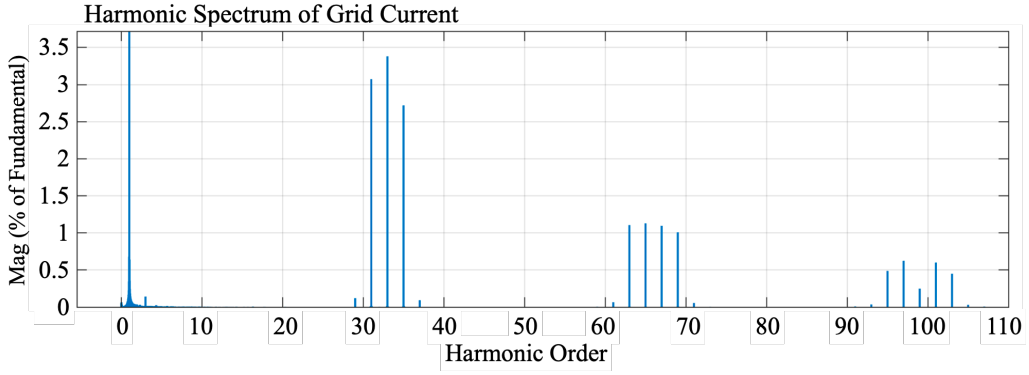

Fig. 5.17. Harmonic Spectrum of Grid Current Without Correction Methods

The voltage balancing capability of the power cell is validated by placing a 100Ω resistor across the capacitor, C_1, and then removing the resistor. The capacitor voltages during the validation are presented in Fig 5.18.

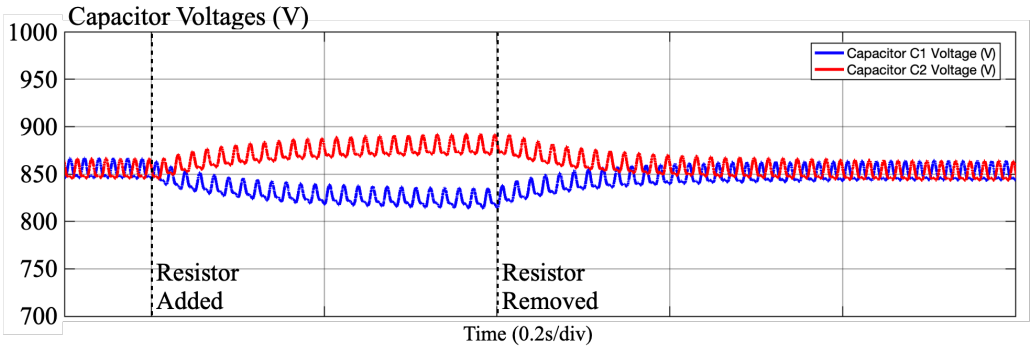

Fig. 5.18. Capacitor Voltages during Voltage Balancing Validation

The capacitor voltages in Fig. 5.18 validate the inherent voltage balancing analysis. The addition of the resistor produces a voltage imbalance between the two DC-link capacitors. Once the resistor is removed, the average DC voltage of the two DC-link capacitors converges to its reference value. The low order harmonic cancellation is observed by setting the motor speed to 0.75pu, corresponding to the 45Hz operation. The harmonic spectrums of the cell input and grid currents are shown in Fig. 5.19.

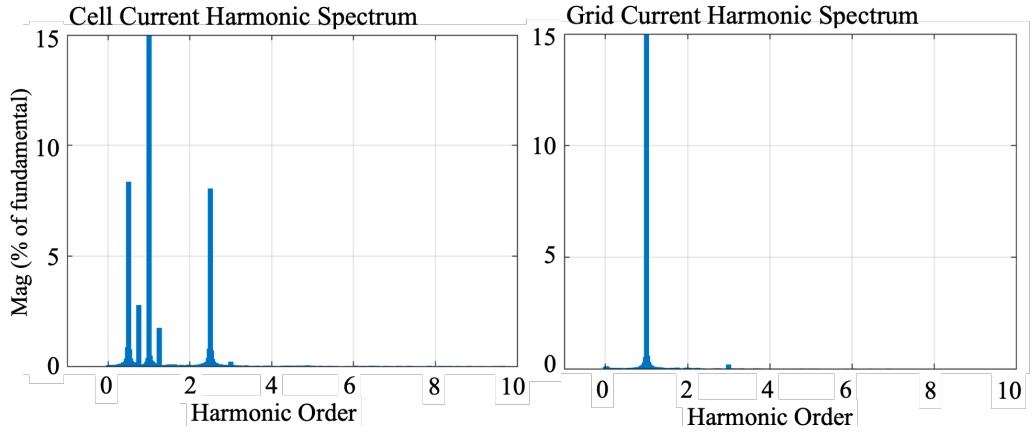

Fig. 5.19. Harmonic Spectrum of Cell Input and Grid Currents Without Correction Methods

In the cell input current harmonic spectrum, four low order harmonics from the output inverter can be identified: ω_o, $2\omega_o$, and $(\omega_{in} \pm 2\omega_o)$. Without any proposed method implemented, the low order harmonics do not exist in the grid current harmonic spectrum as a three-phase transformer allows an inherent low order harmonic cancellation. Fig 5.20 shows the output phase voltage of the motor and its harmonic spectrum.

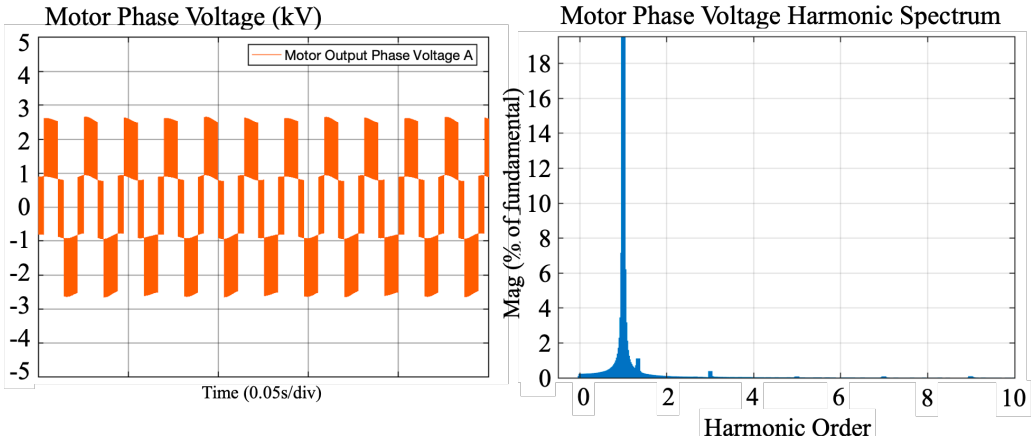

Fig. 5.20. Baseline Model Motor Output Voltage and Harmonic Spectrum

The output phase voltage of the proposed power cell shows the DC-link voltage ripples on the output voltage. Two low order harmonics can be identified: ω_{in} and $3\omega_o$.

5.7.2 Proposed Power Cell using Phase Alternation Method

The first possible configuration of the proposed power cell utilizes phase alternation, the proposed voltage injection method, and switching harmonic elimination. The simulation model is constructed in steps to demonstrate the changes with each method.

a) Phase Alternation Method

Implementing the phase alternation method with the proposed power cell allows the cancellation of triplen and carrier harmonics. Fig 5.21 shows the harmonic spectrum of the grid current after implementing the phase alternation method.

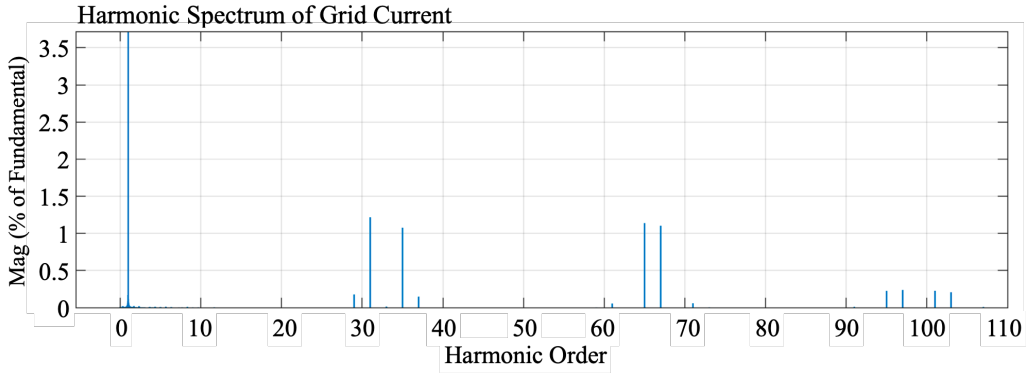

Fig. 5.21. Harmonic Spectrum of Grid Current with Phase Alternation

The harmonic spectrum of the grid current in Fig. 5.20 shows the elimination of the triplen and carrier switching harmonics. The THD drops from 5.94% to 2.39% as a result.

b) Proposed Voltage Injection Method

Implementing the proposed voltage injection method allows the correction of a cell input current unbalance and low order harmonics caused by the DC-link voltage ripples. Fig 5.22 shows the cell input current after implementing the proposed voltage injection method.

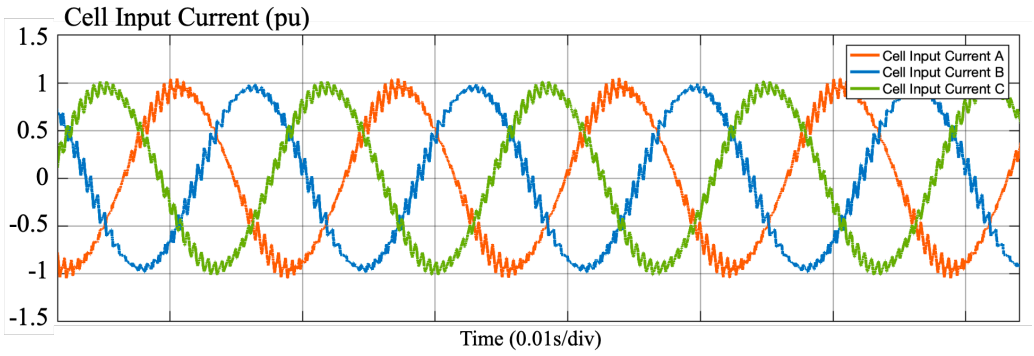

Fig. 5.22. Cell Input Current with Voltage Injection Method

The difference in the cell input current unbalance is seen when comparing Fig. 5.22 to Fig. 5.16. The cell input current is balanced after implementing the voltage injection method. However, as the phase alternation method addresses the current unbalance

observed in the grid current, the THD of the grid current does not change with the implementation of the voltage injection method. Fig. 5.23 shows the harmonic spectrum of the cell input current and motor phase voltage to show the low order harmonic cancellation.

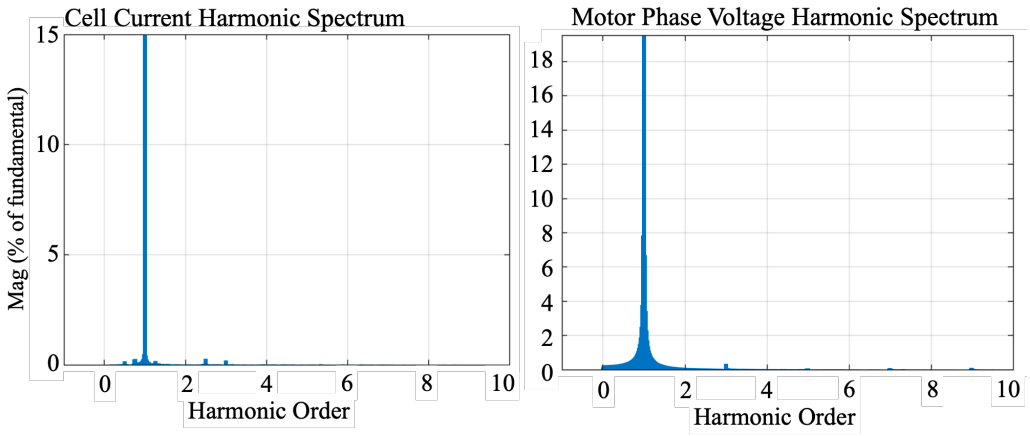

Fig. 5.23 Harmonic Spectrums of Cell Input Current and Motor Phase Voltage with Voltage Injection

Comparing the harmonic spectrums from Fig. 5.23 with those from Fig. 5.19 and Fig. 5.20, the low order harmonics present in the baseline model are eliminated or reduced. The cell input current harmonic spectrum in Fig 5.23 demonstrates a significant reduction in low order harmonics compared to the baseline model. The harmonic spectrum of the motor phase voltage in Fig. 5.23 demonstrates the elimination of grid fundamental voltage in the baseline model.

c) Switching Harmonic Elimination with Phase Alternation Method

The switching harmonic elimination is achieved by applying the carrier phase shift defined in Table 5.3. The carrier phase shift allows the cancellation of the first two sidebands harmonic group. Fig 5.24 shows the grid current and the harmonic spectrum of the grid current after implementing the proposed switching harmonic elimination method.

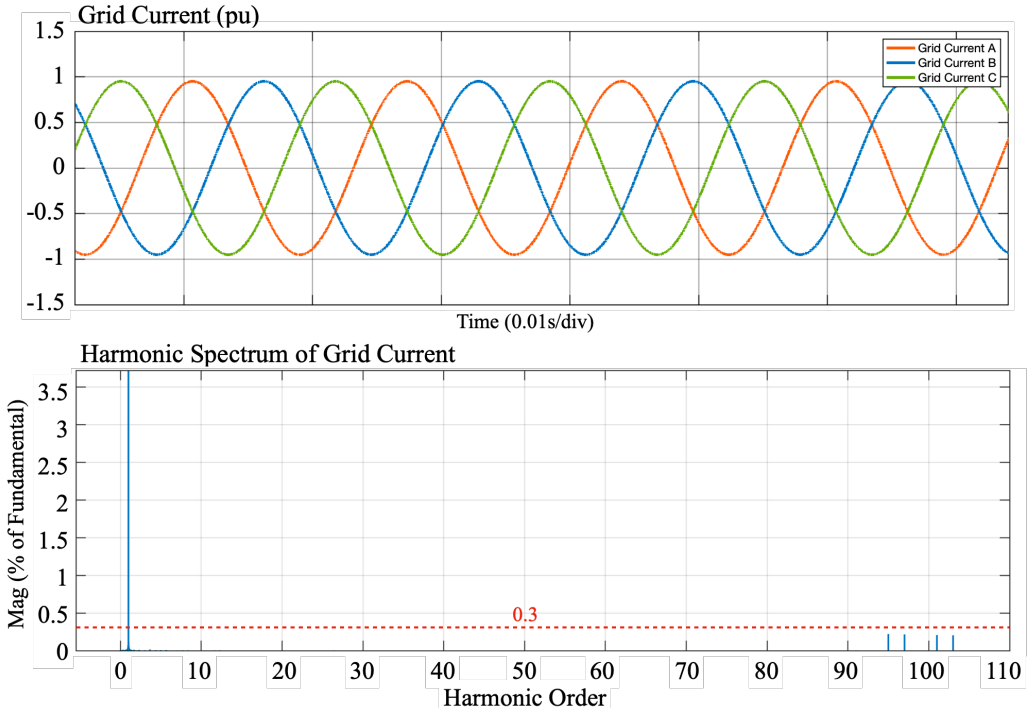

Fig. 5.24. Grid Current and Harmonic Spectrum with Switching Harmonic Elimination and Phase Alternation Method

The grid current shows a drastic reduction in switching harmonics compared to Fig. 5.16. The harmonic spectrum of the grid current reflects the changes in harmonic content. The first two sideband groups are eliminated, and only the third sideband is present. The red line indicates the maximum harmonic content for odd harmonic order of 50 or larger. The third sideband group is well below the maximum allowable harmonic content for grid connection compliance. The THD reduces from 2.39% to 0.49%.

5.7.3 Proposed Power Cell Configuration without Phase Alternation

The second possible configuration of the proposed power cell utilizes only voltage ripple injection and switching harmonic elimination method. Without the phase alternation method, the proposed configuration utilizes a different switching harmonic elimination method that allows the cancellation of all three sideband groups.

a) Proposed Voltage Injection Method without Phase Alternation

Fig. 5.25 shows the grid current and its harmonic spectrum with only voltage injection method implemented.

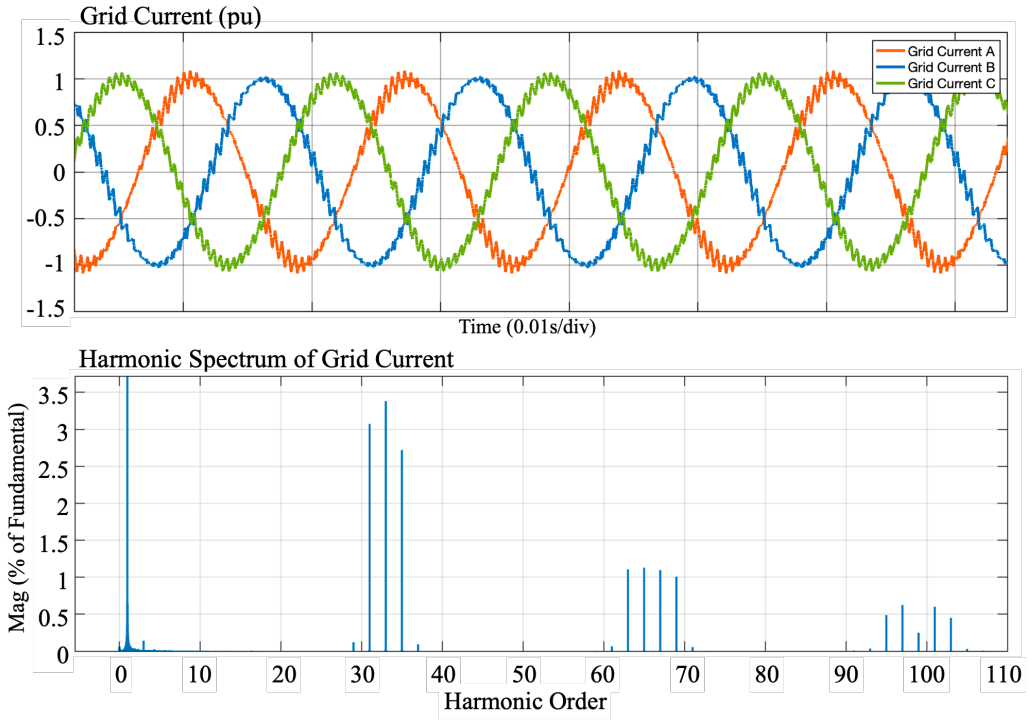

Fig. 5.25. Grid Current and Harmonic Spectrum with Only the Voltage Injection Method

The proposed voltage injection method allows the correction of cell input unbalance and low order harmonic elimination on the load side. The harmonics do not change from the baseline model, only implementing the voltage injection method.

b) Switching Harmonic Elimination without Phase Alternation

Without phase alternation, the proposed power cell configuration utilizes a switching harmonic elimination method to cancel all sideband groups identified. The carrier phase shift defined in Table 5.2 is applied to the simulation model. Fig. 5.26 shows the grid current and harmonic spectrum with switching harmonic elimination.

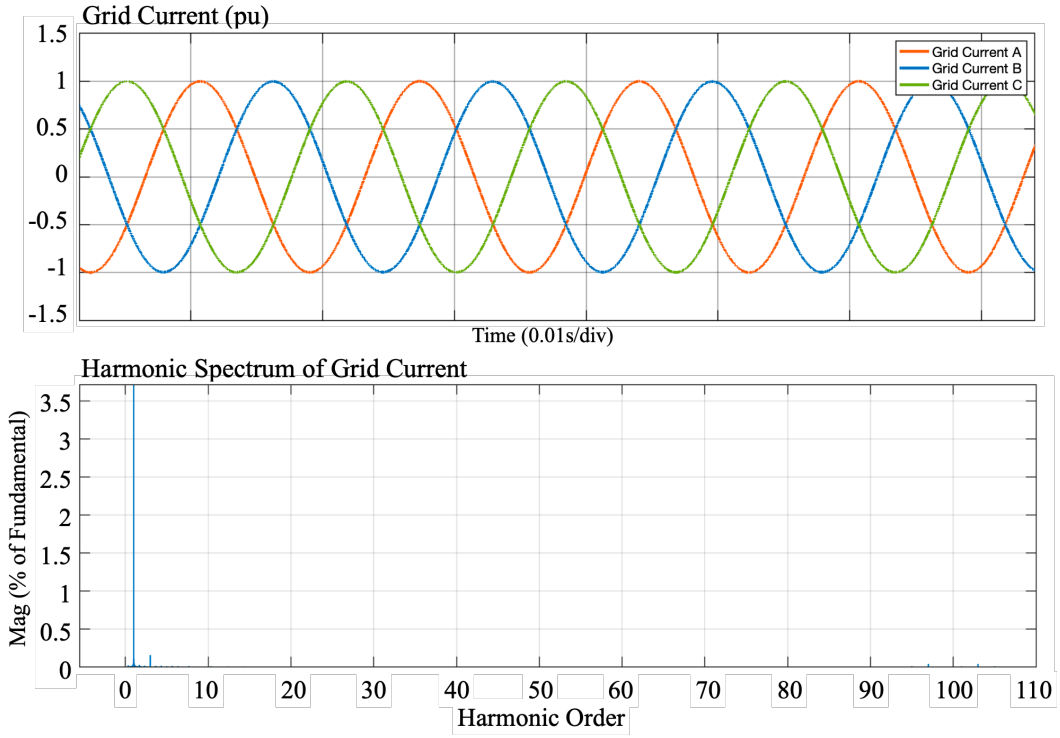

Fig. 5.26. Grid Current and Harmonic Spectrum with Switching Harmonic Elimination without Phase Alternation

Implementing the switching harmonic elimination without phase alternation demonstrates the cancellation of all carrier and sideband harmonics identified in the previous section. The only harmonic that remains in the grid current is the small triplen harmonic component identified. The triplen harmonic identified is well below the maximum third order harmonics identified by IEEE std. 519-2014 of 4.0%. Implementing the switching harmonics elimination without phase alternation reduces the THD of the grid current from 5.98% to 0.25%.

5.8 Summary

A new reduced switch-count regenerative power cell is proposed. The Six-Switch Regenerative I-Bridge power cell utilizes an FSTPI AFE and a single-phase half-bridge inverter with a capacitor midpoint connection to reduce the switch count by four compared to the conventional regenerative CHB power cell. The reduction in switch count reduces the challenges identified with the conventional regenerative CHB power cell, which are cost, size, and complexity. The proposed power cell configuration is analyzed in detail and verified with a 9-cell CHB motor drive simulation model.

The analysis and methods to address challenges with the Six-Switch Regenerative I-Bridge power cell are proposed. Two possible configurations of the proposed configuration show cancellation of low order harmonics, triplen harmonics, high frequency switching harmonics, and current unbalance with the FSTPI. Both configurations demonstrate compliance with grid connection standards, IEEE std. 519-2014.

The first configuration of the Six-Switch Regenerative I-Bridge power cell proposes a voltage injection method to address the current unbalance from the grid current and low order harmonics from the motor current. A phase alternation method is proposed to eliminate triplen harmonic, and a carrier phase-shifting method is proposed to eliminate high frequency switching harmonics from the grid current. The combination of phase alternation and carrier phase-shifting method cancels all harmonics analyzed except for the third sideband harmonic group. However, the third sideband harmonic group does not impact compliance with grid connection standards.

The second configuration of the Six-Switch Regenerative I-Bridge power cell proposes a voltage injection method to address the current unbalance from the grid current and low order harmonics from the motor current. An asymmetric carrier shifting method is proposed to eliminate all carrier, and sideband harmonic groups analyzed. Triplen harmonics exist in the grid current with the configuration. However, the triplen harmonic does not impact compliance with grid connection standards.

Table 5.6 compares the conventional regenerative CHB power cell, existing reduced switch-count power cells, and the proposed Six-Switch Regenerative I-Bridge power cell. All the power cells were compared against a conventional regenerative CHB power cell.

TABLE 5.6. COMPARISON OF REDUCED SWITCH-COUNT REGENERATIVE CHB POWER CELLS WITH CONVENTIONAL REGENERATIVE CELL FOR AN *N*-CELL CHB

<table>
<tr><th rowspan="2">Cell Configuration</th><th colspan="3">Three-Phase AFE</th><th colspan="3">Single-Phase AFE</th></tr>
<tr><th>Conventional Regenerative Cell [15]-[17]</th><th>Reduced Switch-Count Regenerative Cell [27]</th><th>Proposed Six-Switch Regenerative I-Bridge Power Cell</th><th>H-H Cell [22]</th><th>Semi-Reduced Cell [23], [24]</th><th>Reduced Cell [25]</th></tr>
<tr><td># of Switches</td><td>10</td><td>8</td><td>6</td><td>8</td><td>6</td><td>4</td></tr>
<tr><td>Output Voltage Levels</td><td>$2N+1$</td><td>$2N+1$</td><td>$N+1$</td><td colspan="2">$2N+1$</td><td>$N+1$</td></tr>
<tr><td>AFE Control Frame</td><td colspan="3">Rotating d-q</td><td colspan="3">Stationary abc (more complex)</td></tr>
<tr><td>Low order harmonic elimination</td><td colspan="3">Effective for any number of cells/phase</td><td colspan="3">Effective only if number of cells/phase is multiple of three</td></tr>
<tr><td>Low order DC-link ripples</td><td colspan="3">Output 2nd order</td><td colspan="3">Output and input 2nd order</td></tr>
<tr><td rowspan="3">Capacitor ripples</td><td rowspan="3">Output 2nd order</td><td>Output 2nd order</td><td>Output 2nd order</td><td colspan="3">Output and input 2nd order</td></tr>
<tr><td>Input fundamental</td><td>Input fundamental</td><td></td><td colspan="2">Input Fundamental</td></tr>
<tr><td></td><td>Output fundamental</td><td colspan="3">Output fundamental</td></tr>
<tr><td>AFE Switches current rating</td><td>I_{in}</td><td>$2I_{in}$</td><td>I_{in}</td><td>$1.73I_{in}$</td><td>$3.46I_{in}$</td><td>$1.73I_{in}$</td></tr>
<tr><td>Switches voltage ratings</td><td colspan="2">V_{dc}</td><td>$2V_{dc}$</td><td colspan="2">V_{dc}</td><td>$2V_{dc}$</td></tr>
</table>

Chapter 6

Experimental Implementation and Validation

6.1 Experimental Implementation of the CHB Power Cells

A scaled-down single power cell setup with an RL load was implemented to verify the theoretical analysis and simulation studies. The conventional regenerative CHB power cell was constructed in the single power cell setup, later modified to implement the Reduced Switch-Count Regenerative cell and the proposed Six-Switch Regenerative I-Bridge power cell. The Active Front End control scheme identified with each topology was implemented to ensure proper validation, operation, and control. The overall view of the experimental setup is shown in Fig. 6.1.

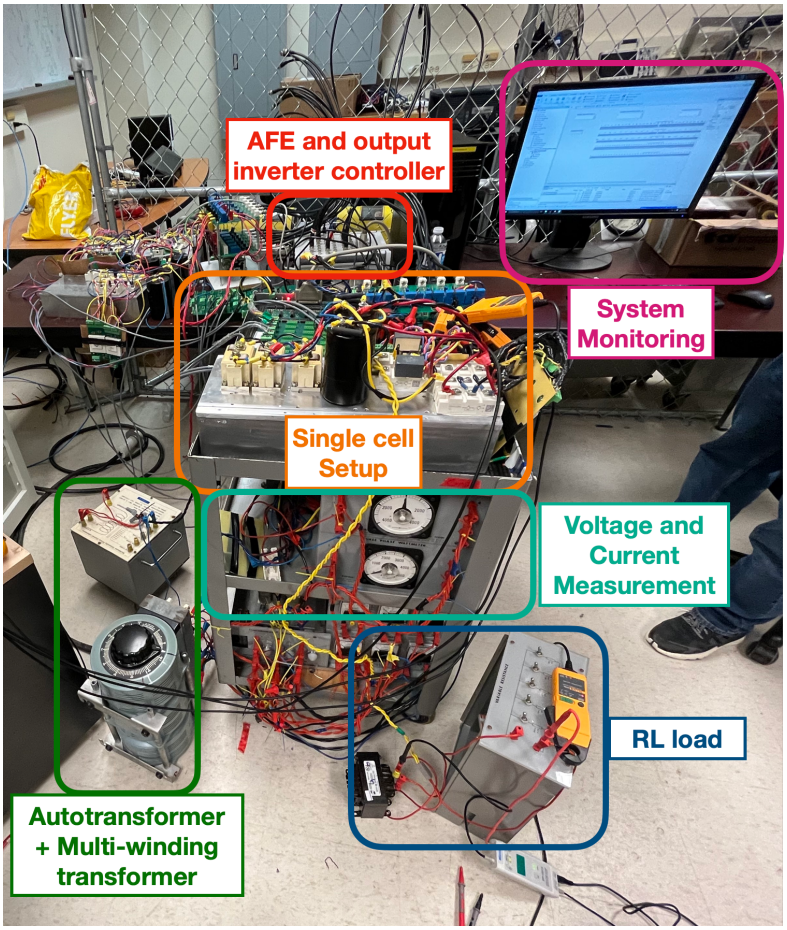

Fig. 6.1. Overview of the Experimental Single Cell Setup

The whole experimental setup can be divided into four separate sections:

1) **Grid Circuits:** Equipment related to the connection with the grid, such as transformers, grid filters, and measurement tools.

2) **Power cell:** Prototype of the power cells to be tested.

3) **Control and Monitoring:** Controller for AFE and inverter modulation. Voltage and current measurement circuits for the controller.

4) **Output load:** RL load connected to the output of the inverter

6.1.1 Grid Circuits

The connection of the AFE inverter to the grid is achieved using an autotransformer shown in Fig. 6.1. The voltage of the three-phase grid connection is adjusted to target a DC-link voltage of 190V with the three single-cell power cell topologies that were tested. A 4-mH three-phase inductor serves as a grid filter for the AFE inverter. The line-to-line output RMS voltage of the autotransformer is measured with the analog measurement tools in Fig. 6.1 and voltage sensors on the measurement circuit in Fig. 6.2.

The multi-winding transformer is utilized to pre-charge the capacitors in the power cell setup. The primary side of the transformer is connected to the grid. The secondary side provides multiple output voltages used with a diode rectifier to charge capacitors to an appropriate voltage prior to starting the controller for the power cell. The pre-charging circuit ensures that the inrush current remains low at the time of starting.

6.1.2 Power Cell

Fig 6.2. shows the single power cell implemented for experimental validation.

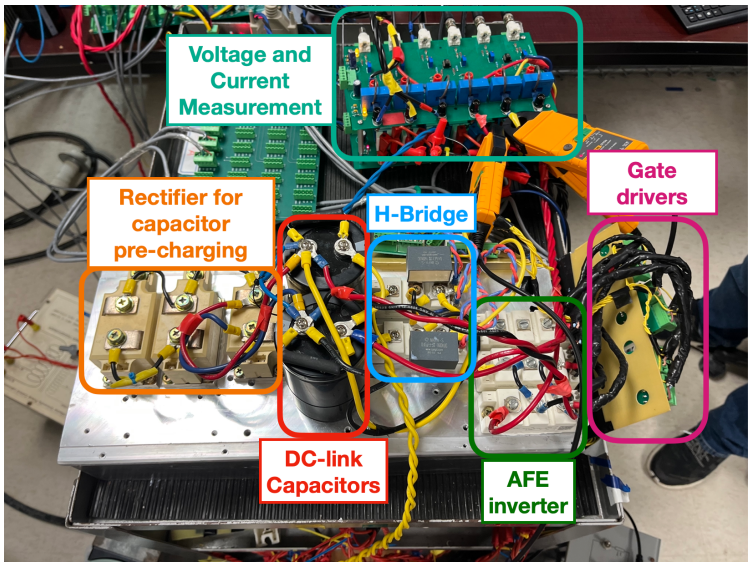

Fig. 6.2. Experimental Power Cell Configuration

The three-phase 3.8kV/380A diode bridge is used to pre-charge the capacitors. As the single power cell was constructed to test multiple three-phase power cell configurations, the AFE inverter utilized three 1.2kV/50A half-bridge IGBT modules to allow the implementation of the 2L-VSI and FSTPI. The output inverter utilized two 1.2kV/50A half-bridge IGBT modules to allow the implementation of an H-bridge and half-bridge inverter. Five gate drivers were used to control the AFE and output inverter. For the single cell to remain flexible with all configurations, two 400V/4700μF electrolytic capacitors were connected in series and then connected in parallel with the IGBT modules. The arrangement of the DC-link capacitors allowed the midpoint connection that the reduced switch-count power cells required.

6.1.3 Control and Monitoring

The experimental setup consisted of three measurement sources. The analog measurement tools shown in Fig. 6.1 measured the three-phase grid voltage, current, and power. The voltage and current measurement circuit shown in Fig. 6.2 measured the three-phase grid voltage, current, and DC-link voltages required for the controller to operate the control scheme for the AFE inverter. The voltage and current measured through the measurement circuit provide the necessary signal for the operation of the PLL and control of the DC-link voltage based on its reference value. In addition, the grid phase voltage, three-phase grid current, DC-link voltage, output voltage, and current were monitored with an oscilloscope. Fig 6.3 shows the dSpace MicroLabBox controller used for the experimental setup. The dSpace MicroLabBox controller is programmed to operate the AFE control scheme and generate modulation signals for the AFE and output inverter.

Fig. 6.3. dSpace MicroLabBox Controller for the Experimental Single-Cell Setup

Fig. 6.4 shows the gate driver interface board for the single cell setup. The gating signal generated from the dSpace MicroLabBox was converted to appropriate signals for the gate drivers seen in Fig. 6.1.

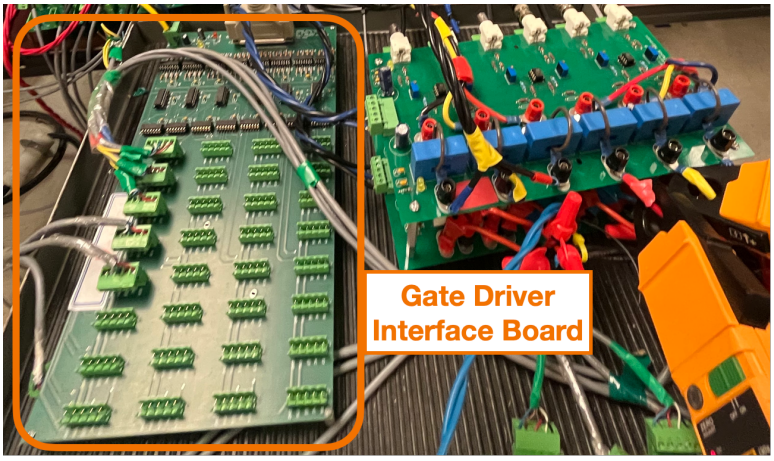

Fig. 6.4. Gate Driver Interface Board for dSpace MicroLabBox

6.1.4 Output Load

One RL load was used across all power cell configurations and is shown in Fig. 6.5. A bank of resistors with all resistors connected in parallel with a single-phase 5-mH inductor was used to create the RL load for the output inverter. The final resistance of the

resistor bank was 12.63Ω. The resistor bank and the single-phase inductor were connected in series for the output RL load.

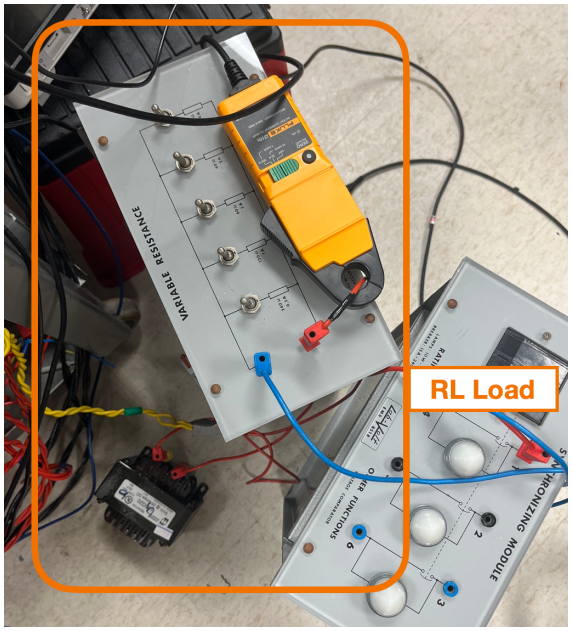

Fig. 6.5. RL load for the Experimental Setup

6.2 Experimental Validation of the Conventional Regenerative CHB Power Cell

The existing and proposed reduced switch-count power cell uses the conventional regenerative power cell as a benchmark. The experimental implementation of the single-cell CHB power cell was first constructed as a conventional regenerative CHB power cell to validate the theoretical and simulation results of the thesis. The experimental implementation utilized an input RMS line voltage of 80V, 4mH grid filter, total DC-link capacitance of 2350uF, and a DC-link voltage of 170V. Fig. 6.6 shows the three-phase grid current with phase A grid voltage.

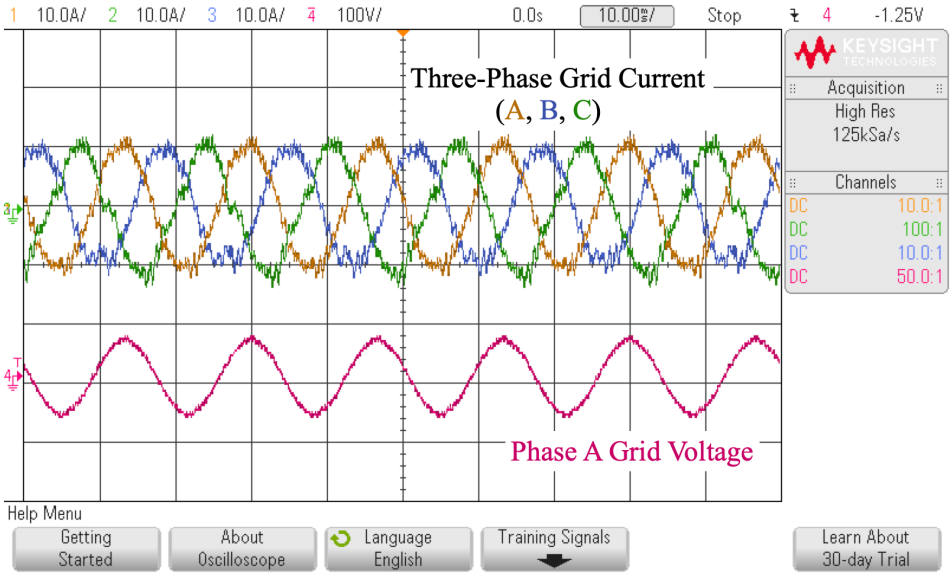

Fig. 6.6. Phase A Grid Voltage and Three-Phase Grid Current of the Conventional Regenerative CHB Power Cell

In the experimental implementation of the conventional regenerative CHB power cell, the reference reactive power for the 2L-VSI AFE was set to 0 VAR for unity power factor operation. Fig 6.7 shows the phase A grid voltage overlaid on the three-phase current.

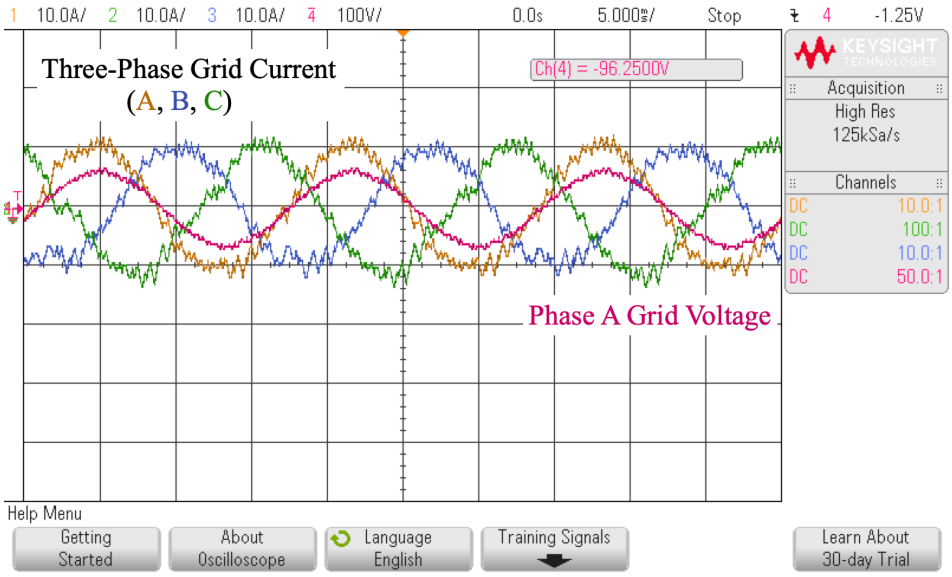

Fig. 6.7. Phase A Grid Voltage and Three-Phase Grid Current of the Conventional Regenerative CHB Power cell (Overlaid).

The grid voltage and current in Fig. 6.7 show the unity power factor operation of the 2L-VSI. Between the grid voltage and current of phase A, the phase angle is equal while the H-Bridge output inverter is connected to the output RL load, and not operating at unity power factor. Fig 6.8 shows the total DC-link voltage and the H-Bridge output current.

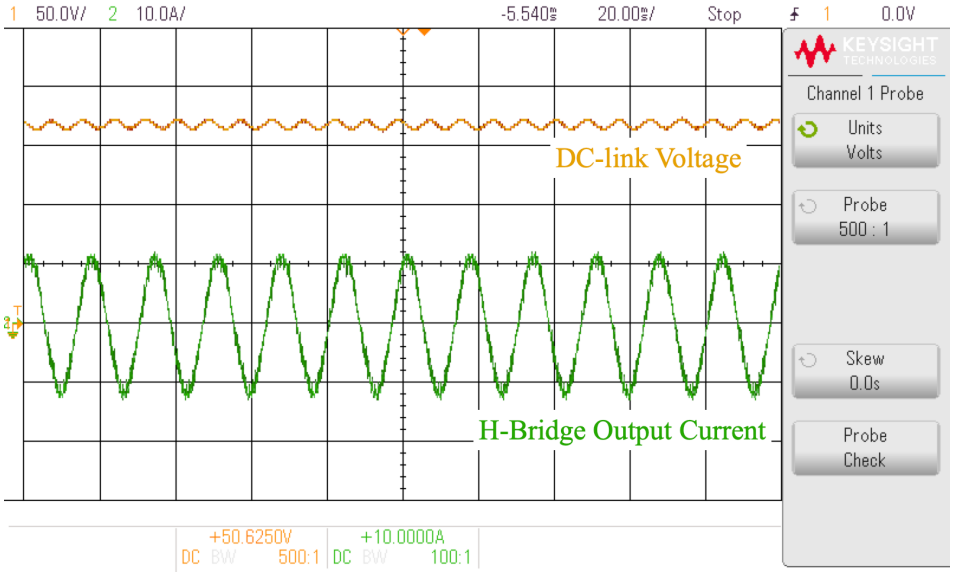

Fig. 6.8. DC-link Voltage and H-Bridge Output Current of the Conventional Regenerative CHB Power Cell.

The average voltage of the DC-link is stable at 170V and contains second order harmonic ripples. The H-Bridge output current is shown in Fig. 6.8 for reference. The frequency of the modulating signal is set to 60Hz. Fig 6.9 shows the H-Bridge output voltage and current. The output voltage and current of the H-Bridge serve as a benchmark for the proposed Six-Switch Regenerative I-Bridge power cell. In Fig 6.9, the output voltage shows three levels. The H-Bridge outputs the positive and negative voltage equivalent to the voltage of the whole DC-link. Additionally, a zero-voltage output level exists.

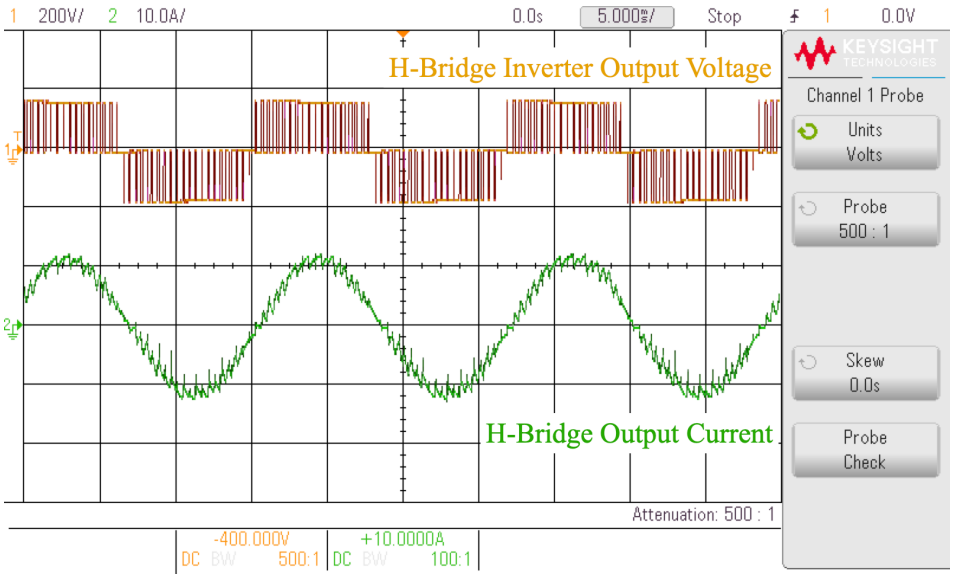

Fig. 6.9. H-Bridge Output Voltage and Current of the Conventional Regenerative CHB Power Cell

6.3 Experimental Validation of the Reduced Switch-Count Regenerative Cell

The experimental validation of the Reduced Switch-Count Regenerative Cell was conducted by replacing the 2L-VSI with an FSTPI in the single-cell experimental setup. The control scheme of the 2L-VSI with the modified modulator was implemented to operate the FSTPI AFE. The experimental implementation utilized an input RMS line voltage of 40V, 4mH grid filter, total DC-link capacitance of 2350uF, and a DC-link voltage of 170V. Fig. 6.10 shows the three-phase grid current with phase A grid voltage.

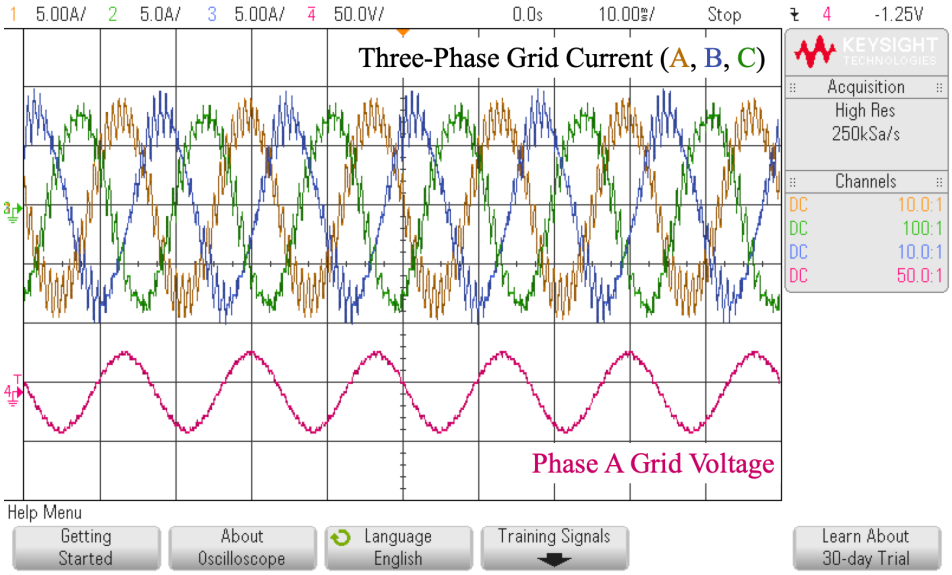

Fig. 6.10. Phase A Grid Voltage and Three-Phase Grid Current of the Reduced Switch-Count Regenerative Cell.

The reference reactive power for the Reduced Switch-Count Regenerative cell was set to 0 VAR for unity power factor operation. Fig 6.11 shows the phase A grid voltage overlaid on the three-phase current.

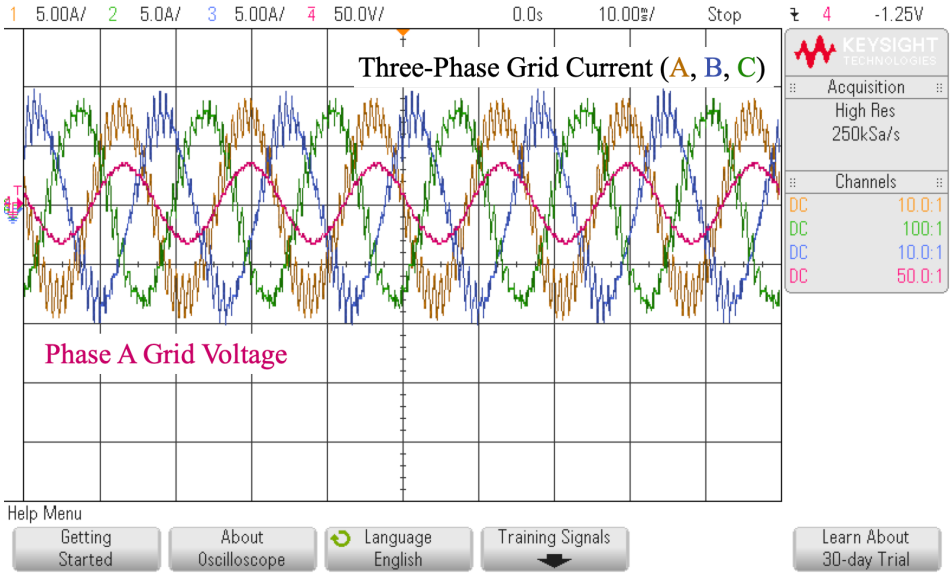

Fig. 6.11. Phase A Grid Voltage and Three-Phase Grid Current of the Reduced Switch-Count Regenerative Cell (Overlaid).

Fig. 6.11 shows a successful unity power factor operation of the FSTPI AFE with an equal phase angle between the grid phase A voltage and current. With the experimental implementation of the FSTPI AFE, an increase in harmonics is observed compared to the 2L-VSI. Fig 6.12 shows the individual voltages of the two DC-link capacitors.

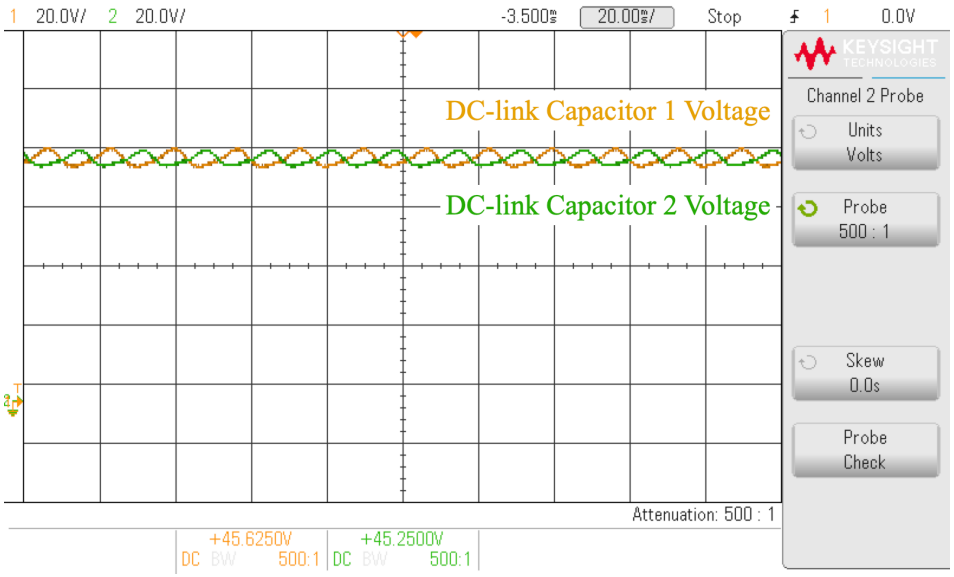

Fig. 6.12. DC-link Capacitor Voltages of the Reduced Switch-Count Regenerative Cell

The analysis of the DC-link ripples for the Reduces Switch-Count Regenerative cell demonstrates the existence of fundamental voltage ripples from the FSTPI that are 180° apart in phase angle. Fig 6.12 validates the analysis as fundamental voltage ripples, and a phase shift between the capacitors is observed. In addition, the average capacitor voltages remain equal between the two capacitors. Fig 6.13 shows the H-Bridge output voltage and current.

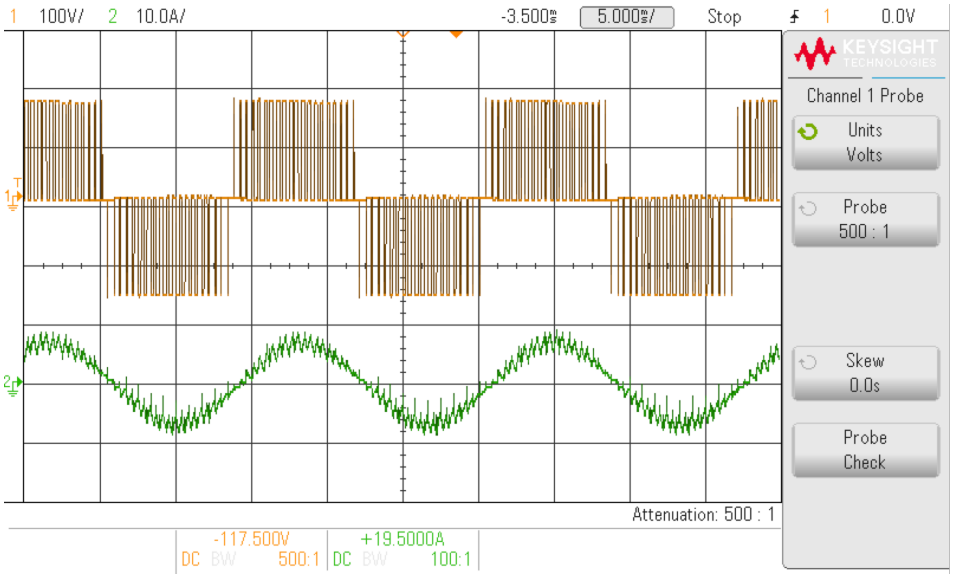

Fig. 6.13. H-Bridge Output Voltage and Current of the Reduced Switch-Count Regenerative Cell

As the Reduced Switch-Count Regenerative Cell does not modify the output inverter of the power cell, the characteristic of the output inverter is expected to remain the same. Fig. 6.13 shows that the output of the H-Bridge between the conventional regenerative CHB power cell and the Reduced Switch-Count Regenerative Cell does not change.

6.4 Experimental Validation of the Proposed Six-Switch Regenerative I-Bridge Power Cell

The experimental validation of the proposed Six-Switch Regenerative I-Bridge power cell was conducted by modifying the output inverter of the Reduced Switch-Count Regenerative Cell. The experimental implementation utilized an input RMS line voltage of 40V, 4mH grid filter, total DC-link capacitance of 2350uF, and a DC-link voltage of 180V. Fig. 6.14 shows the three-phase grid current with phase A grid voltage.

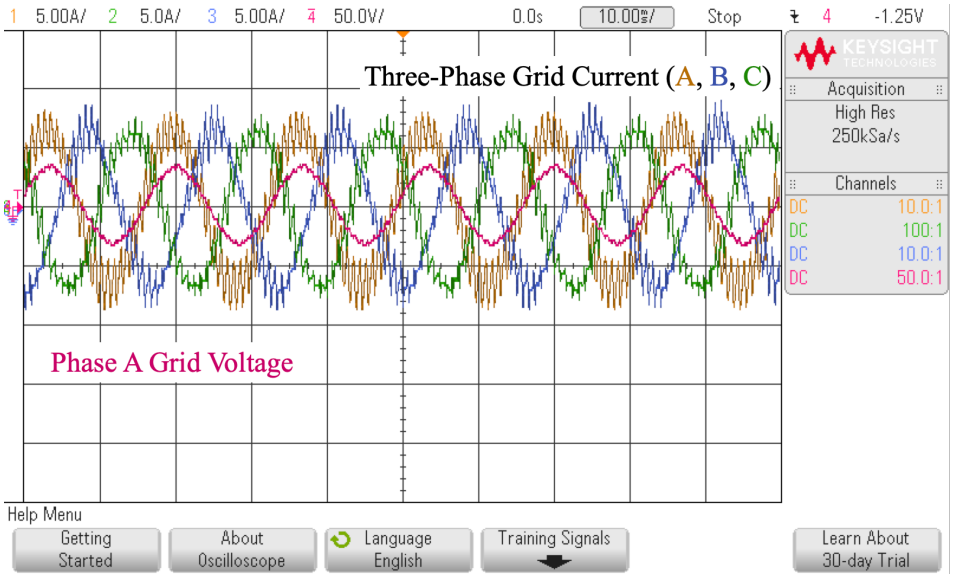

Fig. 6.14. Phase A Grid Voltage and Three-Phase Grid Current of the Reduced Switch-Count Regenerative Cell.

The Six-Switch Regenerative I-Bridge power cell, without any correction, is subject to low order harmonics, current unbalance, and switching harmonics on the cell input current. The cell input current in Fig. 6.14 shows a visible amount of switching harmonics. However, the low order harmonics and current unbalance are not easily visible. The reference reactive power was set to 0 VAR. Comparing the phase difference between the grid current and voltage show that with the Six-Switch Regenerative I-Bridge power cell, FSTPI AFE has good power control and successfully operates in unity power factor. Fig. 6.15 shows the individual voltages of the DC-link capacitors.

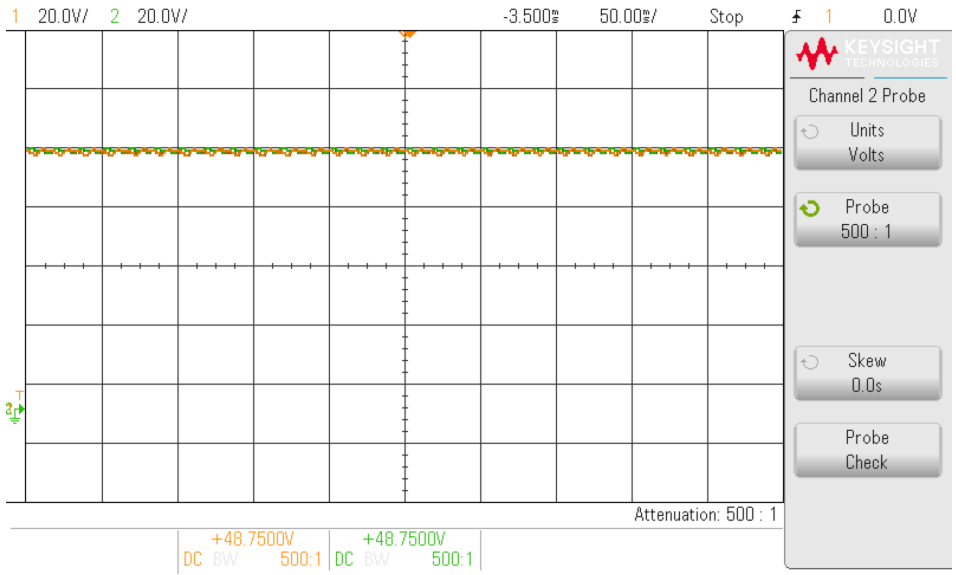

Fig. 6.15. DC-link Capacitor Voltages of the Six-Switch Regenerative I-Bridge Power Cell

The experimental implementation of the Six-Switch Regenerative I-Bridge power cell is a scaled-down single-cell setup. The limitation in available grid power, maximum attainable DC-link voltage, and output RL load is evident when comparing the DC-link ripples and harmonic content with the simulation studies. The low order harmonics and unbalance are directly related to the DC-link voltage ripples in the power cell, and voltage ripples are proportional to the output power of the power cell. As the experimental implementation operates at a fraction of the power in the simulation model, the DC-link ripple, low order harmonics, and current unbalance remain at a low level. Nonetheless, the theoretical analysis is verified through the DC-link capacitor ripples. Fig. 6.16 shows the individual capacitor voltages at a 5V/div.

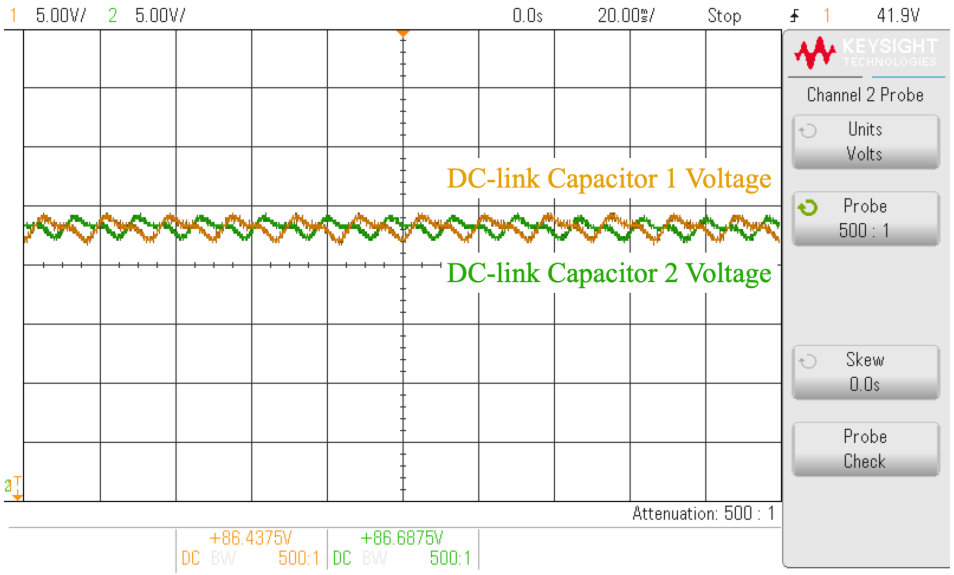

Fig. 6.16. DC-link Capacitor Voltages of the Six-Switch Regenerative I-Bridge Power Cell at 5V/div

The analysis of the DC-link voltage reveals three characteristics of the Six-Switch Regenerative I-Bridge power cell: voltage ripples from both inverters, fundamental voltage ripple cancellation in the whole DC-link, and inherent capacitor voltage balancing. Fig 6.16 demonstrates fundamental voltage ripples on the two DC-link capacitors. The voltage ripples are 180° apart in phase angle, demonstrating the fundamental voltage ripple cancellation in the whole DC-link. The Reduced Switch-Count Regenerative Cell is only subjected to voltage ripples from the FSTPI AFE. In contrast, the Six-Switch Regenerative I-Bridge power cell is subjected to voltage ripples from the FSTPI AFE and the half-bridge inverter. The capacitor voltages in Fig 6.12 and Fig. 6.16 show that the DC-link capacitors are subjected to different voltage ripples despite the control and the parameters of the power cell remaining mostly equivalent. Additionally, the individual capacitor voltages show that the voltage of the two DC-link capacitors remains balanced in the experimental validation. The output voltage and current of the half-bridge inverter are shown in Fig. 6.17.

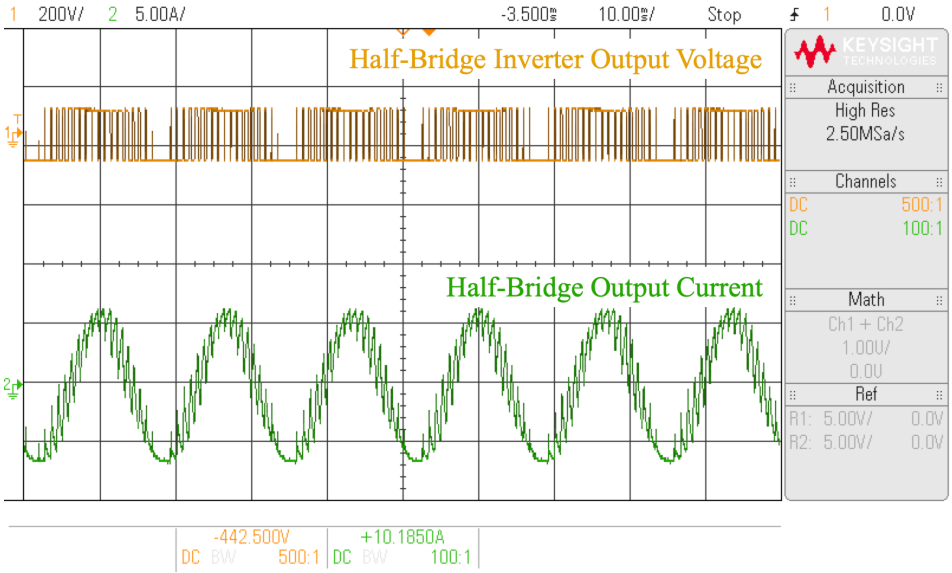

Fig. 6.17. Half-Bridge Output Voltage and Current of the Six-Switch Regenerative I-Bridge Power Cell

The output voltage of the half-bridge inverter shows the reduction in output voltage compared to the H-Bridge inverter and the loss of a voltage level. The analysis of the half-bridge inverter demonstrated that the positive and negative voltage level is based on the voltage of a single DC-link capacitor and does not have a zero-voltage state. The experimental validation reflects the analysis conducted.

Chapter 7

Conclusions and Future Work

7.1 Conclusions

The conventional Cascaded H-Bridge Multilevel inverter is a well-established, popular inverter used in medium voltage motor drive applications. The CHB MV drive provides a modular, reliable, fault-tolerant design that meets the grid and motor harmonic requirements. The typical CHB MV drive only can consume power from the grid. In certain use cases, the unidirectional power capability of the CHB introduces inefficient use of energy as any regenerated power from the load is dissipated through a circuit such as a resistive chopper circuit. The introduction of the conventional regenerative CHB power cell addresses the unidirectional nature of the CHB drive. A conventional regenerative

CHB power cell has been introduced to achieve the bidirectional power capability. However, the conventional regenerative CHB utilizes a 2L-VSI in the rectification stage, increasing complexity, size, and cost. The research in reduced switch-count regenerative CHB power cells has gained significant attention due to the challenges of the conventional regenerative power cell.

This thesis research two new reduced switch-count regenerative CHB power cells that maintain a three-phase connection with the grid and provide a three-phase regenerative CHB power cell with the least switch count.

The conventional non-regenerative and regenerative CHB drives are analyzed to review the operational principles of the configurations. The main challenges of the conventional regenerative power cell are identified to clearly understand the design objectives of the reduced switch-count regenerative CHB power cells.

A literature review of the existing reduced switch count power cells analyzes the structure, methods of switch-count minimization, and challenges involved with switch count reduction. The solutions to address the challenges are investigated, and the analysis of the existing reduced switch-count power cells are compared against the conventional regenerative power cell. The comparison reveals the challenges based on the method of switch count minimization and demonstrates the benefits of maintaining a three-phase grid connection.

The proposed Six-Switch Regenerative H-Bridge CHB power cell reduces the number of switches per power cell by four. An FSTPI and H-Bridge inverters are employed with a common inverter leg. The analysis of the common leg is conducted, and a modulation technique is proposed for proper operation and control of the power cell with

a common inverter leg. The analysis and modulation technique reveals the limitations of the Six-Switch Regenerative H-Bridge CHB power cell. A simulation study is conducted to validate the analysis of the proposed power cell and proposed modulation technique.

The proposed Six-Switch Regenerative I-Bridge CHB power cell addresses the limitations identified with the Six-Switch Regenerative H-Bridge CHB power cell. The proposed power cell maintains the three-phase grid connection and reduces the switch count by four. An FSTPI and half-bridge inverters are employed to minimize the switch count. The analysis of the proposed power cell reveals fundamental and second order voltage ripples on the DC-link, cell input current unbalance, triplen, and switching harmonics that hinder compliance with the IEEE std. 519-2014 grid connection standard. Two possible CHB configurations using the proposed power cell are proposed to address the challenges. In the first configuration, the following methods are proposed:

- Phase alternation method with the FSTPI to eliminate triplen harmonics
- Voltage injection method to address the harmonics caused by the DC-link voltage ripples and cell input current unbalance.
- Switching harmonic elimination method to eliminate two sideband harmonic groups

In the second configuration, the following methods are proposed:

- Voltage injection method to address the harmonics caused by the DC-link voltage ripples and cell input current unbalance
- An asymmetrical switching harmonic elimination method to eliminate the carrier and all three sideband groups identified

Both possible configurations of the proposed Six-Switch Regenerative I-Bridge CHB power cell demonstrate compliance with the grid connection standard and low Total Harmonic Distortion (THD) on the grid current. Simulation studies to validate the analysis and evaluate the performance of the proposed power cell are conducted with three simulation models of a 3kV 9-cell Regenerative CHB. Each model is subjected to a motor load operating in motoring and regenerating modes. The first model of the proposed power cell in a CHB is constructed without any proposed method implemented. The second model implements the first possible CHB configuration with the proposed power cell, and the third model implements the second possible CHB configuration. The simulation studies demonstrate the effectiveness of the proposed method and the proposed Six-Switch Regenerative I-Bridge power cell as a replacement for the conventional regenerative CHB power cell.

The experimental implementation and validation are conducted by constructing a scaled-down single-cell setup that accommodates the conventional regenerative CHB power cell, Reduced Switch-Count Regenerative cell, and the Six-Switch Regenerative I-Bridge power cell. The experimental results validate the theoretical analysis and the simulation studies. Due to time limitations, the experimental implementation of the Six-Switch Regenerative I-Bridge power cell and its proposed methods in a CHB configuration is considered in future work.

7.2 Contributions

The main contributions of the presented work are summarized as follows:

- Proposal of a new Six-Switch Regenerative H-Bridge CHB power cell with an FSTPI AFE and H-Bridge inverter sharing a common leg that reduces the number of switches per power cell by four
- Proposal of a new Six-Switch Regenerative I-Bridge CHB power cell with an FSTPI AFE and half-bridge inverter that reduces the number of switches per power cell by four.
- Proposal of voltage injection, phase alternation, and two switching harmonics elimination methods that address the challenges of the Six-Switch Regenerative I-Bridge power cell.
- Proposal of two possible CHB configurations with the Six-Switch Regenerative I-Bridge power cell to ensure compliance with the IEEE std. 519-2014 grid connection standard.
- Simulation studies for two new proposed reduced switch-count Regenerative CHB power cell
- Experimental implementation and validation of the conventional regenerative CHB power cell, Reduced Switch-Count cell, and new Six-Switch Regenerative I-Bridge power cell with a scaled-down single power cell setup.

7.3 Future Work

The research presented in this thesis reveals some areas of interest worth investigating. The further analysis and validation of the proposed ideas can allow the development of a more economical and better performing regenerative CHB drive. The future work is concluded as follows:

- Evaluation of power cell efficiency as the switch count reduction leads to fewer switching devices with switching and conduction loss.
- Analysis of the proposed power cell with grid side disturbances.
- Analysis of alternative control and modulation strategy with the Six-Switch Regenerative H-Bridge power cell.
- Evaluation of asymmetrical carrier shifting strategy with phase alternation method.
- Analysis of the proposed reduced switch-count power cells utilizing third order harmonic injection and its impact on harmonics.
- Experimental validation of the proposed reduced switch-count power cells and proposed methods based on a regenerative CHB drive configuration.
- Investigation of kVA ratings between the conventional regenerative CHB power cell and proposed reduced switch-count power cells.

References

[1] H. Akagi, "Multilevel Converters: Fundamental Circuits and Systems," in Proceedings of the IEEE, vol. 105, no. 11, pp. 2048-2065, Nov. 2017, doi: 10.1109/JPROC.2017.2682105.

[2] B. K. Bose, *Power Electronics and Motor Drives*, 2nd ed. Knoxville, TN, United States: Academic Press, 2020, pp. 59-109.

[3] B. Wu, and M. Narimani, "High-Power Converters and AC drives ", *Wiley-IEEE Press*, 2017, ISBN: 978-1-119-15603-1.

[4] K. Schiller, "Medium Voltage Drives Report - 2019", IHS Markit, 2019.

[5] B. Bugiardini, and F. Jason, “Matching VFD to Application Requirements”, *Rockwell Automation on demand webinars*, 20-5-2020.

[6] "ALSPA Drive Range", 2001. [Online]. Available: http://alsintec.com/documents/alstom/drives/alspa%20drive%20range_drives%20solutions.pdf. [Accessed: 06- Apr- 2022].

[7] "ACS 1000 Medium Voltage Drives", 2021. [Online]. Available: https://library.e.abb.com/public/a9ba044f69174e2fae063eea07df3448/ACS1000_medium_voltage_drive_catalog_3BHT490400R0001_RevL_EN_lowres.pdf. [Accessed: 06- Apr- 2022].

[8] MV 7000 Flat Pack (FP)", 2021. [Online]. Available: https://www.gepowerconversion.com/sites/default/files/2021-11/GEA33499B%20MV7000%20Flat%20Pack.pdf. [Accessed: 06- Apr- 2022].

[9] "SIMOVERT MV Medium-Voltage Drives 660kVA to 7200kVA", 2001. [Online]. Available: http://w2.siemens.com.cn/news_events/events/common/roadshow/ld/ac/SIMOVERT_MV_DA63_Catalog.pdf. [Accessed: 06- Apr- 2022].

[10] "SINAMICS Perfect Harmony GH180", 2021. [Online]. Available: https://assets.new.siemens.com/siemens/assets/api/uuid:e9d52b04c5acad9232c4c701743b9ec3312a3a3e/genv-gh180-520-brochure-june2018update-lowres.pdf. [Accessed: 06- Apr- 2022].

[11] "HIVECTOL HVI Hardware Overview". [Online]. Available: https://www.hitachi-ip.com/products/direct_inverter/products/direct_inverter_02.html. [Accessed: 06- Apr- 2022].

[12] "PowerFlex 6000 Medium Voltage Variable Frequency Drive", 2019. [Online]. Available: https://literature.rockwellautomation.com/idc/groups/literature/documents/um/6000-um002_-en-p.pdf. [Accessed: 06- Apr- 2022].

[13] M. Vijeh, M. Rezanejad, E. Samadaei and K. Bertilsson, "A General Review of Multilevel Inverters Based on Main Submodules: Structural Point of View," in IEEE Transactions on Power Electronics, vol. 34, no. 10, pp. 9479-9502, Oct. 2019, doi: 10.1109/TPEL.2018.2890649.

[14] K. Benson, "Regeneration for AC drive systems," Proceedings of 1994 IEEE/IAS Annual Textile, Fiber and Film Industry Technical Conference, 1994, pp. 1-3, doi: 10.1109/TEXCON.1994.320728.

[15] M. Rastogi, R. H. Osman, and Y. Fukuta, "Variable-frequency drive with regeneration capability", *US7508147B2*.

[16] J. Wang, and Y. Li, "PWM rectifier in power cell of cascaded H-bridge multilevel converter," *2007 International Conference on Electrical Machines and Systems (ICEMS)*, Seoul, 2007, pp. 18-21.

[17] M. A. Perez, J. R. Espinoza, J. R. Rodriguez and P. Lezana, "Regenerative medium-voltage AC drive based on a multicell arrangement with reduced energy storage requirements," in *IEEE Transactions on Industrial Electronics*, vol. 52, no. 1, pp. 171-180, Feb. 2005, doi: 10.1109/TIE.2004.841095.

[18] "PowerFlex 6000 Medium Voltage AC Drives", 2020. [Online]. Available: https://literature.rockwellautomation.com/idc/groups/literature/documents/pp/6000-pp003_-en-p.pdf. [Accessed: 24- Apr- 2022].

[19] R. Attia, K. Abdellah and H. Ahmed, "Space Vector Pulse Width Modulation for Three Phase Cascaded H-Bridge Inverter," 2018 International Conference on Applied Smart Systems (ICASS), 2018, pp. 1-6, doi: 10.1109/ICASS.2018.8652080.

[20] "PowerFlex 6000 Medium Voltage Variable Frequency Drive Firmware, Parameters, and Troubleshooting Manual", 2017. [Online]. Available: https://literature.rockwellautomation.com/idc/groups/literature/documents/td/6000-td004_-en-p.pdf. [Accessed: 29- Apr- 2022].

[21] J. Rodriguez, J. Pontt, N. Becker and A. Weinstein, "Regenerative drives in the megawatt range for high-performance downhill belt conveyors," in IEEE

Transactions on Industry Applications, vol. 38, no. 1, pp. 203-210, Jan.-Feb. 2002, doi: 10.1109/28.980377.

[22] J. Rodriguez et al., "High-voltage multilevel converter with regeneration capability," in *IEEE Transactions on Industrial Electronics*, vol. 49, no. 4, pp. 839-846, Aug. 2002, doi: 10.1109/TIE.2002.801238.

[23] P. Lezana, J. Rodriguez, D. Rojas and J. Pontt, "Novel cell based on reduced single-phase active front end for multicell converters," *31st Annual Conference of IEEE Industrial Electronics Society, 2005*. IECON 2005, Raleigh, NC, 2005, pp. 6 pp.-, doi: 10.1109/IECON.2005.1568995.

[24] P. Lezana, J. Rodriguez and D. A. Oyarzun, "Cascaded Multilevel Inverter With Regeneration Capability and Reduced Number of Switches," in *IEEE Transactions on Industrial Electronics*, vol. 55, no. 3, pp. 1059-1066, March 2008, doi: 10.1109/TIE.2008.917095.

[25] J. Rodriguez, J. Pontt, E. Silva, J. Espinoza and M. Perez, "Topologies for regenerative cascaded multilevel inverters," *IEEE 34th Annual Conference on Power Electronics Specialist, 2003. PESC '03*. Acapulco, Mexico, 2003, pp. 519-524 vol.2, doi: 10.1109/PESC.2003.1218109.

[26] J. R. Rodriguez, J. W. Dixon, J. R. Espinoza, J. Pontt and P. Lezana, "PWM regenerative rectifiers: state of the art," in IEEE Transactions on Industrial Electronics, vol. 52, no. 1, pp. 5-22, Feb. 2005, doi: 10.1109/TIE.2004.841149.

[27] S. Badawi et al., "Utilization of a Reduced Switch-Count Topology in Regenerative Cascaded H-Bridge (CHB) Medium-Voltage Drives," in IEEE Journal of Emerging and Selected Topics in Power Electronics, doi: 10.1109/JESTPE.2021.3129137.

[28] Gi-Taek Kim and T. A. Lipo, "VSI-PWM rectifier/inverter system with a reduced switch count," IAS '95. Conference Record of the 1995 IEEE Industry Applications Conference Thirtieth IAS Annual Meeting, 1995, pp. 2327-2332 vol.3, doi: 10.1109/IAS.1995.530598.

[29] H. Zhang, "A Simplified Space Vector PWM Algorithm for Four-Switch Three-phase Inverters," 2021 IEEE 12th International Symposium on Power Electronics for Distributed Generation Systems (PEDG), 2021, pp. 1-6, doi: 10.1109/PEDG51384.2021.9494166.

[30] P. Q. Dzung, Le Minh Phuong, P. Q. Vinh, N. M. Hoang and N. X. Bac, "A New Switching Technique for Direct Torque Control of Induction Motor using Four-Switch Three-Phase Inverter," 2007 7th International Conference on Power Electronics and Drive Systems, 2007, pp. 1331-1336, doi: 10.1109/PEDS.2007.4487877.

[31] Hong Hee Lee, Phan Quoc Dzung, Le Dinh Khoa, Le Minh Phuong and Huynh Tan Thanh, "The adaptive space vector PWM for four switch three phase inverter fed induction motor with DC - link voltage imbalance," TENCON 2008 - 2008 IEEE Region 10 Conference, 2008, pp. 1-6, doi: 10.1109/TENCON.2008.4766516.

[32] C. B. Jacobina, E. R. C. da Silva, A. M. N. Lima and R. L. A. Ribeiro, "Vector and scalar control of a four switch three phase inverter," IAS '95. Conference Record of the 1995 IEEE Industry Applications Conference Thirtieth IAS Annual Meeting, 1995, pp. 2422-2429 vol.3, doi: 10.1109/IAS.1995.530611.

[33] "IFS100B12N3E4 | 1200V, 100A sixpack IGBT module". [Online]. Available: https://www.infineon.com/cms/en/product/power/igbt/igbt-modules/ifs100b12n3e4_b31/. [Accessed: 04- May- 2022].

[34] IEEE Recommended Practice and Requirements for Harmonic Control in Electric Power Systems," in *IEEE Std 519-2014 (Revision of IEEE Std 519-1992)*, pp.1-29, 11 June 2014, doi: 10.1109/IEEESTD.2014.6826459.

[35] D. G. Holmes, and T. A. Lipo, " Pulse Width Modulation for Power Converters: Principles and Practice, " *Wiley-IEEE Press*, 2003, ISBN: 978-0-471-20814-3.

[36] Z. Ni et al., "A New Approach to Input Filter Design for Regenerative Cascaded H-Bridge Drives," in IEEE Transactions on Industrial Electronics, vol. 69, no. 4, pp. 3266-3277, April 2022, doi: 10.1109/TIE.2021.3071694.

[37] J. Rodriguez, J.S. Lai, and F.Z. Peng, "Multilevel inverters: a survey of topologies, controls, and applications," in *IEEE Transactions on Industrial Electronics*, vol. 49, no. 4, pp. 724-738, Aug. 2002, doi: 10.1109/TIE.2002.801052.

[38] C. Brandao Jacobina, M. Beltrao de Rossiter Correa, A. M. Nogueira Lima and E. R. Cabral da Silva, "AC motor drive systems with a reduced-switch-count

converter," in IEEE Transactions on Industry Applications, vol. 39, no. 5, pp. 1333-1342, Sept.-Oct. 2003, doi: 10.1109/TIA.2003.816526.

[39] S. Kouro, M. Malinowski, K. Gopakumar, J. Pou, L. G. Franquelo, B. Wu, J. Rodriguez, M. A. Pérez, and J. I. Leon, "Recent Advances and Industrial Applications of Multilevel Converters," in *IEEE Transactions on Industrial Electronics*, vol. 57, no. 8, pp. 2553-2580, Aug. 2010, doi: 10.1109/TIE.2010.2049719.

[40] J. D. Glover, M. S. Sarma, T. J. Overbye, "Power system analysis and design, " *Cengage Learning*, 2012, ISBN: 978-1-111-42577-7.

[41] M. Vijeh, M. Rezanejad, E. Samadaei and K. Bertilsson, "A General Review of Multilevel Inverters Based on Main Submodules: Structural Point of View," in *IEEE Transactions on Power Electronics*, vol. 34, no. 10, pp. 9479-9502, Oct. 2019, doi: 10.1109/TPEL.2018.2890649.